Interfaces of Graphene and Biological Systems: Applications in Biomedicine and Energy

BY

BIJENTIMALA KEISHAM

B.Tech, Amity University, Noida, India, 2010

M.Tech, National Institute of Technology, Tiruchirappalli, India, 2012

THESIS

Submitted as partial fulfillment of the requirements for the degree of
Doctor of Philosophy in Chemical Engineering in the
Graduate College of the University of Illinois at Chicago, 2020

Chicago, Illinois

Defense Committee:

Dr. Vikas Berry, Chair and Advisor, Department of Chemical Engineering

Dr. Ying Liu, Department of Chemical Engineering

Dr. Gang Cheng, Department of Chemical Engineering

Dr. Ankit Mehta, Department of Neurosurgery

Dr. Jie Xu, Department of Mechanical and Industrial Engineering

ACKNOWLEDGEMENTS

I would like to thank Dr. Vikas Berry for his guidance throughout my professional and graduate career. I started my PhD career because I wanted to do research in the field of nanobiotechnology. However, I had no idea what graphene was. That changed when I met Dr. Berry. The enthusiasm with which Dr. Berry described his research motivated me to learn about graphene and its exciting properties. And within a couple of months, I started my first PhD project on cancer detection using graphene as a sensitive platform.

I also wish to extend my sincere appreciation to Dr. Mehta, my committee member, with whom I have collaborated in multiple projects, including my first research. I have learned a lot about neurosurgery and its related topic from working with Dr. Mehta and attending his research group meetings. I would also like to thank my other committee members, Dr. Ying Liu, Dr. Gang Cheng and Dr. Jie Xu, who have graciously agreed to take out time from their busy schedules and attend my defense.

Sincere thanks to Dr. George Papadantonakis as well with whom I have worked as a teaching assistant for the past 5 years. Dr. P had always encouraged me and supported me throughout my PhD.

Further, I would like to thank my colleagues from Berry research laboratory (Phong Nguyen, Rousan Debbarma, Shikai Deng, Songwei Che, Deisy Arrington, Sheldon Cotts, Sungjoon Kim, Lan Nguyen, Chen Wang and Roshan Nemade). They made working in a research laboratory

everyday fun and exciting. I would also like to thank my co-authors (Akop Seksenyan, Sheldon Cotts, Mandana Behbahani, Sungjoon Kim and Steven Denyer).

Finally, I want to thank my family and friends outside of research. My mom and my siblings have always supported me in every decision I have made in my life. Their unconditional love and encouragement have helped me pursue excellence in my studies. Lastly, I want to thank my boyfriend, Michael Wallin, who has supported me through all the up and downs and taught me life is not just about work.

CONTRIBUTION OF AUTHORS

Keisham, B.; Cole, A.; Nguyen, P.; Mehta, A.; Berry, V. Cancer Cell Hyperactivity and Membrane Dipolarity Monitoring via Raman Mapping of Interfaced Graphene: Towards Non-Invasive Cancer Diagnostics. ***ACS Appl. Mater. Interfaces*** **2016, 8, 48, 32717-32722**

BK conducted most of the experiments and analysis, AC directed the cell cultures and PN contributed in the calculations. VB and AM conceived and directed the project. All authors contributed towards writing the manuscript.

Keisham, B.; Seksenyan, A.; Denyer, S.; Kheirkhah, P.; Arnone, G. D.; Avalos, P.; Bhimani, A. D.; Svendsen, C.; Berry, V.; Mehta, A. I. Quantum Capacitance Based Amplified Graphene Phononics for Studying Neurodegenerative Diseases. ***ACS Appl. Mater. Interfaces*** **2019,** ***11*** **(1), 169–175.**

AS conceived the idea of using the detection technology developed by VB, AM and BK for ALS detection. BK, AS, CS, VB and AM designed the experiments. BK fabricated the graphene detection system and performed the detection experiments. AS, SD, PK, GDA, ADB contributed in obtaining the CSF samples. BK and AS analyzed the Raman data and made the figures in the manuscript. PA and CS developed and characterized the transgenic rat model and provided the CSF samples from this model. BK, AS, VB and AM wrote the manuscript. All authors contributed to the discussion, analysis and interpretation of the results and reviewed the manuscript and have given approval to the final version of the manuscript. BK and AS contributed equally and share first authorship.

Sheldon Cotts, Bijentimala Keisham, Jay Rawal and Vikas Berry, "Graphene-Interface with Electrogenic Bacterial Membrane for Electron-Harvestation", Submitted

VB conceived and directed the project. SC, BK and JR performed the rGO synthesis and the experiments. SC and BK analyzed the results. The manuscript was written through contributions of all the authors. All authors have given approval to the final version of the manuscript. BK and SC contributed equally and share first authorship.

TABLE OF CONTENTS

TABLE OF CONTENTS (Continued)

TABLE OF CONTENTS (Continued)

TABLE OF CONTENTS (Continued)

LIST OF TABLES

LIST OF FIGURES

LIST OF ABBREVIATIONS

2D Two-dimensional

CVD Chemical Vapor Deposition

GO Graphene Oxide

rGO Reduced Graphene Oxide

CNT Carbon Nanotube

MSC Mesenchymal Stem Cell

hNSC Human Neural Stem Cell

GBM Glioblastoma Multiforme

CSF Cerebrospinal Fluid

ALS Amyotropic Lateral Sclerosis

MS Multiple Sclerosis

MND Motor Neuron Disease

CNS Central Nervous System

MFC Microbial Fuel Cell

FESEM Field Emission Scanning Electron Microscopy

SERS Surface Enhanced Raman Spectroscopy

GQD Graphene Quantum Dots

AFM Atomic Force Microscopy

ABSTRACT

Interfacing of graphene (and other 2D materials) with biocomponents has led to its translation into a wide spectrum of applications in biotechnology, biomedicine and energy via development of a wide spectrum of novel bio-nanodevices. Graphene is the newest member of carbon-allotrope family, which consists of various nanomaterials including carbon nanotubes and quantum dots. The fundamental electronic, vibrational and optical phenomena derived from this stable, free-standing nanomaterial in the form of an atomically-thick, 2D flat sheet is what makes graphene unique.

Several 2D materials, including graphene, are being investigated intensively for their unique physicochemical properties arising from their atomically planar structure. They possess a range of fundamentally superior properties including the highest surface area to volume ratio, high conductivity and exceptional optical and electrical phenomena. These properties could enable the development of efficient graphene biointerfaces for fabricating multifunctional biomedical devices and alternate energy sources. To successfully define the capabilities and limitations of such devices, it is important to understand the mechanisms involved in systems where biological components are interfaced with graphene.

One of the ways to characterize graphene is using Raman spectroscopy which has shown to be a powerful tool to study materials. Although the electrical properties of graphene have been extensively studied for numerous applications including biosensing, research on graphene phononics to investigate nanobiointerface is limited. To gain insight in this field, we interfaced monolayer graphene with different cell systems - cancerous: Glioblastoma multiforme (GBM) cells and normal: Astrocytes, and investigated the interaction using Raman spectroscopy. The 2D

Raman peak of graphene with GBM cells showed a large blue shift, ~6.3 cm^{-1}, indicating a high degree of p-doping compared to when interfaced with astrocytes, ~2.3 cm^{-1}. This is attributed to the different metabolic activity and surface chemistry among the two cell types. Such sensitive doping of graphene is attributed to its large quantum capacitance and the surface potential of the GBM cell was calculated to be ~310 mV.

Following the cell study, we then investigated different cerebrospinal fluids (CSFs) obtained from patients with diseases affecting the central nervous system (CNS) including ALS, multiple sclerosis (MS) and other forms of motor neuron diseases (MND). The CSF with ALS n-doped the graphene lattice (red-shifted the 2D peak) to a different degree compared to other disease groups (MS and MND). Currently, there are no reliable biomarker to accurately detect ALS and often, patients with monomelic amyotrophy, primary lateral sclerosis and cervical myelopathy are misdiagnosed as ALS. Hence, the graphene-bio interface could potentially be used as a diagnostic tool for detecting ALS. The graphene platform could also be used to monitor the progression of ALS disease. CSF samples from $SOD1^{G93A}$ transgenic rat model corresponding to different stages: early symptomatic (onset) and end point were investigated, which exhibited different n-doping trends. This offers a technique to monitor the progression of the disease, which has been difficult to quantitatively measure until now.

We further investigated the utilization of the graphene- bio interfaces in other fields including bioenergy. Here, we interfaced graphene (reduced graphene oxide, rGO) with electrogenic bacteria (*Geobacter sulferreducens*) to understand the electron transport mechanism. In this study, the high conductivity and flexibility of graphenic sheets was leveraged. When rGO sheets interfaced with *Geobacter sulferreducens*, the electrons produced by the electrogenic bacteria by metabolizing the

substrate are transferred to the rGO sheets, adding ~34400 electrons per μm^2 under steady state as confirmed by phononic characterization. The interaction of bacteria with rGO led to addition of electrons (n-doping) (~5.3 cm^{-1}) in the rGO lattice. This interface was also studied in a microbial fuel cell (MFC) like device, where the introduction of graphene in the anode chamber resulted in an estimated 2-fold higher rate of electron transfer. The flexible rGO sheet conforms to the bacterial cell, connecting the membrane proteins and enhancing the efficient transport of the electrons from the cellular surface. Exploring the bacterial-graphene interaction and the energetics involved at a single cellular level would help us understand the nano-biointerface and utilize it for fabricating efficient nanodevices.

In addition, the interaction of graphene quantum dots (GQDs) with bacteria was characterized using Raman spectroscopy. In this study, we observed an enhancement in the bacterial peaks due to the presence of GQDs. Previously, SERS of bacteria was observed using various metal substrates including silver and gold. This is the first time, GQD was used as the SERS substrate.

CHAPTER 1

1. Introduction

1.1. Graphene

Graphene is a planar sheet of sp^2 hybridized carbon atoms arranged in a honeycomb lattice(Schedin et al. 2007; Mohanty and Berry 2008; Mohanty et al. 2011; X. Wang, Zhi, and Müllen 2008; Pumera 2011) and is the precursor of all graphitic material including fullerenes (0D), carbon nanotubes (1D) and graphite (3D). This wonder material is associated with numerous superlatives. It is the thinnest known material (~0.3 nm, vibration modes are active). The π-electrons(Geim and Novoselov 2007) within a single-layer of atoms(Novoselov et al. 2004) ensure that the effect of events on graphene's carrier density remains confined to graphene. In contrast, the effect of a molecular event on graphite surface is diminished due to its thickness (distribution of the effect over thickness). Due to this, graphene exhibits a high quantum capacitance which changes the density-of-states of graphene with a small electric field from interfacing molecules, making it extremely sensitive to doping. Here, the quantum-coupling of the electric-field from the molecular dipoles on graphene is enhanced, significantly influencing the conductivity of graphene. Graphene exhibits ultrahigh mobility (200,000 $cm^2/V/s$; highest ever measured), which acts as a signal-amplifier ($\Delta I/V_{DS} \propto nA\,\mu$) for ultrasensitive detection. The high mobility originates from its π-orbitals being atop its lattice plane reducing scattering(Meyer et al. 2007; Geim and Novoselov 2007). Graphene also exhibits strong phonon coupling with phononic energies which is extremely sensitive to its Fermi level(Das et al. 2008b; Basko, Piscanec, and Ferrari 2009). Further, graphene possesses a large interfacial area providing an ideal platform for attachment of large biological

cells(Nguyen and Berry 2012; Paulus et al. 2014). These properties are considered tremendously advantageous for various applications, especially in the biomedical field.

Numerous procedures have been developed to synthesize graphene. Novoselov et al.(Novoselov et al. 2004) first synthesized graphene micromechanical cleavage method which uses scotch tape to peel the graphitic layers apart. This method produces very high quality graphene. However, it is rather tedious with extremely low throughput and produces graphene of micro-scale dimensions, which demand precision handling (large areal graphene such as inch scale would enable easier handling and processing). Another way to synthesize large quantity of graphene is via exfoliation of graphite with strong acids/ oxidizing agents(Hummers and Offeman 1958) and subsequent reduction of the resulting graphene oxide using various chemical, electrochemical, thermal and photocatalytic processes(Dreyer et al. 2010; Tung et al. 2009). Graphene oxide (GO) consists of several oxy-functional groups (carboxyl, carbonyl, hydroxyl, epoxy, etc) sp^3 bonded on the sp^2 graphenic structure which helps in the exfoliation and subsequent stabilization in solution(Si and Samulski 2008). The subsequent reduction of GO into reduced GO (rGO) can be effectively done using a variety of reagents including hydrazine(Dikin et al. 2007; Stankovich et al. 2007), hydrogen plasma(Zhu et al. 2010; Sundaram et al. 2008), microbes(Zhu et al. 2010; Salas et al. 2010), and even microwave(Voiry et al. 2016). However, the quality of rGO produced is generally lower than that of the micromechanical exfoliated graphene(Schwamb et al. 2009), due to the resilient oxy-functional groups in GO such as the carbonyl groups, which are difficult to remove upon reduction(Gao et al. 2009; Stankovich et al. 2006) as well as some defects. Later, the chemical vapor deposition (CVD) process was employed to produce large-scale, and single or few layered graphene on various substrates. Here, hydrocarbon precursors such as CH_4 are fed into the

reactor at a high temperature, which will be decomposed to carbon radicals on catalytic metal surfaces and then form graphene(Zhang, Zhang, and Zhou 2013). Ni is one of major substrates used for CVD graphene process due to its highly-matched lattice with graphene(Batzill 2012). However, the high solubility of carbon (C) in Ni limits the yield of monolayer graphene sheets. Another promising substrate is Cu, which possesses low solubility of C resulting in a self-limiting deposition mechanism on Cu surface. CVD growth of graphene using Cu was pioneered by Ruoff et al.(Xuesong Li et al. 2009) producing continuous, high quality, and large scale monolayer graphene (>95% of area mono layered). The CVD produced graphene is then transferred onto arbitrary substrates such silica to investigate its various properties. However, the CVD graphene suffers from some critical issues including lower mobility and formation of wrinkles, tears, and other structural defects during the transfer process.

1.2. Characterization of Graphene

Various characterization tools, including atomic force microscopy (AFM), TEM, and Raman spectroscopy, have been utilized to characterize the structure and properties of graphene. In our study, the main emphasis will be given to Raman spectroscopy which is a fast and non-destructive method. Further, it offers high resolution, provides electronic and structural information, and is also applicable at both laboratory and mass-production scales(Andrea C. Ferrari and Basko 2013).

1.2.1. Raman spectroscopy

Raman scattering is referred to the inelastic scattering of photons by optical phonons which is typically classified as two photon events, namely the simultaneous annihilation of an incident photon and the formation of a scattered photon. The probability of Raman scattering is much lower

than Rayleigh scattering and happens when some of the energy of the incident photon ($\hbar\vartheta_i$) is lost during the interaction process, thereby creating a scattered photon with lower energy ($\hbar\vartheta_{sc}$). Such event is referred to as a Stokes (S) process. The energy lost during this interaction must correspond

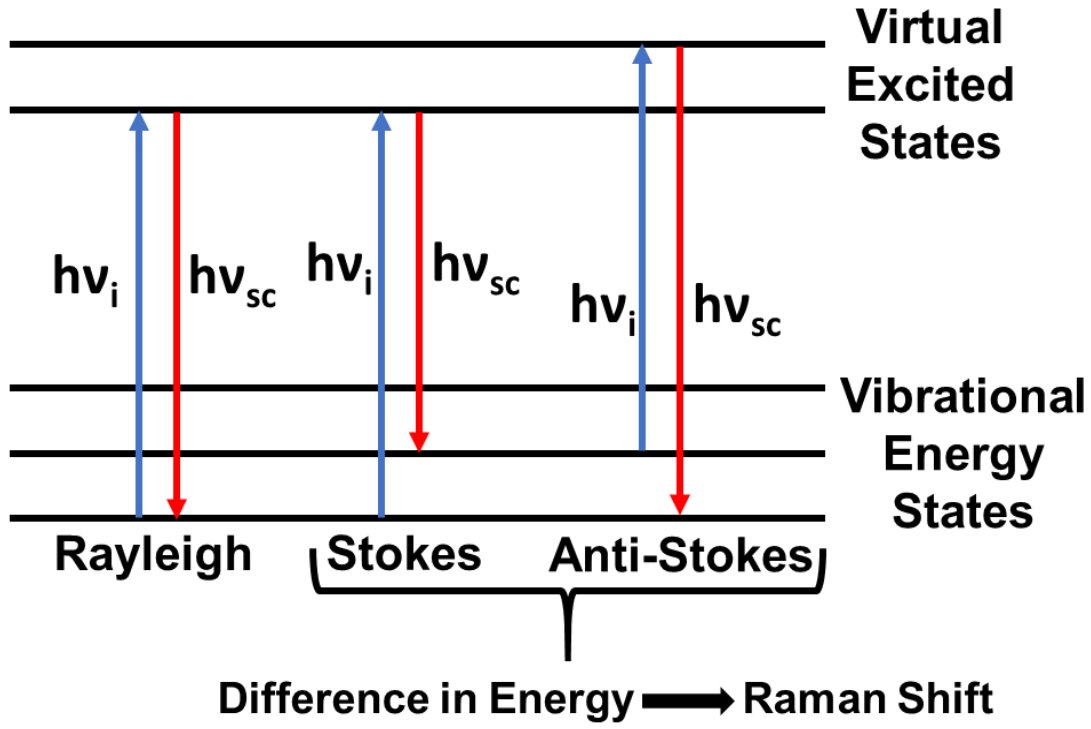

Figure 1.1. Mechanism of Raman spectroscopy involving inelastic scattering processes (Stokes and Anti-Stokes)

to a phonon energy, $\hbar\vartheta_i - \hbar\vartheta_{sc} = \hbar\Omega$, since the sample should return to a stationary state. Alternatively, the incident photon can leave the crystal with an increased energy, $\hbar\vartheta_{sc} = \hbar\vartheta_i + \hbar\Omega$, after the interaction with the system if the sample was already in an excited vibrational state. This corresponds to the Anti-Stokes (AS) process (Figure 1.1).

Stokes processes are studied more in literature due to its higher probability(P. Y. Yu and Cardona 2005) where the measurements are conducted by plotting the intensity of the scattered light as a function of the difference between scattered photon energy and incident energy, referred to as the

"Raman shift". The unit of Raman shift is generally represented as cm^{-1}, even though it should resemble that of energy.

Electrons play a big role in determining the Raman scattering process on phonons including their movements and scattering behavior. Therefore, one can effectively probe the electrons via phonons to investigate any modifications of the electronic properties of a system attributed to edges, doping, defects or magnetic fields by observing the widths, positions, and intensities of the Raman peaks.(Andrea C. Ferrari and Basko 2013) In this section, the phononic properties of graphene probed using Raman spectroscopy, will be discussed.

1.2.1.1. The Raman spectrum of Graphene

Raman spectroscopy has become increasingly famous to characterize carbon nanomaterials like graphene. In case of graphene, this scattering technique is essentially advantageous due to the non-existence of band gap, rendering incident radiation of any wavelength resonant. Thus, the Raman spectra of graphene provides information ranging from the atomic structure as well as the electronic properties. However, it is essential to understand the phonon dispersion of graphene to accurately interpret the Raman spectra of graphene. Monolayer graphene consists of 2 carbon atoms, A and B, and thus represented by 6 phonon dispersion bands: three acoustic branches (A) and the other three optic (O) phonon branches (Figure 1.2a), two being doubly degenerate(Malard et al. 2009; Andrea C. Ferrari and Basko 2013). The Raman spectra of graphene is represented by 3 characteristic peaks as shown in Figure 1.2b. The D peak, also known as the disorder-induced band, occurs around 1350 cm-1, G peak around 1580-1590 cm^{-1} and 2D (also called G') peak between 2600-2700 cm^{-1}.

The G band is associated with the doubly degenerate (iTO and LO) phonon mode and corresponds to the high-frequency E_{2g} phonon at the Brillouin zone center, **Γ**. The D band originate from a second order process involving iTO phonon near the Brillouin zone corner, K and a defect. It is strongly dispersive with the laser excitation energy due to Kohn Anomaly at K. The 2D band is also a second order process which involves two iTO phonons near the K point. This peak is always present regardless of the presence of defects since its process involves momentum conservation satisfied by two phonons with opposite wave vectors(Andrea C. Ferrari and Basko 2013; Malard et al. 2009).

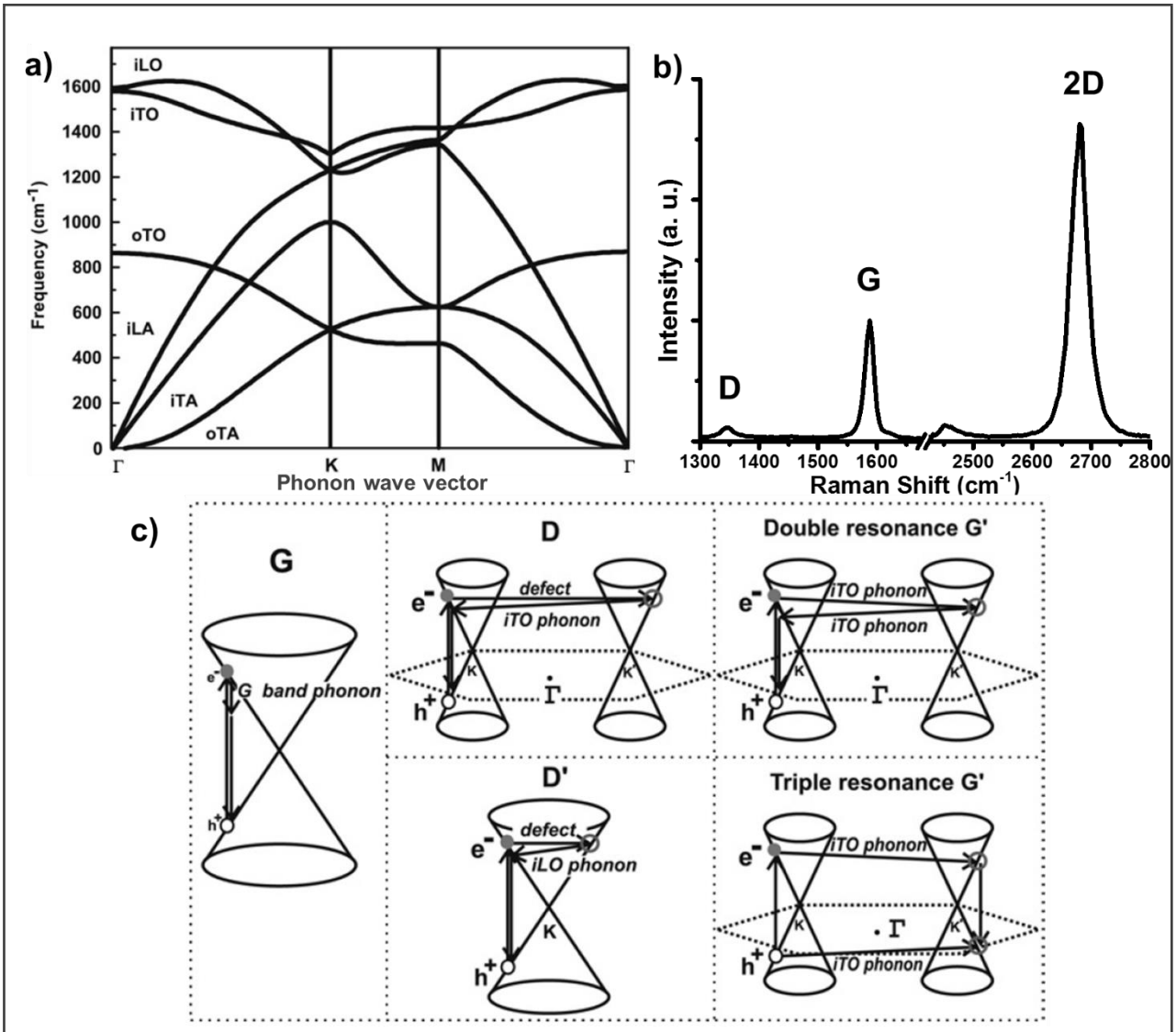

Figure 1.2. Characterization of graphene phonons. a) Dispersion of graphene phonons depicting the iLO, iTO, oTO, iLA, iTA and oTA phonon branches(Malard et al. 2009); i: in-plane, o: out-of-plane, A: acoustic, O: optical, T: transverse, L: longitudinal. b) The Raman spectrum of monolayer graphene showing D, G and 2D bands, and c) First-order G band phononics (Left); intervalley process involving the second-order double resonance process for the D-band with one-phonon and a defect (Center top) and intravalley process for the D' band (Center bottom); and second-order resonance Raman processes involving 2 phonons (Right top) for the 2D band double resonance process, and for the 2D band triple resonance process for monolayer graphene (Right bottom). The resonance points are indicated by the open circles near the K point (left) and the K' point (right). Physics Reports. 2009, pp 51–87

The G band process involves one phonon mode (where the wave vector $q = 0$) and is the only one which follows the normal first order Raman scattering process in graphene. Alternatively, the D and 2D bands, which are second order processes, are associated with the double resonance (DR) Raman process. The DR Raman process starts with the absorption of a photon of energy, E_{laser}, by an electron of wave-vector k around K (as shown in Figure 1.2c, the center and right side), which is then scattered inelastically by a phonon or a defect of wave vector q and energy E_{phonon} to a K' point (related to K by time reversal symmetry(Dresselhaus, Dresselhaus, and Jorio 2008)), with a wave vector $k + q$. The electron then gets scattered back to a k state, and recombines with a hole at a k state, thereby emitting a photon.

The DR Raman process involves three scattering events which should fulfill two resonance conditions: a) the intermediate k + q state represents a real electronic state, and b) either the initial or the final k state indicates a real electronic state(Reich and Thomsen 2004). There is another special case when it comes to graphene, known as the triple resonance (TR) Raman process, wherein the valence band is almost a mirror band of the conduction band, that is relative to the Fermi energy. As shown in the bottom right side of Figure 1.2c, the hole from a K point is scattered to a K' point by a phonon wave vector + q, instead of scattering back the electron (from K' to K point) by a wave vector – q. Here, the scattering processes of both the electron and hole is considered resonant, thus the electron-hole recombination occurs around the K' point in resonance states. This could potentially explain the higher intensity of the 2D bank peak compared to the G peak(Malard et al. 2009).

1.3. Understanding graphene biointerfaces

The integration of biological cells with graphene material has significantly evolved over the years with a wide range of applications including biosensing, disease detection and drug delivery. Hence, understanding the fundamental interaction mechanism involved at the interface of graphene and cells is essential. To successfully integrate 2D nanomaterials in the development of biomedical devices, it is imperative to understand the mechanism involved during the interaction between interfaced biological components (such as cells) and the nanomaterials. Due to the complexity of the system, numerous factors must be considered, including the characteristics of the involved material, the type of interactions pertaining to different biological components and, the outcomes of such biological activities.

1.3.1. Graphene Chemistry

An important attribute of nanomaterials is its large surface area to volume ratio.(Cheng et al. 2013) This property has enabled the extensive integration of nanotechnology in biomedical analysis. Graphene is an extreme example in this regard. Every atom in a monolayer graphene lies on the surface and are exposed on both sides with a theoretical maximum of 2600 m^2/g for a sp^2-hybridized carbon sheet. It is important to understand how the exceptionally high surface area of a single layer graphene could affect the surface phenomena involved when it interfaces with biological entities. Furthermore, due to its 2-D planar structure and flexibility, it conforms well to the cell membrane.(Mohanty et al. 2011; Nguyen and Berry 2012; Deng et al. 2016) Another important property to consider is the number of layers of graphene. This is because the surface area of graphene gradually decreases with increasing number of layers. Hence, it is necessary to control the graphene's number of layers to fully utilize its useful characteristics. Additionally,

graphene materials exist in different forms, with distinct surface chemistry. Graphene oxide (GO) sheet contains several types of lattice disorders and oxygen functional groups, including hydroxyl, carboxy and epoxy groups. This results in GO being a high resistance material(Eda, Fanchini, and Chhowalla 2008; Pope and Aksay 2015; Dreyer et al. 2010; Sreeprasad and Berry 2013), as well as being a heavily self-doped material. A monolayer GO sheet (~1 nm) is thicker than graphene (0.34 nm) due to the presence of various functional groups, structural/lattice defects and adsorbed water molecules(Eda, Fanchini, and Chhowalla 2008).

1.3.2. Dimensionality of Graphenic Structures

The compatibility between the dimensions of the biological systems and the materials plays a crucial role in developing an efficient bio-interface. Graphene materials with different dimensions including 0D, 1D, 2D and 3D have been utilized for fabricating functional biointerfaces. The target biological structure defines the appropriate dimension of the graphene material. Further, the size of these materials influences their mechanical and chemical properties.

The interface formed with a biological entity like cell can be intercellular or intracellular depending on the nanomaterial used. Graphene materials which can exist as freestanding systems including graphene quantum dots (0D) can be readily internalized *via* endocytosis. This process results in an extracellular interface whereby GQDs can directly interact with organelles or cytosol, giving insights about the subcellular entities. In contrast, substrate bound graphene sheets often form intercellular interface through which the surface properties of the cells could be examined.

1.3.3. Surface Chemistry of Biological Systems

Along with the characteristics of the graphene materials, another significant factor to understand is the surface science of the biosystems. Different applications can be developed based on the biological system used. For example, bacterial cells have been thoroughly investigated by interfacing with graphene systems to develop a sensitive and reliable platform for screening microbes. However, it is important to note there are different types of bacteria based on their surface chemistries, mainly: gram-negative and gram-positive bacteria. Aside from microbes, there have been numerous researches to explore the interface of diverse mammalian (human) systems with graphene to develop an ultrasensitive platform for applications including disease detection. Some important criteria to consider for different human systems are discussed below:

1. Cells: Cell-material interface are widely studied in the biomedicine field for applications including reliable and sensitive biosensors. Most cell-material interactions are mediated by the cell membrane; hence, it is important to investigate the surface chemistry of the membrane.(Mager, Lapointe, and Stevens 2011) The chemical composition of the outer cell membrane plays a significant role in such interactions. Diseases like cancer affect the cells altering their surface characteristics.

2. Tissues: Composed of specialized cells, tissues have specific properties defined by the type of cells they are composed of. Characterizing material-tissue interface is crucial for successful development of implants including neural and bone. The integrity of tissue architecture depends on the proper functioning and organization of the cells which depends on the polarity or the spatial orientation of the specific cells in their place. Hence, alteration

or mutation in these cells pertaining to specific diseases significantly changes the properties of the associated tissues.

3. Biofluids (blood and CSF): Biofluids like blood and cerebrospinal fluid (CSF) can provide plentiful information regarding the state of the human body. The chemical compositions in these fluids provide a fingerprint of any disease present. When interfaced with graphene materials, these chemical components change the properties of graphene due to their specific dipole moments.

1.3.4. Biocompatibility of graphene

As discussed, the interfaces formed by graphene systems with biological systems are influenced by various factors. Over the years, the literature on graphene-bio interactions has rapidly increased. The interaction of graphene with biological entities like cells can be broadly classified into 2 groups: (a) interaction with the outer surface of the cell membrane (extracellular) and (b) incorporation of the material inside the cell (intracellular). Here, focus will be on exploring extracellular nano-biointerfaces and understanding the surface chemical properties of biosystems for applications including disease diagnosis.

One of the main concerns of integrating graphene into biomedical research is its toxicity. As biointerfaces formed by 0D graphene material (GQDs, fullerenes) are predominantly intracellular, functionalization of the nanomaterial and the biosystems are typically required to develop extracellular interfaces.(Sreeprasad et al. 2015) Since majority of the biocompatibility studies of GQDs and fullerenes are based intracellular interactions, they fall beyond the scope of this review. Further, the biocompatibility studies on 1D material like CNTs are often inconclusive as the

toxicology of CNT and CNT based materials often depends on the presence of transition metal catalysts.(Smart et al. 2006; Y. Liu et al. 2013; Cui et al. 2005) As for 2D graphene systems, the surface chemistries of each graphene sheets (pristine graphene, GO or reduced GO) differ widely, so it is unrealistic to expect them to have similar biocompatibilities. Numerous studies on the interaction of GO (or rGO) with biological systems are available compared to pristine graphene (mechanically exfoliated or CVD based). In 2010, Kalbacova et al. showed for the first time the biocompatibility of CVD graphene towards human osteoblasts and MSCs.(Kalbacova et al. 2010) These cells were plated on graphene and SiO_2 substrates by incubating for 48 hrs. Increased cell growth and density was observed on graphene substrates compared to SiO_2, as shown in figure 1.3. The favored cell differentiation on graphene film indicates its potential application towards

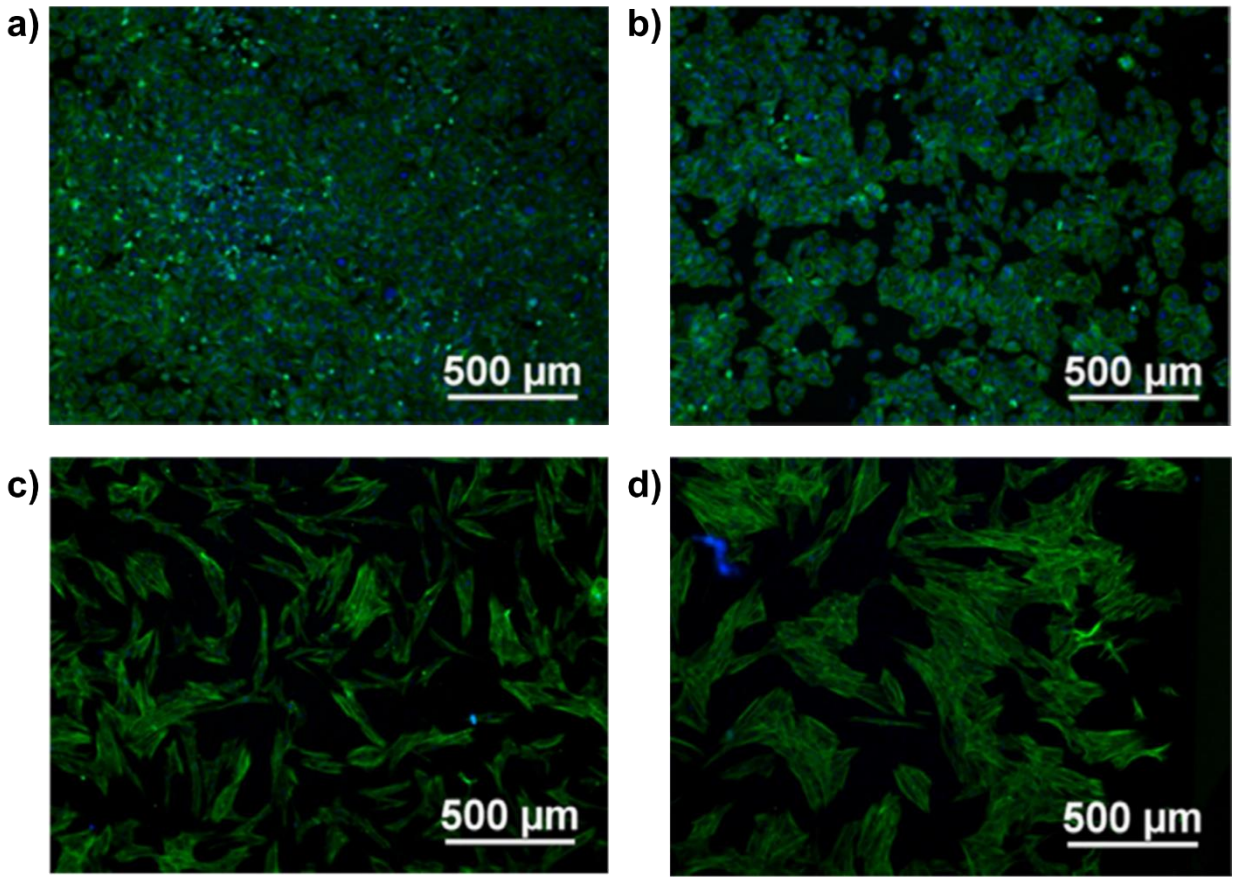

Figure 1.3. Optical images of human cells on graphene and SiO_2 substrate incubated for 48 hrs. Fluorescent optical images of human osteoblasts incubated on a) graphene substrate, and b) SiO_2 substrate, where the actin filaments are stained green and nuclei stained blue. Fluorescent optical images of human MSCs on c) graphene substrate, and d) SiO_2 substrate, where the actin filaments are stained green. The scale bar is 500 µm. Carbon N. Y. **2010**, 48 (15), 4323–4329

surface engineering of implants with MSCs, which is a major area of interest in bone reconstruction surgery.

The biocompatibility studies on graphene substrate showed that graphene provides a great platform for developing bio-interfaces with wide-ranging applications including implants. In case of neural

implants, graphene has especially shown to be beneficial due to its exceptional electrical, electrochemical and mechanical properties. In recent years, research focused on incorporating graphene in neural interfaces has increased tremendously. In 2011, Park et al(Park et al. 2011) utilized CVD grown graphene to grow human neural stem cells (hNSCs) and direct their differentiation towards neurons (Figure 1.4). Previous studies had shown that hNSCs differentiated more towards glial cells rather than neurons, in the absence of co-cultures and biochemical motifs. Such directed differentiation towards neurons would be beneficial for utilizing hNSCs for brain repair and neural regeneration.

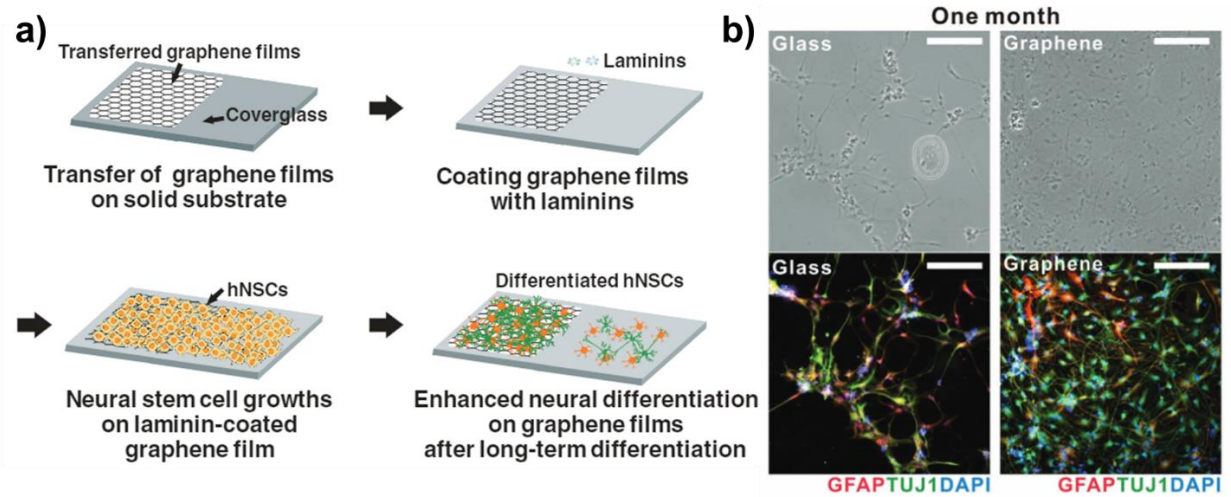

Figure 1.4. Growth and differentiation of human neural stem cells (hNSCs). a) Schematic showing the proliferation of hNSCs on graphene and glass substrates. CVD grown graphene was transferred to a cover glass and then coated with laminins (both graphene and glass regions) to promote hNSC attachment. The substrates were then incubated with hNSc and allowed to grow and differentiate (~1 month). b) Optical images (top) hNSCs on glass and graphene after 1 month of differentiation. The fluorescence images of these systems are also shown (below). The cells were stained with GFAP (red) for glial cells, TUJ1 (green) for neurons and DAPI (blue) for nuclei. The images show that the hNSCs adhered more to graphene than to glass. Also, the growth of neurons is more pronounced on graphene substrate. The scale bar is 200 μm. *Adv. Mater.* **2011**, *23* (36), H263–H267

Furthermore, with the intent to develop electrically functional implants, Fabbro et al.(Fabbro et al. 2016) incorporated electrically active graphene based substrates (GBSs) towards neuronal growth and development of neural interfaces. Although previous studies(N. Li et al. 2011) involving peptide coated graphene exhibited a neuro compatible substrate leading to improved neural growth, the peptide coating could potentially lead to weaker neuron/interface electrical contacts, altering the charge transfer properties. Uncoated GBSs produced *via* liquid phase exfoliation (LPE) promoted efficient cell adhesion with unaltered neuronal signal properties. This study demonstrated the impact of graphene on neuronal electrophysiological behavior, indicating its biocompatibility and potential application in reliable neural implants.

1.4. Graphene Phononics

The properties of graphene have been extensively documented in literature and can be well characterized using Raman spectroscopy, as discussed earlier. The ultrasensitive nature of graphene as well as its high quantum capacitance makes it highly susceptible to doping. Graphene also exhibits strong phonon coupling with phononic energies which is extremely sensitive to its Fermi level(Das et al. 2008b; Basko, Piscanec, and Ferrari 2009). Further, graphene possesses a large interfacial area providing an ideal platform for attachment of biological cells with a wide spectrum of sizes(Nguyen and Berry 2012; Paulus et al. 2014). These properties are considered tremendously advantageous for various applications, especially in the biomedical field, and are discussed in detail below.

1.4.1. Quantum Capacitance

The dipole potential of any biomolecule interfaced with a monolayer graphene significantly influences its phononic properties.(Sreeprasad and Berry 2013; Geim and Novoselov 2007) When graphene interfaces with cells or biomolecules, the dipole originating from the interfaced biomolecule (or cell membrane) apply an electric field. (Deng et al. 2016) The large quantum capacitance of graphene makes it highly sensitive to doping (electron or hole carriers) by the dipole induced electric field,(Keisham et al. 2016, 2019) which significantly alters the vibrational energies of graphene.(Sreeprasad and Berry 2013; Sreeprasad et al. 2015; Geim and Novoselov 2007) The quantum capacitance of graphene is expressed as: $C_Q = \frac{4e^2\sqrt{\pi}}{h\vartheta_F}\sqrt{n}$, where e is the charge of an electron, h is the Planck's constant, ϑ_F is the Fermi velocity of the Dirac electron, and n is the total carrier concentration of graphene, including the intrinsic carrier concentration of graphene as well as the carrier concentration from the potential of the interfaced biomolecules.

1.4.2. Carrier Density and doping

The sensitivity of graphene phononics towards the interfaced biomolecules are directly translated to the change in carrier density of graphene. Further, any change in the chemical potential of the cell membrane or the components of the biofluids is amplified by the drastic change in graphene's carrier density, due to the confinement of charge carriers to graphene's monolayer 2-dimensional plane. These changes in the carrier density of graphene can be quantitatively monitored using Raman spectroscopy.(Malard et al. 2009; Andrea C. Ferrari and Basko 2013; Das et al. 2008b) Furthermore, the dopant concentration may be accurately measured due to the sensitive Raman peak positions changes(Das et al. 2008b): the G band position increases with both n or p-type of

doping, while the 2D band increases with p-doping and decreases with n-doping,(Andrea C. Ferrari 2007; A. C. Ferrari et al. 2006; Casiraghi et al. 2007; Ni et al. 2008) as shown in figure 1.5.

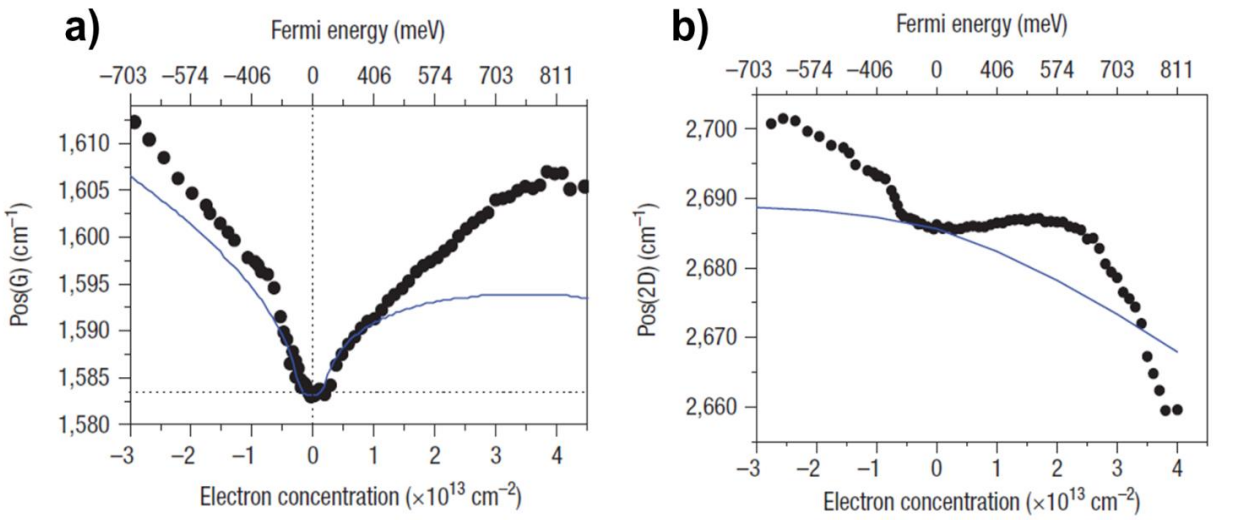

Figure 1.5. Correlation of carrier concentration of graphene with its Raman peak positions. a) Graphs showing the relation between G peak positions of graphene with its electron concentration (doping). b) Graphs showing the 2D peak positions of graphene as a function of its electron concentration (doping). The black dots represent the experimental data points and the blue line represents the theoretical adiabatic DFT calculations. Nat. Nanotechnol. **2008**, 3 (4), 210–215

The sensitivity of graphene has been widely utilized to develop graphene-based pH sensors, which is limited to only changes in the pH. However, biological systems are quite diverse with complex surface chemistries. Biological entities like cells, tissues and biofluids have unique chemical components with distinct dipole moments. When interfaced with graphene, these molecules exert a potential on the graphene lattice, specific to the interfaced biomolecule, as discussed earlier. The potential arising from the quantum coupling of the dipole moments of the biomolecules with graphene can be expressed as:

$$V_{potential} = \frac{\mu\rho\sin(45^o)}{4\varepsilon_o\pi}\left(4\left\{\sum_{i=1}\left(\sqrt{(i\times d)^2+(r)^2}\right)^{-2}\right\}+8\left\{\sum_{i=1}\left(\sqrt{\left(i\times d\sqrt{2}\right)^2+(r)^2}\right)^{-2}\right\}+4\left\{\sum_{i=1}\left(\sqrt{\left(i\times d\sqrt{5}\right)^2+(r)^2}\right)^{-2}\right\}+\{r^{-2}\}\right)$$

where ε_o is vacuum permittivity (8.85 x 10^{-12} F/m), r is the distance from the center biomolecule to the surface of graphene (~ 1 nm), $d = \sqrt{\frac{\sqrt{2}}{\rho}}$ is the distance of dipole of the biomolecule to the point of interest, i is the index (representing the distance of the dipole of the interfaced molecule and the point of interest), and r is vertical distance between the biomolecule to graphene surface (assume to be 1 nm).(Kim, Keisham, and Berry 2020; Keisham et al. 2019, 2016)

CHAPTER 2

2. Detection of Cancer Cell via Raman Mapping of Interfaced Graphene: Towards Non-Invasive Cancer Diagnostics

Previously published as Keisham, B.; Cole, A.; Nguyen, P.; Mehta, A.; Berry, V. Cancer Cell Hyperactivity and Membrane Dipolarity Monitoring via Raman Mapping of Interfaced Graphene: Towards Non-Invasive Cancer Diagnostics. *ACS Appl. Mater. Interfaces* 2016, 8, 48, 32717-32722

2.1. ABSTRACT

Ultra-sensitive detection, mapping and monitoring of the activity of cancer cells is critical for treatment evaluation and patient care. Here, we demonstrate that a cancer cell's glycolysis-induced hyperactivity and enhanced electronegative membrane (from sialic acid) can sensitively modify the second-order overtone of in-plane phonon vibration energies (2D) of interfaced graphene *via* a hole-doping mechanism. By leveraging ultrathin graphene's high quantum capacitance and responsive phononics, we sensitively differentiated the activity of interfaced Glioblastoma Multiforme (GBM) cells, a malignant brain tumor, from that of human astrocytes at a single-cell resolution. GBM cell's high surface electronegativity (potential ~310 mV) and hyperacidic-release induces hole-doping in graphene with a 3-fold higher 2D vibration energy shift of approximately 6±0.5 cm^{-1} than astrocytes. From molecular dipole induced quantum coupling, we estimate that the sialic acid density on the cell membrane increases from one molecule per ~17 nm^2 to one molecule per ~7 nm^2. Further, graphene phononic response also identified enhanced acidity of cancer cell's growth medium. Graphene's phonon-sensitive platform to determine interfaced cell's

activity/chemistry will potentially open avenues for studying activity of other cancer cell types, including metastatic tumors and characterizing different grades of their malignancy.

2.2. Introduction

Cancer is one of the leading causes of death worldwide, and its diagnosis is critical to initiate therapies(Siegel, Miller, and Jemal 2015). Successful cancer treatment relies on early detection at high sensitivity and specificity. Hence, it is imperative to develop sensitive detection technologies that can identify cancer at early stages.

Over the past couple of decades, research efforts have leveraged the sensitive quantum mechanical effects and high surface area to volume ratio of nanoparticle to develop several cancer detectors.(Perfézou, Turner, and Merkoçi 2012; Choi, Kwak, and Park 2010; Mansoori et al. 2007; M. Ferrari 2005) Some of the employed nanomaterials include gold nanoparticles,(Bhattacharyya et al. 2012; X. Huang and El-Sayed 2010; Cai et al. 2008) quantum dots,(Pericleous et al. 2012) and carbon nanotubes.(X. Yu et al. 2006) These sensors operate on the principle of optical, magnetic, mechanical, chemical and/or physical actuation at interfacing with cancer biomarkers.

Similarly, Raman spectroscopy (or surface enhanced Raman spectroscopy) and other spectroscopy methods have been used for determining the chemical fingerprints of cancer biomarkers to differentiate normal and cancerous cells(Vendrell et al. 2013). They can also provide information on the chemistry of the cell membrane molecules. However, such spectroscopic techniques generally do not provide information about the activity of the cell or its effect on its local environment. There is a critical need of a sensitive platform, which can detect, differentiate, and quantify such cell activity. Here, we measure the change in the frequency of one of graphene's

prominent Raman peaks upon interfacing of a single cell to determine if the cell is hyperactive. Graphene – a planar sheet of sp^2 hybridized carbon atoms arranged in a honeycomb lattice(Schedin et al. 2007; Mohanty and Berry 2008; Mohanty et al. 2011; X. Wang, Zhi, and Müllen 2008; Pumera 2011) – possesses superior properties(Sreeprasad and Berry 2013; Palermo 2013; Geim 2009; Geim and Novoselov 2007) to enable this application: (a) graphene is the thinnest material (~0.3 nm, vibration modes are active), (b) high quantum capacitance (highly sensitive to doping), (c) high carrier-phonon coupling with phononic energies sensitive to its Fermi level(Das et al. 2008b; Basko, Piscanec, and Ferrari 2009), and (d) a large interfacial area, providing an ideal platform for cell attachment(Nguyen and Berry 2012; Paulus et al. 2014). When the cell interfaces with graphene, the molecular dipoles on the membrane apply an electric field(Deng et al. 2016), which sensitively changes the charge-carrier concentration of graphene due to its large quantum capacitance. Further, the cell also injects ions to the membrane, which can gate graphene. The carrier doping modifies Graphene's Raman peak frequencies, which can be recorded at high spectral, spatial, and temporal resolution. Since the cell's activity is manifested in its membrane chemistry and ion-exchange, the Raman imaging provides the level of activity and chemical density. Based on this principle, we have developed a facile, non-invasive, Raman-based early-stage cancer diagnostic device. It is important to note that graphene-based electronic sensors for cells do not provide spatially resolved activity of the cell. Also, graphene oxide which comprises of heavy lattice disorders and oxygen functional groups(Dreyer et al. 2010; Sreeprasad and Berry 2013), do not provide a sensitive Raman detection platform due to the lack of clarity of Raman peaks. The detection study here was methodically conducted for cultured Glioblastoma Multiforme (GBM) cells immobilized on graphene substrate. GBM, WHO Grade IV malignant

astrocytomas, are the most aggressive and common malignant tumor with a poor prognosis of approximately 14 months(Holland 2000; Mehta et al. 2015). Human astrocytes (normal) were cultured and utilized as a control.

2.3. Experimental Methods

2.3.1. Cell preparation

For this study, the U138 human Glioblastoma Multiforme (GBM) and normal human astrocyte (NHA, Lonza Inc.) cell lines were used. Cells were grown in flasks under aseptic conditions, maintained at 37°C with a 5% CO_2 humidified atmosphere. Media used in this study was Gibco's DMEM media without phenol red and supplemented with 10% fetal bovine serum (FBS) and 1% penicillin/streptomycin. This media formulation is required to both ensure proper growth of the cells, and to prevent unwanted interference with Raman spectroscopy upon analysis due to the aromaticity of phenol red.

During the preparation of each cell sample, attached cells were checked for confluence and contamination under a light microscope. Old media was aspirated using a vacuum apparatus, and 10mL of phosphate buffered saline (PBS) was added to flask followed by vacuum aspiration. Subsequently, 1-2mL of Trypsin was added to the flask with gentle agitation and incubated until cells were fully detached (1-5 minutes). 10mL of fresh supplemented media was then added back to the flask and transferred to a conical tube. The cells were then centrifuged at 1000-1500RPM for 10 minutes and re-suspended in media. Total number of cells and percent viability were determined using a hemocytometer, to obtain a sample density between 10^4 - 10^6 cells.

2.3.2. Synthesis and transfer of graphene

A 25 μm thick 1 in x 3 in Cu foil (99.8%, Alfa-Aesar, annealed, uncoated) was pretreated in 1 M nitric and 3 M iron (III) nitrate for 10 min to remove the native copper oxide layer and the contaminants. After the Cu foil had been thoroughly rinsed with copious amount of DI water, it was immersed in a sonicating bath of Isopropyl alcohol (IPA) and acetone for 30 minutes.

Subsequently, the Cu foil was placed inside the standard 1-inch quartz tube of the home build LP-CVD system. The reaction chamber was evacuated to ~ 1.5 mTorr and flushed with 100 sccm of H_2 (99.9999% purity, Praxair) at total pressure of 650 mTorr for 20 minutes. Then, the temperature was increased to 1050ºC with the same H_2 condition for 35 minutes. The Cu foil was annealed at 1050ºC to increase the grainsize and to smoothen the surface. Afterwards, 10 sccm of CH_4 (99.999% purity, Praxair) at partial pressure of 100 mTorr was introduced into the tube for 10 seconds. Following CH_4 exposure, the reaction chamber was cooled down to room temperature in 40 minutes (25ºC/minutes).

Graphene (from CVD) was synthesized on both sides of the Cu foil. One side was spin coated with PMMA solution to mask the graphene while the other side was exposed to RIE to remove the graphene present there. The PMMA/graphene/Cu system was placed on dilute HNO_3 solution (1:3) for 1 hour, to etch away the Cu. The PMMA/Graphene system was then transferred to two consecutive DI water baths to remove any residual ions or impurities.

The PMMA-graphene system was scooped out from the water bath using a 1 cm x 1 cm SiO_2/Si chip (300 nm SiO_2). The SiO_2/Si chip was cleaned using Piranha solution and then washed with DI water, acetone and IPA, until the surface was clean. When the SiO_2/Si chip with PMMA-

Graphene was dry (~1 hour), it was heated to 160°C for 25 min and then transferred to acetone bath (~60°C, 5 min), to remove PMMA. The chip was then washed with IPA and blown dry with air.

2.3.3. Preparation of graphene-cells ensemble

Monolayer graphene was synthesized *via* chemical vapor deposition (CVD) process and transferred onto a SiO_2/Si chip (300nm SiO_2). The U138 human Glioblastoma Multiforme (GBM) and normal human astrocyte (NHA, Lonza) cell lines, employed in our study, were grown and later suspended in Dulbecco's Modified Eagle Medium (DMEM). To interface the cells with graphene, 3 drops of the cell suspension were deposited on the transferred graphene surface. The graphene/cell sample was capped using a cover slip to minimize the evaporation of the media. In order to allow the proper attachment of the cells on the surface, the sample was incubated at 37º C for 2 and half hours. Optical microscopy and Raman spectroscopy were employed to visualize and analyze the three samples (probed from the top) including: (1) monolayer graphene on SiO_2/Si substrate, (2) monolayer graphene with DMEM on SiO_2/Si substrate, and (3) monolayer graphene with cell/DMEM (GBM cell and astrocyte) on SiO_2/Si substrate.

2.3.4. Data analysis

The data for Raman spectroscopy was obtained using WITEC Raman Alpha 300-RA, with a laser excitation wavelength of 532 nm and an exposure time of ~5 min. The 100X objective was used to examine all the graphene samples (on air, with media and with media and cells). The spot size was determined using the equation:

$$Spot\ size = \frac{1.22\lambda}{NA}$$

Where, λ is the wavelength of the laser and NA is the numerical aperture.

Also, all the Raman spectra have been normalized to the intensity of G peak and the 2D Raman peaks have been custom fitted to Lorentzian curve fit.

2.4. Results and discussion

2.4.1. Cell adhesion

To interface the cell with the graphene, an aliquot of the cell culture suspension was placed on graphene/SiO_2 and incubated at 37º C for 1 to 3 hours. The cells showed strong adherence on the graphene surface when incubated for 2.5 hours. Cells adhered with 1.5-hour incubation time were susceptible to detachment when exposed to the Raman laser with power as low as 10 mW. Further, the cell growth medium plays an important role in the cell attachment process. When the cells were suspended in phosphate buffer solution (PBS), they exhibited poor adhesion to the graphene surface, even after 3 hours of incubation. The (DMEM) used here contains fetal bovine serum (FBS), which includes numerous growth factors and proteins that stimulate cell adhesion(Khan, Auner, and Newaz 2005). At the microscopic level, the spreading of the cell, which flattens it from the initial circular form is enabled by the polymerization of the cytoskeleton component, actin. Actin filaments act on the plasma membrane and its polymerization force pushes the membrane forward, allowing the cell to establish contact with the substrate(Fardin et al. 2010). Figure 2.1 depicts the representative micrograph of a well-adhered GBM cell and a less-adhered cell on the graphene-SiO_2 substrate. The cells that are not adhered and still suspended in medium look circular in shape. As the cell attaches to a surface, it flattens out and forms protrusions (and retractile regions)(Fardin et al. 2010).

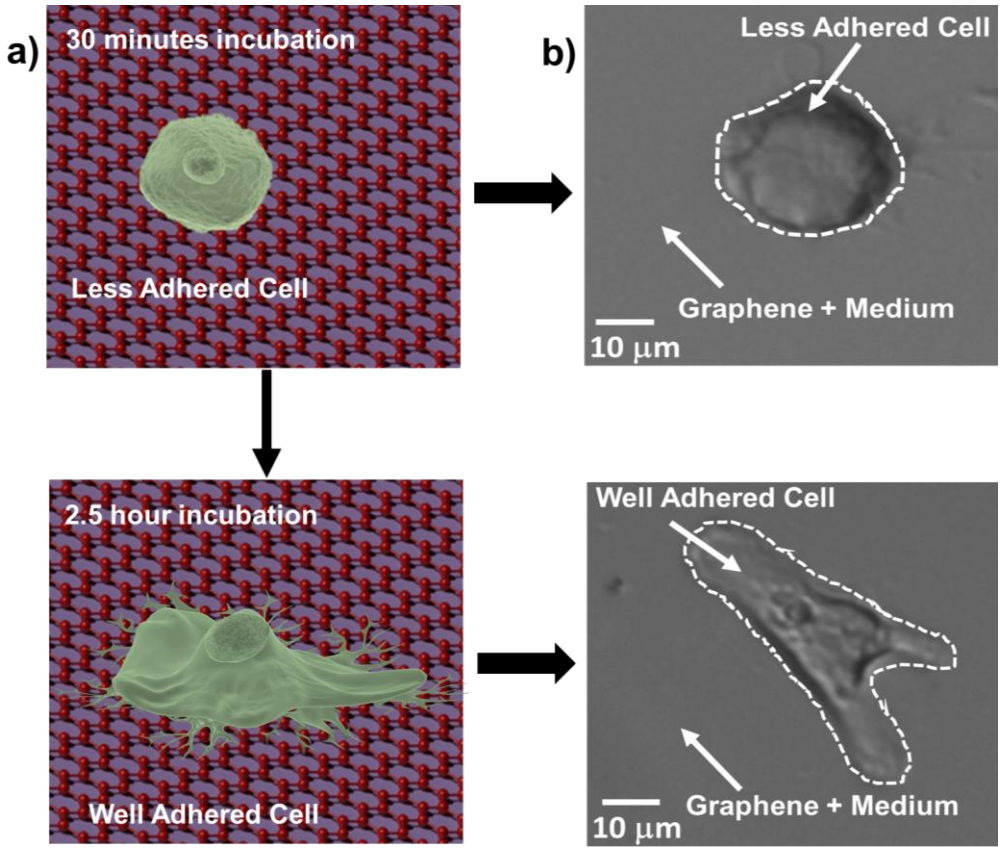

Figure 2.1. a) A representative model showing the cell attachment process on graphene. b) Optical images showing a less-adhered GBM cell and a well-adhered cell on graphene/SiO_2 surface. Scale bar 10 μm. ACS Appl. Mater. Interfaces 2016, 8 (48), 32717–32722

2.4.2. Mechanism

Since the sensor is based on cell activity, it is important to understand the biochemical activity of a normal and cancer cell. Cancer cells undergo anaerobic fermentation (not respiring), where the electron transport mechanism and oxygen-dependency for energy production are disrupted(Kato et al. 2013; Warburg 1956). This conversion of the primary mechanism for energy production results in excessive (~200 folds higher) accumulation of organic acids (*via* glycolysis) and pH modifications in cancerous cells and tissues, leading to an acidic microenvironment around the

cell(Griffiths 1991; Tannock and Rotin 1989; Haltiwanger 2010; Kato et al. 2013). Further, cancer cells have increased negative charges on the outer cell coat (glycocalyx) which are due to the presence of sialic acid residues making them more electronegative than normal cells(Haltiwanger 2010). The increased acidic efflux from the cell [H^+] onto the graphene surface(Kiani et al. 2013; Paulus et al. 2014) and the heightened negative charge on the cell surface, [E] induces p-doping on graphene's surface(Nguyen et al. 2013; Nguyen and Berry 2012) (consistent with the observation). Further, these cells can infiltrate the nearby tissues and change their micro-environment(Holland 2000). This property might be leveraged to study the body fluids, including blood and cerebrospinal fluid, and its potential application in cancer diagnostics.

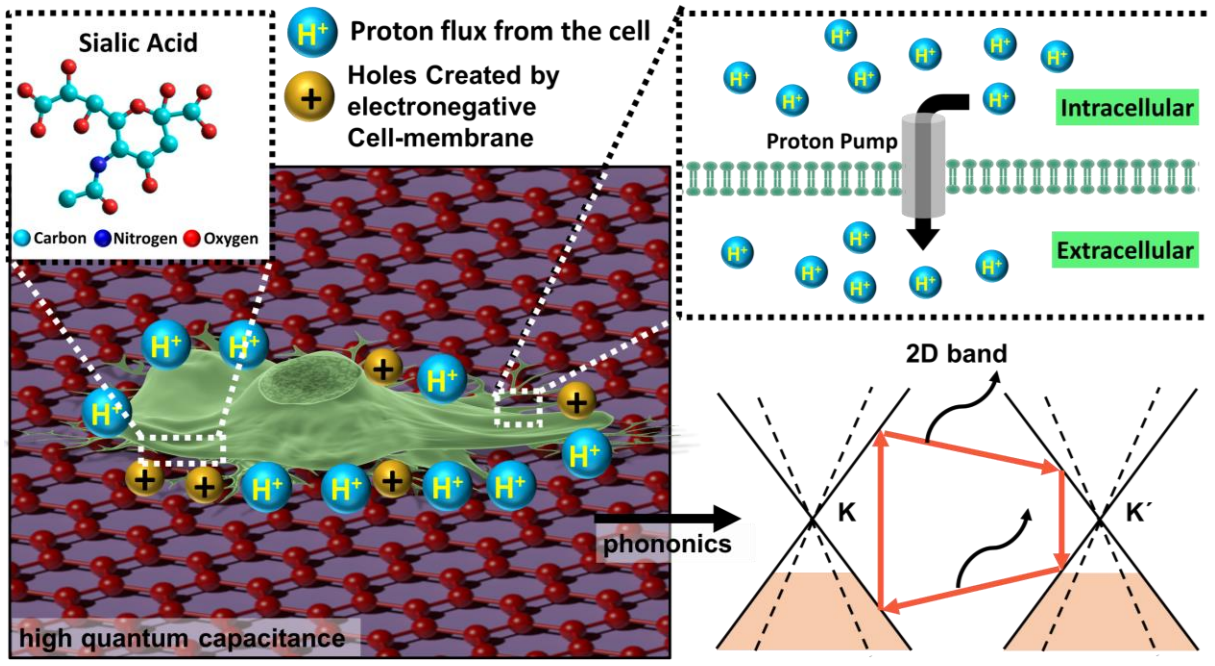

Figure 2.2. Schematic depicting the doping mechanism of graphene by a well-attached GBM cell and the resultant modification of phonon dispersion in 2D peak. Doping influences the electronic bands of graphene (solid lines) to become flatter compared to the intrinsic one (dashed lines). ACS Appl. Mater. Interfaces 2016, 8 (48), 32717–32722

The p-doping on graphene affects the resonance condition of the 2D phonons causing the renormalization of the electronic band, as shown in Figure 2.2. The absolute electron energies reduce and the electronic bands are pushed further away from the K and K' points, decreasing the lifetime of the excited quasiparticles and phonon momentum(Y. Li 2014). This abnormal phonon dispersion process results in an increase in the 2D mode Raman shift caused by 2D Raman scattering involving phonons of higher energies.

2.4.3. Raman spectroscopy

The CVD graphene was characterized using Raman Spectroscopy and its Raman spectra is represented by three characteristic Raman bands, a small D-band peak around 1350 cm^{-1}, a G-band peak near 1580-1590 cm^{-1} (corresponding to the in-plane vibration mode) and a 2D-band peak between 2600-2700 cm^{-1} (second order overtone of in-plane vibration)(A. C. Ferrari et al. 2006), depending on the energy of the excitation laser (D and 2D peaks). These three primary peaks are associated with phonon vibrational modes in graphene(A. C. Ferrari et al. 2006; Malard et al. 2009; Andrea C. Ferrari 2007; Andrea C. Ferrari and Basko 2013), and are sensitive to the electronic, structural and interfacial properties of graphene.

Das *et al*(Das et al. 2008b) quantitatively correlated the concentration of injected carriers in graphene (dopants/cm^2) to the Raman peak positions by monitoring the amount of charge carriers at various gate voltages. The position of G peak increases with the addition of either electrons or holes, however the 2D peak position responds differently to holes and electrons: increases with p-doping and decreases with n-doping(Casiraghi 2009; Das et al. 2008b; Basko, Piscanec, and Ferrari 2009). Thus, 2D band provides a comprehensive information on the polarity and density of charge carriers in graphene, while the G band only provides the carrier density. Also, it is well-known that graphene exhibits Kohn anomaly for the Raman-active E_{2g} Γ phonon (G band)(Andrea C. Ferrari and Basko 2013; Malard et al. 2009; Andrea C. Ferrari 2007; A. C. Ferrari et al. 2006). Upon extensive doping, this abnormal phonon dispersion behavior (Kohn anomaly) is removed non-adiabatically (beyond the adiabatic Born-Oppenheimer approximation) from the Γ point which leads to stiffening of G peak and saturation (at high doping level)(Pisana et al. 2007; Lazzeri and Mauri 2006; Das et al. 2008b; Casiraghi 2009). However, the 2D position is not restricted by

the carrier concentration level as the 2D phonons are not influenced by the non-adiabatic effects. Therefore, the 2D peak position analysis was used in this work.

The doping activity of the interfaced GBM cells and astrocytes (Lonza) on the graphene platform was analyzed using Raman spectroscopy. A typical cell is 40 – 50 μm in size and can be probed with a diffraction-limited spatial resolution of 300 nm Raman spot size (area of 0.7 μm^2). Figure 2.3a shows the 2D band Raman spectra of the bare graphene exposed to air (black), graphene interfaced with Astrocyte covered in medium (blue) and graphene interfaced with the GBM cell covered in medium (red). The GBM cells exhibit a large blue shift in the 2D peak position (~6.3 cm^{-1}), indicating a high degree of p-doping in graphene and a significant decrease in 2D signal intensity. On the other hand, the astrocyte cells (control, Lonza Inc.) show a weaker p-doping on graphene (2D band blue shifts by ~2.3 cm^{-1}) and lower reduction in the 2D intensity. Further, the graphene under the cell is more doped than that just outside the cell's periphery. The overall effective doping outside the GBM cell's boundary is higher than in pure graphene, and lower than that for graphene interfaced with cell. This is apparent in the spatial plot of 2D peak position, which maps the footprint of the cell (inset of figure 2.3a). Since, the GBM cancer cells exhibit enhanced $[H^+]$ diffusion from the cell and an increased surface electronegativity in comparison to the astrocytes, this confirms that graphene's 2D phonon vibration mechanism is sensitive to the difference in the activity levels of interfaced astrocytes and GBM cells. Further, the results also show that [H+] can diffuse from the cell into the medium, which can then dope graphene. The doping induced shift in graphene's G band peak-position is also consistent with the observations

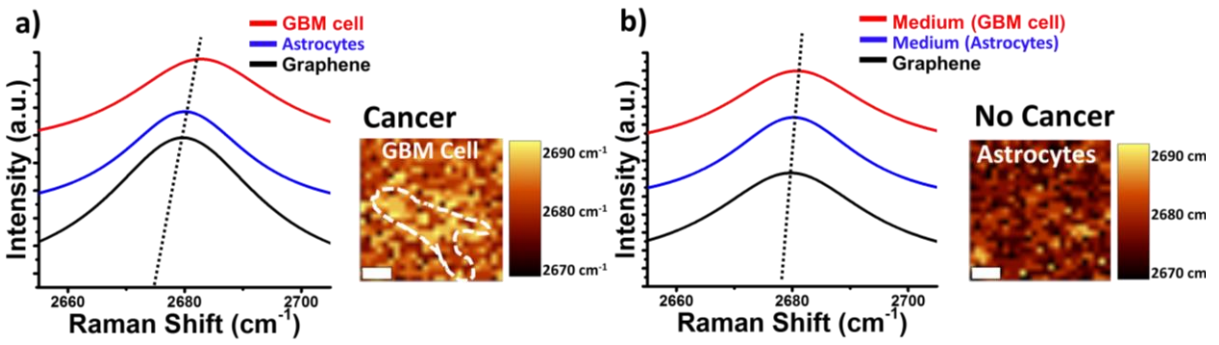

Figure 2.3. a) Raman spectra showing the 2D peak positions of graphene interfaced with air (black), Astrocyte (blue) and GBM cell (red) covered in medium. (Inset) 2D position mapping of GBM cell, scale 10 μm. b) Raman spectra showing the 2D peak positions of graphene interfaced with air (black), cellular growth medium influenced by Astrocyte (blue) and GBM cell (red). (Inset) 2D position mapping of Astrocyte, scale 10 μm. All the Raman spectra have been normalized to the intensity of G peak. ACS Appl. Mater. Interfaces 2016, 8 (48), 32717–32722

mentioned above.

As mentioned above, the cells decrease the pH of the surrounding medium environment by releasing acidic biomolecules. The modified acidity of the medium in turn p-dopes graphene(Voggu et al. 2008; Riveragil et al. 2013; Jiang et al. 2013; Wu et al. 2015). Since enhanced glycolysis in GBM cells must cause more [H^+] release than in astrocytes, to confirm increased GBM activity, we compared the media of the cells. Figure 2.3b shows the 2D peak positions of graphene in air (black), graphene covered in cellular growth medium acidified by an astrocyte (blue) (blue shift ~0.5 cm^{-1}) and that acidified by a GBM cell (red) (blue shift ~ 1.3 cm^{-1}). To minimize the doping effects from the cell, the Raman spectra for graphene-in-medium was acquired from an area > 100 μm away from the cells. Higher 2D peak-shift for GBM's media confirmed enhanced [H^+] release. Further, pure medium when interfaced with graphene caused reduction of p-doping in graphene.

2.4.4. Determination of surface potential

Graphene's surface is ultrasensitive to the interfacial attachment, which can dope graphene and modify its phononic (Raman) properties. The sensitive doping is a consequence of graphene's high quantum capacitance given by (for monolayer)

$$C_Q = \frac{4e^2\sqrt{\pi}}{h\vartheta_F}\sqrt{n_R},$$

where e is the electron charge, h is Planck's constant, ϑ_F is the Fermi velocity of the Dirac electron, and n_R is the total carrier concentration of graphene(Xia et al. 2009).

In the present case, the total carrier concentration of graphene (n_R) is a combination of intrinsic carrier concentration of graphene (n_G), the [H^+] doping on graphene sheet from the cell ($n_{[H^+]}$), and the induced carrier doping *via* the electronegative cell membrane ($n_{[E]}$):

$$n_R = n_{[H^+]} + n_{[E]} + n_G.$$

The quantum coupling of the interfacial sialic acid molecules with graphene enhances the effective electric field due to its dipole moment(Ang et al. 2008; Olson et al. 2015; Xia et al. 2009; Nguyen et al. 2013). The effective cell potential doping graphene ($V_{\lfloor G \rfloor}$) can be estimated by the following expression:

$$V_{\lfloor G \rfloor} = \frac{e.n_R}{C_Q}.$$

Further, the effective potential (cellular potential, $V_{\lfloor G \rfloor}$) is the total contribution of (1) the cell-membrane's dipole potential ($V_{\lfloor Cell \rfloor}$), and (2) the [H^+] absorbed on graphene (proton potential, $V_{\lfloor Proton \rfloor}$). The contribution of proton potential towards the total cellular potential is only 10 %

(Table I), while a dominant role is played by the cellular membrane's dipole potential in the change of graphene's Fermi level. For calculations, this cellular membrane's dipole potential is assumed to originate from the coverage of sialic acid molecules with a dipole moment of 2.5 Debye.

From the calculations, the estimated density of sialic acid molecules on GBM cell, and Astrocyte are 0.15 nm^{-2} (~ 1 per 7 nm^2) and 0.06 nm^{-2} (~ 1 per 17 nm^2) respectively. Consequently, the effective potential of GBM on graphene are estimated to be two-folds higher than those of Astrocyte (Table 1). These values are in agreement with typical voltage difference of cells across membranes, 10-100 mV("Nerve Cells" 2003).

Table I. Summary of the doping effects of various chemical environments and potential values associated with GBM cells as well as the Astrocytes.

Doping type	Chemical system	Doping ($\times 10^{12}$ cm^{-2})	Cellular Potential, mV ($V_{\lfloor G \rfloor}$)	Proton potential, mV($V_{\lfloor Proton \rfloor}$)
n	Medium influenced by Astrocytes	-1.00		
p	Medium influenced by GBM	5.56		

p	Astrocytes	7.24	114-172	12.3-17.5
p	GBM cells	23.4	222-310	38.8-78.9

2.5. Conclusion

In conclusion, graphene's ultrasensitive second-order-overtone of in-plane phonon vibration makes it ideal for spatially resolved (0.7 μm^2) detection of the activity of a single cancer cell. The cell potential of GBM cells (range: 222 – 310 mV) was found to be significantly higher than that of astrocytes (114 – 172 mV). This is attributed to the estimated ~2.5 folds higher density of sialic acid in GBM cell membrane. Further, the higher influence of the GBM cell's glycolysis-induced hyperactivity on the medium (by 2.2 to 6.4 folds) was also confirmed. Futuristically, this phonon-energy-sensitivity can be extended to other cancer cells, tissues and in-vivo samples to spatially map, study or detect cell activity

CHAPTER 3

3. Graphene Phononics Based Sensing Platform for Studying Neurodegenerative Diseases

Previously published as Keisham, B.; Seksenyan, A.; Denyer, S.; Kheirkhah, P.; Arnone, G. D.; Avalos, P.; Bhimani, A. D.; Svendsen, C.; Berry, V.; Mehta, A. I. Quantum Capacitance Based Amplified Graphene Phononics for Studying Neurodegenerative Diseases. *ACS Appl. Mater. Interfaces* **2019**, *11* (1), 169–175.

3.1. ABSTRACT:

Amyotrophic lateral sclerosis (ALS) is the most common adult-onset motor neuron disease, characterized by a rapid loss of upper and lower motor-neurons resulting in patient death from respiratory failure within 3-5 years of initial symptoms onset. Although at least 30 genes of major effect have been reported, the pathobiology of ALS is not well understood. Compounding this is the lack of a reliable laboratory test which can accurately diagnose this rapidly deteriorating disease. Herein, we report on graphene's phonon vibration-energies as a sensitive measure of the composite dipole moment of the components of the interfaced cerebrospinal fluid (CSF) to specifically identify patients with ALS disease. The second-order overtone of in-plane phonon vibration energy (2D) of graphene shifts by 3.2±0.5 cm^{-1} for all ALS patients studied in this work. Further, the amount of *n*-doping induced shift in phonon energy of graphene, interfaced with CSF, is specific to the investigated neurodegenerative disease (ALS, Multiple Sclerosis and Motor Neuron Disease). By removing a severe roadblock in disease detection, this technology can be applied to study diagnostic biomarkers for researchers developing therapeutics and clinicians initiating treatments for neurodegenerative diseases.

3.2. Introduction

Amyotrophic lateral sclerosis (ALS) is an adult onset neurodegenerative disease characterized by rapid loss of motor neurons controlling skeletal muscles.(Talbott, Malek, and Lacomis 2016) The pathological and molecular features of ALS include mitochondrial dysfunction, increased oxidative stress, detrimental immune activation and break down of the blood brain barrier.(van Es et al. 2017; Bozzo et al. 2017) These pathological mechanisms have been previously shown to be reflected in the cerebrospinal fluid (CSF) of both human patients and in animal models of ALS.(Gray et al. 2015; Dodge et al. 2013) Although, proteomic and genomic studies of CSF from ALS patients have shown unique differences reflecting the disease pathophysiology, currently there are no reliable biomarkers which can accurately diagnose and monitor the progression of this rapidly deteriorating disease.(Chiò and Traynor 2015; Tarasiuk et al. 2012) Moreover, patients with monomelic amyotrophy, primary lateral sclerosis and cervical myelopathy are sometimes misdiagnosed as having ALS and vice versa. Although, these diseases manifest with similar clinical motor neuron symptoms, ALS patients have a significantly different and more rapid disease course.(Bäumer, Talbot, and Turner 2014; Turner and Benatar 2015; Staff and Appel 2016) Given the clinical heterogeneity of ALS, having a disease biomarker will be important for clinicians initiating treatments and basic scientists studying the pathophysiology of the disease. More importantly, a biomarker will be of utmost importance in helping with patient selection when designing therapeutic clinical trials.

Graphene, a two-dimensional (2D) sheet with a honeycomb lattice comprising of sp^2 hybridized carbon atoms,(Schedin et al. 2007; Mohanty and Berry 2008; Mohanty et al. 2011; X. Wang, Zhi, and Müllen 2008; Pumera 2011) possesses an ultrasensitive surface with a detection resolution of

a single molecule.(Geim and Novoselov 2007; Y. Wang et al. 2011) The phononic properties of the single-atom-thick graphene are influenced by the dipole potential of any biomaterial or biomolecule interfaced on its surface.(Sreeprasad and Berry 2013; Geim and Novoselov 2007) When graphene comes in contact with the molecules within the CSF, the dipole of the interfaced molecules induce an electric field.(Deng et al. 2016) Due to graphene's large quantum capacitance (sensitivity to be doped by an electric field), the dipolar field from the expressed molecular species dopes graphene with electron or hole carriers.(Keisham et al. 2016) This altered density-of-states affects the vibrational energies of graphene,(Sreeprasad and Berry 2013; Sreeprasad et al. 2015; Geim and Novoselov 2007) which can be mapped using Raman spectroscopy.(Malard et al. 2009; Andrea C. Ferrari and Basko 2013) It has been previously established that the Raman peak positions of graphene changes with the concentration of carriers injected in the lattice.(Das et al. 2008b) Specifically, the 2D peak position observed between 2600-2700 cm^{-1}, decreases with *n*-doping (electron) and increases with *p*-doping (hole) unlike the G peak, whose position increases with either type of doping (Kohn anomaly for Raman active G band).(Andrea C. Ferrari 2007; A. C. Ferrari et al. 2006; Casiraghi et al. 2007; Ni et al. 2008) Further, the G peak-position gets saturated with increasing doping since doping leads to the non-adiabatic removal of the G–phonon dispersion. Hence, 2D peak provides a comprehensive information regarding the polarity as well as the density of injected charge carriers.(Das et al. 2008b; Basko, Piscanec, and Ferrari 2009; Nguyen and Berry 2012) Further, it is important to note that the sensitive platform provided by graphene cannot be expected from graphene oxide, as the latter suffers from heavy and inconsistent lattice disorders, with relatively weak 2D Raman signals (prominent D and G peaks), due to the presence of many defects and oxygen functional groups(Eda, Fanchini, and Chhowalla 2008;

Nguyen et al. 2013; Pope and Aksay 2015; Akhavan 2015; Voiry et al. 2016).

Previously, we applied this ultrasensitive property of graphene to differentiate human glioma cells from human astrocytes.(Keisham et al. 2016) Extrapolating from these findings, we monitored the phononic properties of CSF-interfaced graphene to study the effectiveness of this tool in differentiating ALS from other neurodegenerative diseases.

3.3. Experimental Section

3.3.1. Rat CSF Samples.

Male transgenic rats were euthanized using ketamine/xylazine administered through an intraperitoneal injection. Once the animal lost response to stimuli, it was positioned prone and the head was flexed downward at approximately 45-degrees. A 25-gauge needle attached to a 1cc syringe was percutaneously introduced into the cisterna magna and approximately 50-100µl of CSF was collected. CSF was frozen on dry ice and kept at -80±10°C. Rats (ages 130+/-10 days) were defined to be "early symptomatic" when weakness was observed in locomotion and at "end point" (ages 170+/-20 days) when the animals were not able to right themselves in less than 30 seconds when placed on their side.

3.3.2. Interfacing CSF Samples with Graphene and Analysis

Post-mortem human CSF samples were obtained from the Human Brain and Spinal Fluid Resource Center, which is sponsored by NINDS/NIMH, National Multiple Sclerosis Society and Department of Veterans Affairs. CSF samples were collected from patients with amyotrophic lateral sclerosis (ALS), Multiple Sclerosis (MS), Motor Neuron Diseases (MND) and Control subjects. The CSF was then interfaced with CVD produced graphene transferred onto SiO_2/Si substrate, with a cover slip on top to reduce evaporation. The graphene-CSF system was then

characterized using Raman Spectroscopy, with a laser wavelength of 532 nm. Similar protocol was followed for analyzing the CSF from $SOD1^{G93A}$ transgenic rat model of ALS, at 2 distinct disease stages- early symptomatic (ES) and end point (EP).

3.3.3. pH measurement. The pH of all the CSF samples were obtained using Oakton pH150.

3.3.4. Statistical Analysis. Student's t-test was performed throughout the study and a $p<0.05$ was used for statistical significance cutoff.

3.4. Results and Discussion

3.4.1. Doping effect of CSF on graphene.

We first tested whether human CSF (Figure 3.1a) will have any influence on the phononic properties of graphene. Using a previously published protocol from our own laboratory,(Keisham et al. 2016) graphene on SiO_2/Si substrate was interfaced with 30μL of CSF from postmortem control subjects (non-neurological causes of death) (Table II) and studied under Raman spectroscopy (area of analysis ~ 0.5 μm^2) (Figure 3.1b). We focused our spectral analysis on the second-order overtone of in-plane phonon vibration energies (2D peak) of graphene, as this peak has been previously established to be altered distinctly by the concentration of different carrier types injected in the lattice.(Das et al. 2008b) Relative to pristine graphene, we found that control CSF samples induced a slight, but significant, *n*-doping effect and a red shift of ~1.2-2.4 cm^{-1} in the 2D peak of the Raman spectra (Figure 3.1d). These results point to the existence of dopants in the control CSF. The presence of any dopants changes the properties of graphene, including the electrical and phononic attributes. Analyzing the electronic band structure of graphene is an effective approach to interpret the effects of doping,(Elias et al. 2011; Sasaki et al. 2012) which can be achieved by examining the shape of the Dirac cones of graphene.(Elias et al. 2011; M.

Huang et al. 2010) Graphene on SiO_2/Si is *p*-doped, which modifies the resonance conditions of the 2D phonons and hence renormalizing the electronic bands.(Y. Li 2014) This renormalization pushes the electronic bands away from the K and K' points (Figure 1c), thereby increasing the corresponding 2D mode energy. When the CSF is interfaced with graphene, it *n*-dopes the graphene lattice. The resulting *n*-doping renormalizes the electronic bands again, which in turn shifts them towards the K and K' points reducing the 2D energy (Figure 3.1c). These alterations in graphene phononics are an indication that components in the CSF cause meaningful and measurable changes, which can be monitored using Raman spectroscopy.

Table II. Demographic and clinical characteristics of subjects included in this study.

Sample	Age	Gender	Clinical Diagnosis	Neuropathological Diagnosis	Clinical and Pathological Features
Control	57	M	Heart Disease	n/a	Cytomegalovirus Inclusion Body Disease, Renal Failure
	59	M	Cancer (Esophageal)	n/a	n/a
	59	M	Pulmonary Embolism	Normal	Arthritis
	65	F	Cancer (Lung)	n/a	n/a
	72	M	Pulmonary Embolism	n/a	n/a

	84	F	Cancer (unknown)	n/a	n/a
	101	F	Cancer (colon)	n/a	Hypertension, Osteoporosis
ALS	32	M	Amyotrophic Lateral Sclerosis	Amyotrophic Lateral Sclerosis	n/a
	45	M	Amyotrophic Lateral Sclerosis	Amyotrophic Lateral Sclerosis	n/a
	50	M	Amyotrophic Lateral Sclerosis	Amyotrophic Lateral Sclerosis	Recent Hypoxic Changes in Cerebrum
	52	F	Amyotrophic Lateral Sclerosis	Clinical Diagnosis Only	n/a
	58	F	Amyotrophic Lateral Sclerosis	Amyotrophic Lateral Sclerosis	n/a
	58	M	Amyotrophic Lateral Sclerosis	Clinical Diagnosis Only	Depression
	66	F	Amyotrophic Lateral Sclerosis	Amyotrophic Lateral Sclerosis	Polyneuritis
	66	M	Amyotrophic Lateral	Amyotrophic	Cancer (unknown)

			Sclerosis	Lateral Sclerosis	
	68	M	Amyotrophic Lateral Sclerosis	Amyotrophic Lateral Sclerosis	n/a
	70	M	Amyotrophic Lateral Sclerosis	Amyotrophic Lateral Sclerosis	Diabetes Mellitus, Hypertension
	70	M	Amyotrophic Lateral Sclerosis	Amyotrophic Lateral Sclerosis	Recent Hypoxic Changes in Cerebrum
	74	F	Amyotrophic Lateral Sclerosis	Amyotrophic Lateral Sclerosis	n/a
	76	F	Amyotrophic Lateral Sclerosis	Amyotrophic Lateral Sclerosis	Moderate Cerebral Atherosclerosis
MS	64	F	Secondary Progressive Multiple Sclerosis (MS)	n/a	n/a
	79	F	Secondary Progressive Multiple Sclerosis (MS)	n/a	n/a
	81	M	Secondary Progressive	n/a	n/a

			Multiple Sclerosis (MS)		
MND	52	M	Motor Neuron Disease	n/a	n/a
	60	M	Motor Neuron Disease	n/a	Dementia
	67	M	Motor Neuron Disease	n/a	n/a

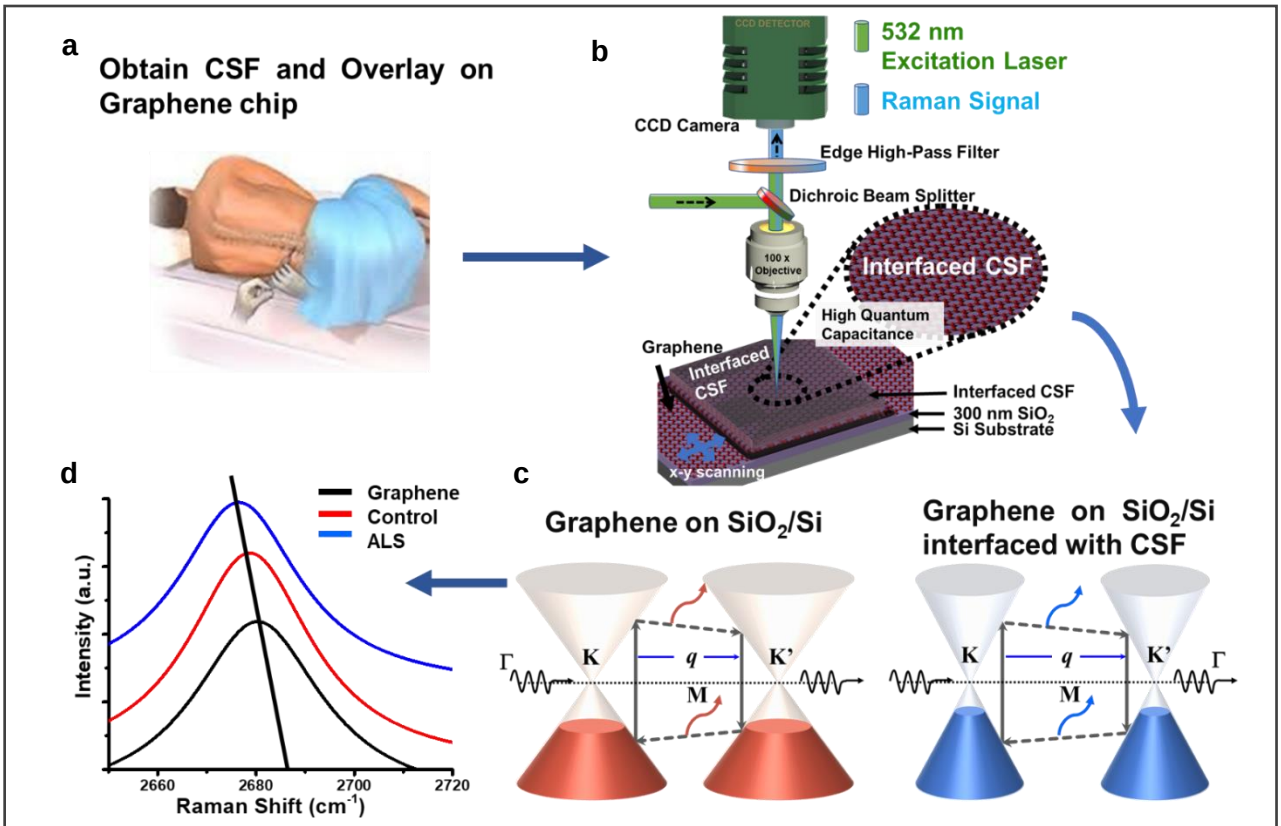

Figure 3.1. Interfaced CSF induces *n*-doping of graphene. (a) Graphic representation of obtaining CSF *via* lumbar puncture. **(b)** Schematic depicting the set-up of graphene-based detection of ALS using Raman spectroscopy. CSF's composite dipole moment coupled with the high quantum capacitance of graphene sensitively modify the 2D band phononics. **(c)** Graphical depiction of the Dirac energy barrier alterations in the presence of human CSF, with wave-vector q, Brillouin zone center Γ, M points in the middle of the hexagonal sides and K and K' points representing the corners of the hexagons. (**d**) Graphene's 2D Raman peak in the presence of control and ALS CSF samples. ACS Appl. Mater. Interfaces 2019, 11 (1), 169–175

3.4.2. Effects of CSFs from neurodegenerative diseases on graphene

Once we established that human CSF has detectable influence on the phononic properties of graphene, we investigated whether this measured effect can be used to distinguish ALS from other neurodegenerative diseases, namely multiple sclerosis (MS) and other motor neuron diseases (MND). Even though these diseases affect the central nervous system (CNS), the driving pathological processes are widely different.(Bäumer, Talbot, and Turner 2014) We hypothesized that the disease-specific components in the CSF will interact differently with graphene and therefore change its properties in a disease-specific manner.

We first tested postmortem CSF samples from 13 ALS patients, 11 of which had pathologically corroborating diagnosis of the disease in addition to the clinical findings (Table II). In these group of patients, we found the shift of the Raman 2D peak to be more pronounced (~3-3.5 cm^{-1}) (Figure 3.1d), indicating a higher *n*-doping of graphene. This difference between the controls and ALS patients is possibly related to the underlying neuroinflammation, metabolic alteration and increased production of reactive oxygen species (ROS) in ALS patients.(Bozzo et al. 2017; Al-Chalabi et al. 2016; D'Amico et al. 2013; Hooten et al. 2015) Subsequently, we tested 3 CSF samples from patients who were diagnosed with secondary progressive multiple sclerosis (MS) and 3 samples from MND patients, who had a form of motor neuron pathology that is not ALS. Interfacing the CSF of MS and MND patients demonstrated a marked difference in the extent of graphene doping compared to ALS and control samples (Figure 3.2a-c). These findings suggest that disease-related changes in the CSF have a pronounced effect on the doping of graphene and the degree of doping is related to the underlying disease. To rule out the possibility that these changes were mainly due to alterations in pH, since this has been previously shown to influence

the doping of graphene,(Paulus et al. 2014) we measured the pH of the pooled CSF samples. Interestingly, we found no significant correlation between pH and the amount of n-doping (Figure 3.2d). This argues for the hypothesis that other disease specific factors (cytokines, ROS, lipids) in the CSF, with different dipole moments, are the main reason for the observed differences among the disease group.

3.4.3. Monitoring the progression of ALS disease

The disease-specific effects on graphene's sensitive phonon vibration energies motivated us to investigate whether the alteration in the doping level of graphene changes with the disease course. For this purpose, we studied the CSF from $SOD1^{G93A}$ transgenic rat model generated by forced overexpression of the mutated human SOD1 protein.(Howland et al. 2002) The mutations in the SOD1 gene, specifically the G93A amino acid alteration, has been well established as one of the causes of ALS.(Bäumer, Talbot, and Turner 2014) Thus, overexpression of the mutated protein reproduces many of the pathological features of human ALS. More importantly, this rat model has been previously characterized and the clinical stages correlated with the neuropathological severity.(Thomsen et al. 2014) As such, this allowed us to test whether the measured doping in graphene from human CSF is also present in the rat and whether the amount of doping can be used to monitor the progression of the disease. The CSF samples from rats at the early symptomatic (ES) and the end point (EP) stages of the disease were tested. Crudely, the ES stage is comparable to the time point at which human patients generally first present to the clinic with neurological symptoms. Results from these experiments showed significantly enhanced doping in both animal groups, with the ES rats exhibiting a much higher shift in the vibrational energy of the 2D band of graphene (Figure 3.2e).

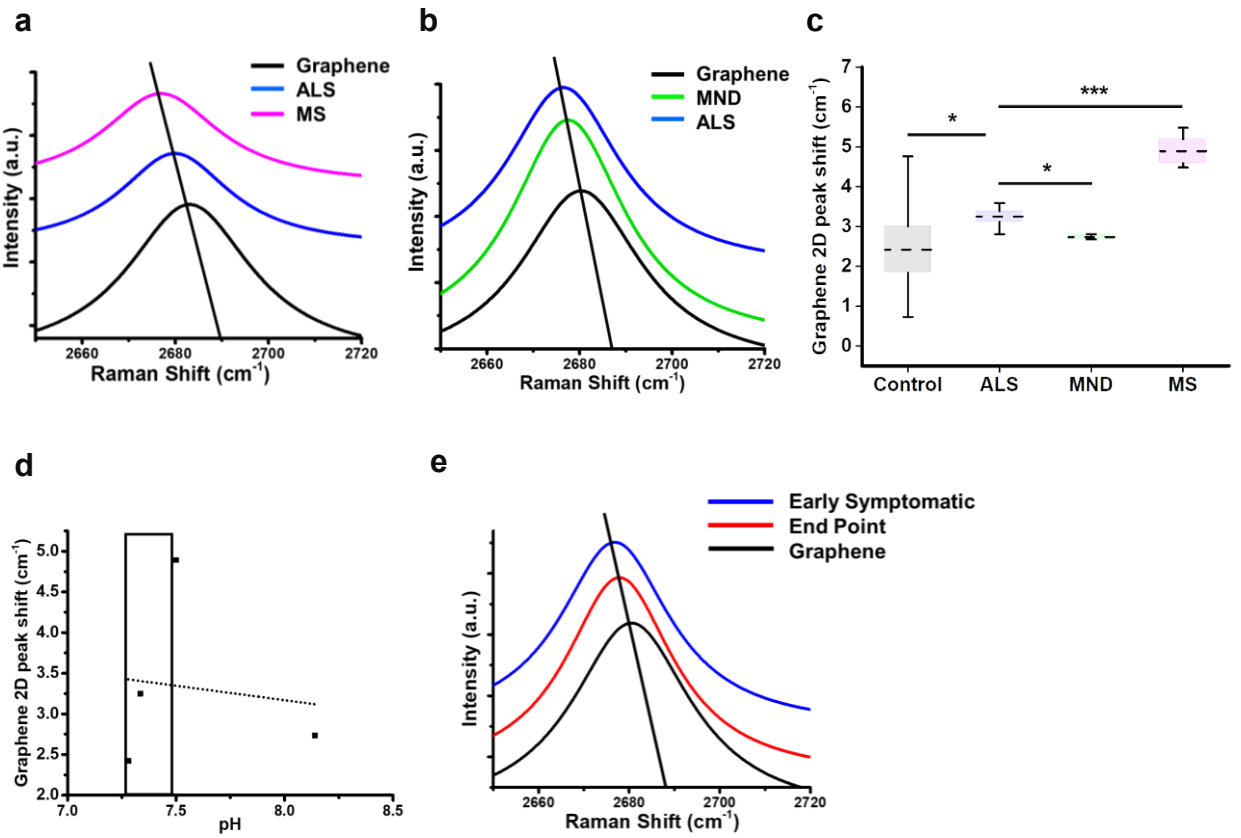

Figure 3.2. *n*-doping of graphene by CSF from neurodegenerative diseases. (a) Relative to ALS 2D peak changes of Multiple Sclerosis (MS) (n=3) and **(b)** Motor Neuron Disease (MND) (n=3). **(c)** quantification of 2D peak shift by human CSF samples. **(d)** Human CSF samples for each group was pooled and pH was measured, demonstrating no correlation between pH and 2D peak shifts (box indicates normal physiologic pH range). **(e)** $SOD1^{G93A}$ transgenic rat CSF samples taken at early symptomatic (n=2) and end point (n=4) subjected to Raman spectroscopy. Error bars, outliers; box, standard error of the mean; dashed line, mean; *P<0.05, **P<0.01, ***P<0.001, Student's t-test. ACS Appl. Mater. Interfaces **2019**, *11* (1), 169–175

3.4.4. Correlation of the age of ALS patients with varying levels of graphene's vibrational energies.

Our experimental results support the hypothesis that biological factors in the CSF have a direct influence on graphene-phononics and that any difference in their quantity can be detected by Raman spectroscopy. This motivated us to investigate whether there are any graphene doping differences among ALS patients and if such differences correlated with demographic parameters. We noticed that ALS patients clustered into two distinct groups based on age. Patients below the age of 55, interestingly this being the average age at diagnosis, had statistically higher 2D shifts compared to patients above the age of 55 (Figure 3.3a). It is well documented that patients diagnosed before the age of 55 generally have the familial form ALS, whereas the older patients tend to be more of the sporadic type. In support of this observation, 2 out of the 3 patients who had documented family history of ALS fell into the "younger" (<55 years of age) patient group whereas 3 out of 3 sporadic patients fell into the "older" (>55 years of age) group. Moreover, out of all the disease groups in our study, only ALS patients tended to have a positive correlation with age (Figure 3.3b). The other diseases displayed a negative correlation and the control samples had no correlation with age, suggesting that the biology of these different diseases is being captured by graphene and reflected in the alteration of its phononic properties.

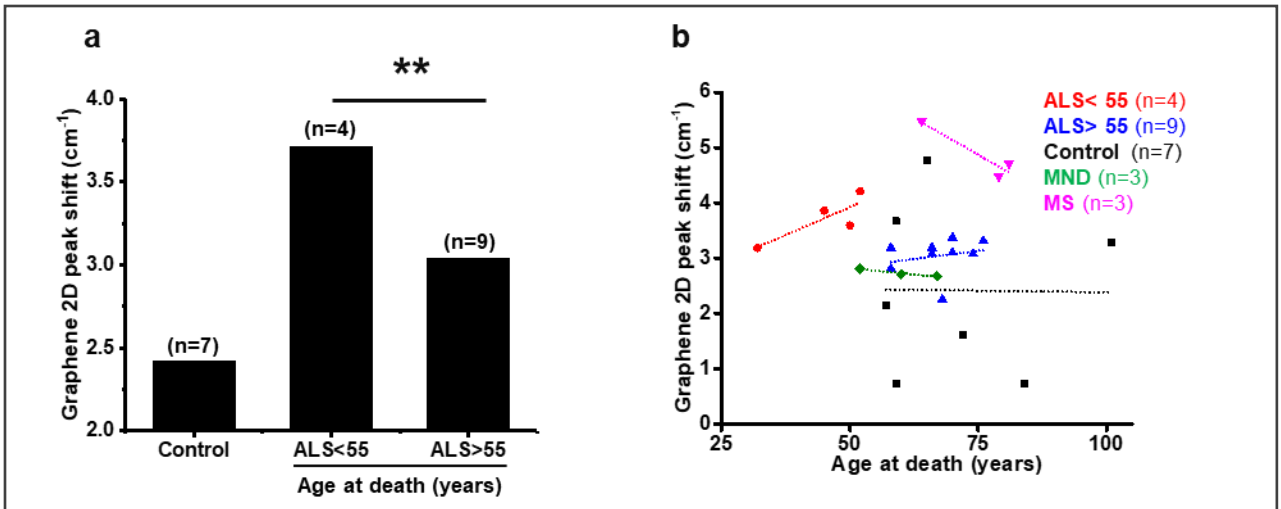

Figure 3.3. Age of ALS patients correlates with amount of graphene 2D peak shift. (a) The amount of 2D peak shift was compared among ALS patients after stratifying them into two age groups at the time of death (<55 years old (n=4) and >55years old (n=9), with 55 years of age being the average age of ALS diagnosis). Comparing these two ALS age groups gave a statistically significant difference with a *p*-value of 0.006. **(b)** The age at death of all the study samples was graphed against the amount of 2D peak shift to look for possible correlation between these two parameters. Both ALS age groups demonstrated a positive correlation with age (red and blue lines), while the other two diseases had a negative correlation (green and purple lines), and the control samples (black line) had no correlation with age. ACS Appl. Mater. Interfaces **2019**, *11* (1), 169–175

3.4.5. Modification of carrier density of graphene by interfaced CSF.

The ultrasensitivity of graphene to any kind of doping stems from its high quantum capacitance, given by $C_Q = \frac{4e^2\sqrt{\pi}}{h\vartheta_F}\sqrt{n_R}$, where e is the charge of electron, h is Planck's constant, ϑ_F is the Fermi

velocity of the Dirac electron, and n_R is the total carrier concentration of graphene.(Xia et al. 2009) The phononic properties of graphene modified by doping is monitored via Raman spectroscopy through which the carrier concentration of graphene can be determined.(Das et al. 2008b) Here, the intrinsic concentration of graphene and the carrier doping, via the components of CSF, comprise the total carrier concentration of graphene. Previous studies have demonstrated that the CSF of ALS and MS patients contain different concentration and types of secreted factors, such as cytokines, lipids and reactive oxygen species (Figure 3.4a). Therefore, we hypothesized that the dipole moment of these CSF factors will enhance the effective electrical field of graphene,(Xia et al. 2009; Nguyen et al. 2013; Ang et al. 2008; Olson et al. 2015) essentially doping the graphene lattice *via* quantum coupling and modifying its carrier concentration, in a disease specific manner. Calculating the total carrier concentration of CSF interfaced graphene demonstrated a clear distinction between ALS and the other diseases (Figure 3.4b). Similar calculations done on the rat CSF samples demonstrated a statistically significant difference (Figure 3.4c). Since the concentration of these proteins, lipids, nucleic acids and reactive oxygen species are also expected to be different in these diseases and vary across the graphene surface, a range of average dipole moments and density of these molecules were also calculated (Figure 3.4d). These results suggest that the change in the carrier concentration of graphene can be attributed to the varying dipole moments of the CSF components.

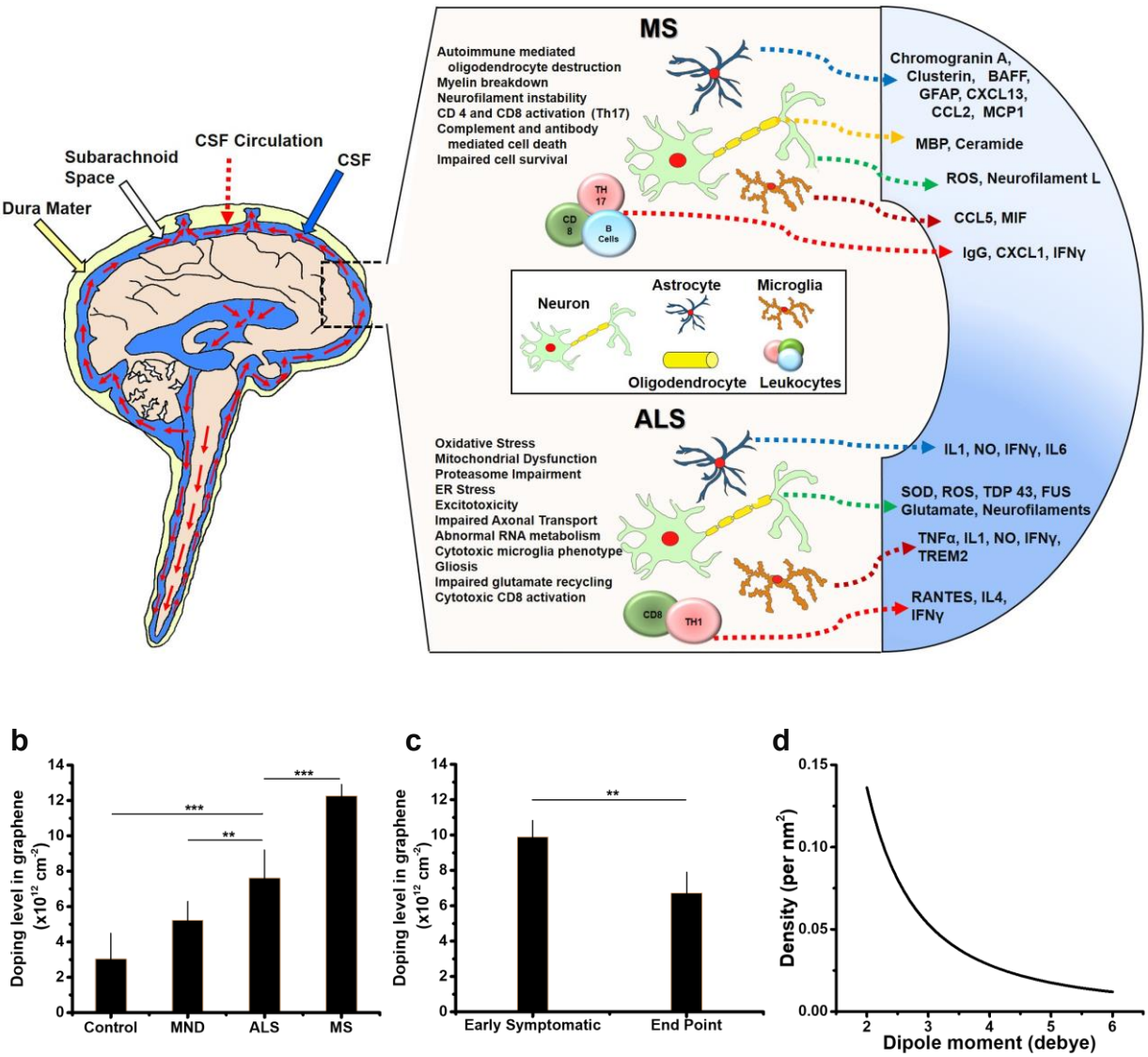

Figure 3.4. Carrier concentrations of graphene interfaced with CSF. **(a)** Flow of CSF in the central nervous system and the previously reported secreted factors found in the CSF of MS and ALS patients. **(b)** Calculated graphene carrier concentration in the presence of human and **(c)** $SOD1^{G93A}$ rat CSF samples. **(d)** Calculated average induced dipole moment of human ALS CSF samples. Error bar, standard error of the mean; *P<0.05, **P<0.01, ***P<0.001, Student's t-test. ACS Appl. Mater. Interfaces **2019**, *11* (1), 169–175

3.5. Conclusion

Development of a disease biomarker for ALS has been challenging.(Bäumer, Talbot, and Turner 2014; Turner and Benatar 2015) Various strategies, including mass spectroscopy and large-scale sequencing, have been employed with limited success thus far.(Turner and Benatar 2015) Here, the ultrasensitive property of graphene was used to study the CSF of ALS patients and disease controls as a novel approach to a possible disease biomarker. We found that the interaction of CSF with graphene causes significant changes in its vibrational energies which can be measured using Raman spectroscopy. Our findings of the measured differences between ALS and MND offer a unique strategy to developing a diagnostic biomarker that can be used to distinguish ALS from other forms of motor neuron diseases. Moreover, the differences in the density curves reflect the disease specific composition of the biomolecules, with varying dipole moments, found in each of the neurodegenerative diseases. These results indicate that graphene is able to sense even the slight variations of the concentration of biological species that are potentially contributing to the specificity of each disease. Even with the limited sample size, it is tempting to speculate that the alterations in graphene is a reflection of the underlying biology and that the amount of *n*-doping is potentially stratifying ALS patients into biologically distinct groups. In combination with the results from the rat studies, we believe these findings raise the exciting possibility that graphene can be eventually used to stratify ALS patients into distinct clinical and biological groups. These results can have profound clinical implications and applications.

In summary, we demonstrate a robust system to investigate ALS by using graphene. The second over-tone of in plane vibration of graphene provides an ultrasensitive platform to study the interface of CSF and graphene. It is important to note that this strategy does not analyze the Raman

signal of the CSF; rather it looks at the change in the Raman signal from interfaced graphene. Based on our analysis, it can be concluded that this ultrasensitive platform can efficaciously differentiate neurodegenerative diseases. Although the exact causes for these differences is beyond the scope of this study, we hypothesize that the composite effect of the inflammatory molecules, reactive oxygen species, and other bioactive substances that have been previously demonstrated in ALS, is the contributing factor for the measured changes in the properties of graphene.(Zhao et al. 2017) Further, monitoring the progression of ALS has always been challenging and understanding this process is critical in the fight against this disease. Our results from the $SOD1^{G93A}$ transgenic rat model argues for the ability to use the measured changes in the graphene's 2D peak to monitor the progression of the disease. These results suggest that our graphene platform cannot only be used to potentially diagnose ALS, but also to monitor its progression and in the future, to study the efficacy of therapeutics. A prospective study will be needed to test whether our findings correlate with more extensive clinical parameters and whether it can stratify patients into distinct subgroups, as suggested by Appel et.al.(Zhao et al. 2017) Even with the limitations of our study, the initial results offer an unprecedented phononic mechanism in graphene to study human CSF for diagnosis of neurodegenerative diseases.

CHAPTER 4

4. Graphene-Interface with Electrogenic Bacterial Membrane: Electron Transport and Energetics

4.1. ABSTRACT.

A synergistic, nanoscale electrical-interface with the membranes of exoelectrogenic microbes will have transformative impact on biological cell based electronic-devices. Here, we report that a conformal graphenic interface on biocatalytic *Geobacter sulfurreducens* membrane results in quantum-capacitance induced n-doping in graphene that further enhances electron shuttling from the membrane to improve electron harvesting from the electrogenic membrane. The quantum coupling of reduced graphene oxide (rGO) with the connected protein-membrane channels leads to an additional electron density of 3.44 x 10^{12} cm^{-2} and an increase in the in-plane phonon vibration energies (G) of rGO by 5 cm^{-1}. This n-doping enhances the electron transfer-rate from the cell membrane into the rGO improving the power density of a simplistic microbial fuel cell (MFC) by ~ 2 folds. The synergistic electron-harvesting and conformal membrane-interfacing of flexible 2D nanomaterials can lead to an evolution in the design of microbe-circuitry to power stand-alone nanodevices.

4.2. Introduction

Electrogenic bacteria are the central components of a microbial fuel cell (MFC) – a bio-electrochemical device, where bacteria oxidize substrates into electrons, which are transferred through an interfaced electrode towards the cathode to undergo a reduction reaction.**1–**(Bond and Lovley 2003) As opposed to a metallic catalyst in a conventional fuel cell, the anodic mechanism in a MFC is derived from biological activity within organisms catalyzing the electrochemical reaction. The removal of the metallic catalyst eliminates the fuel-impurity sensitivity of the conventional fuel cell, thus making MFCs more economically viable.(Blum, Marzari, and Car 2004; Holton and Stevenson 2013) The overall biochemical conversion of substrate to electrons has high stoichiometric quantum conversion (each molecule of acetate produces 8 electrons, $C_2H_3O_2^- + 2H_2O \rightarrow 2CO_2 + 7H^+ + 8e^-$; or 768,000 Coulombs per mole of oxidizing acetate).

While, several studies have focused on engineering the electrode-bacteria interface(Santoro, Kodali, et al. 2017) (even with reduced graphene oxide), there are limited studies on the influence of exoelectronic membrane on interfaced conductive nanomaterials and their electron harvesting properties. These studies are important since there is a significant loss of electrons transported from the cell membrane to the anode electrode, resulting in reduced electronic-current output.

Due to a unique combination of electronic and structural attributes, graphene, a planar sheet of sp^2 hybridized carbon atoms,(Schedin et al. 2007; Mohanty and Berry 2008; Mohanty et al. 2011; X. Wang, Zhi, and Müllen 2008) possesses numerous superior properties(Sreeprasad and Berry 2013; Geim and Novoselov 2007; Geim 2009) suitable for membrane interfacing for electron harvesting. Graphenic materials exhibit high conductivity (pristine graphene's carrier mobility can be as high as 200,000 $cm^2/V/s$) originating from the presence of π–orbitals atop its lattice

plane.(Meyer et al. 2007; Geim and Novoselov 2007) Graphenic sheets also possess a flexible and bendable carbon-carbon bond, enabling a conformal interface for soft biological cells.(Deng et al. 2016) Moreover, the effect of cellular interface on graphene's electronic structure is quantifiable. When a cell interfaces with graphene, it changes the carrier properties of graphene due to the dipolar-interaction with the cell wall,(Nguyen and Berry 2012; Keisham et al. 2016) which in turn is strongly coupled with its phononic properties, measurable via Raman spectroscopy. Graphene's high electron-conductivity at room temperature(Novoselov et al. 2004, 2005) and its ability to interfacially conform to a cell(Deng et al. 2016; Mohanty et al. 2011; Nguyen and Berry 2012) are leveraged here for studying electron-harvesting efficiency in the anodic section of a simplistic (without biofilm) MFC device. Also, graphene's large quantum capacitance will enable detailed analysis of the electron-doping process; and its phononic sensitivity(Das et al. 2008a; Keisham et al. 2016) will allow its interfacial characterization (Figure 4.1).

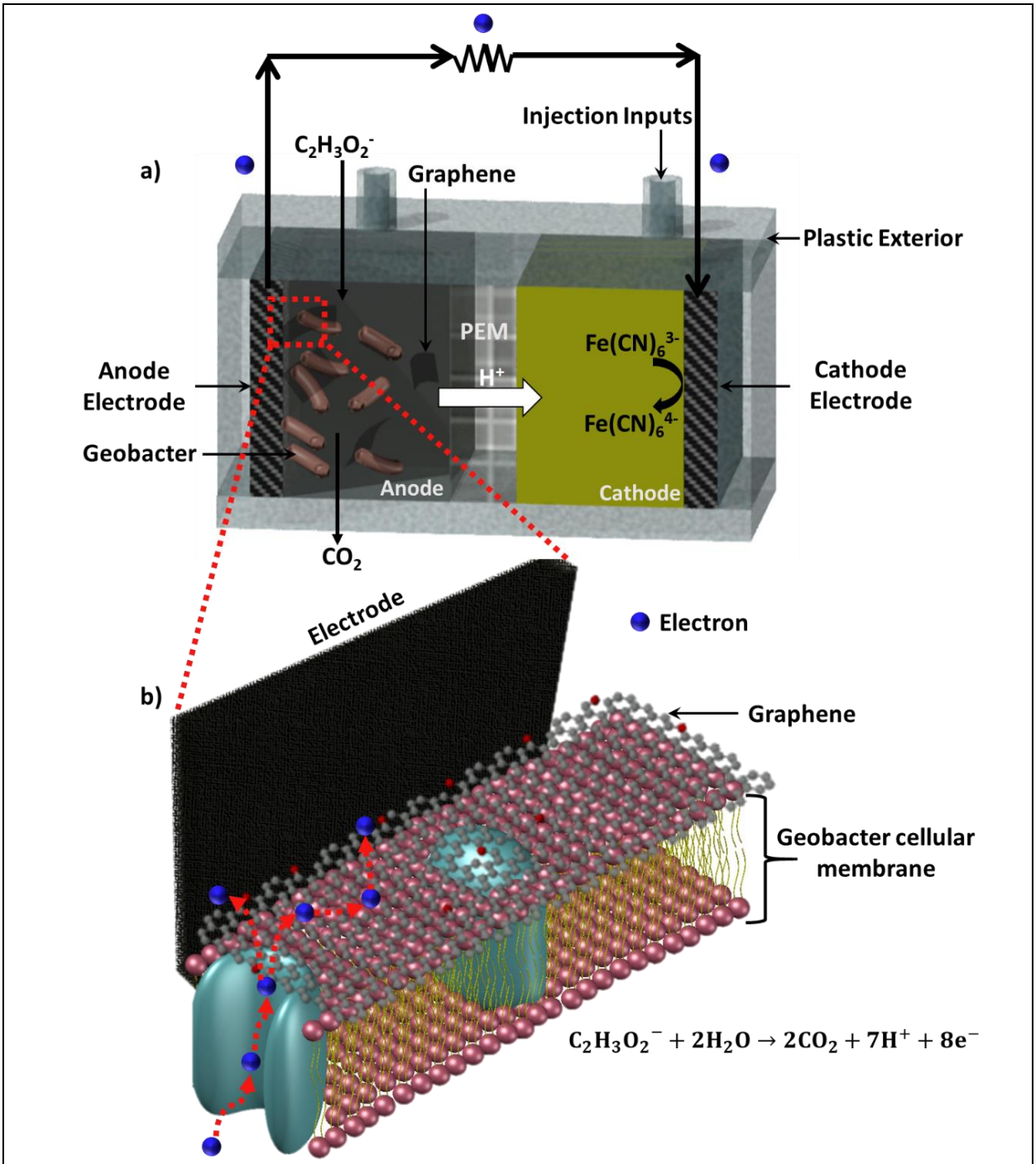

Figure 4.1. a) Cross-sectional view of the MFC construct depicting the device operation after the injection of rGO solution. b) Schematic diagram showing the interaction between graphene (rGO sheet) and geobacter cell. The electrons produced during the cell's metabolic activity are transferred via direct contact with the conductive protein and the rGO sheet. Due to rGO's high conducitvity, the electrons are transported to the interfaced electrode with ease.

Geobacter Sulfurreducens' efficient, enzymatic metabolism (it has been reported that >90% of the substrate is converted to electricity) of the organic substrate is a model characteristic of the electrogenic bacterium for power generation inside the bio-catalytic device(Bond and Lovley 2003; Bond et al. 2002; Nevin et al. 2008; Richter et al. 2008). Geobacter is a small rod-shaped microorganism that contains conductive proteins(Leang et al. 2010; Schröder 2007) on the extracellular surface which allows the direct transfer of the produced electrons to the adhered electrode. The potential difference between the electrodes acts as the driving force for the bacterial attachment. However, only a fraction (α) of the conductive proteins on the bacterium membrane is in direct contact with the unmodified anode (Figure 4.2). A significant portion that is not in contact ($1-\alpha$) limits the overall efficiency of electronic harvestation. The larger relative size of the graphenic sheets combined with its conformational characteristic makes it a great candidate to interface with the unconnected electron-channels on the organism's membrane and increase the connectivity with the unmodified anode.

The biocatalyst breaks the substrate into protons and electrons. The protons hop across the proton exchange membrane to the cathode, while the generated electrons are shuttled from the proteins on the extracellular membrane directly to the electrode or by the graphene-electrode junction. The circuit is completed when the produced electrons travel from the anode to the cathode across a resistor and recombine with the protons and the reducing agent to complete the redox cycle (Figure 4.1). This research outlines the mechanism of interfacing graphenic sheets on exoelectrogens (*Geobacter sulfurreducens*) and electronic transport mechanism from its exterior cell-membrane *via* the graphenic sheets to a generic, unmodified MFC-anode.

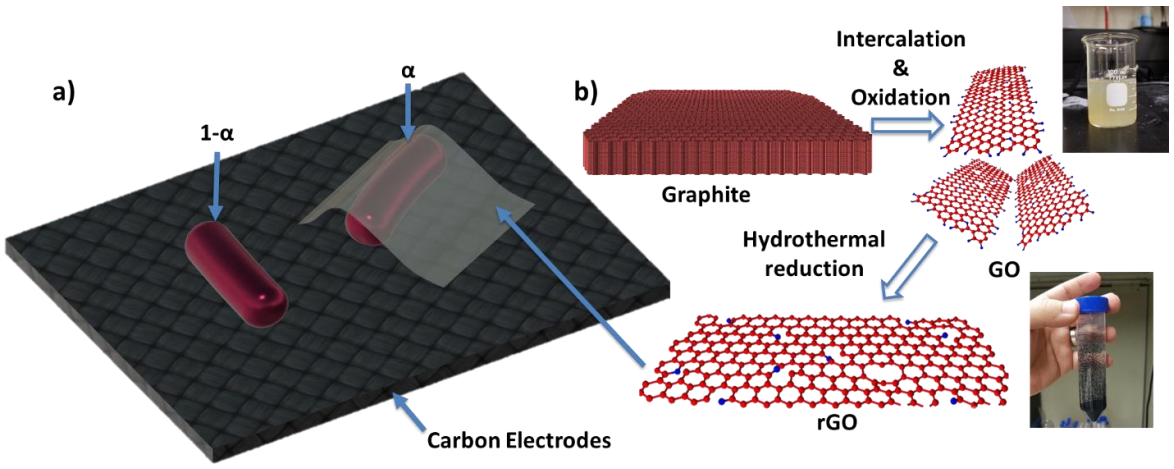

Figure 4.2. a) Well adhered bacterium to the carbon electrode showing an exposed fraction (1-α) of the cellular membrane, along with an rGO encased bacterium where the rGO sheet increases the fraction of connected membrane proteins (α) to the device. b) Schematic showing the synthesis of rGO from graphite via modified Hummer's method.

4.3. Experimental Methods

4.3.1. rGO synthesis

Graphene oxide (GO) was synthesized by a modified Hummers method. Here, 1.0 gram of 7 mesh graphite flakes (Sigma-Aldrich) was added to a beaker in an ice bath. 40 ml of Sulfuric acid (Fisher Chemical, 96%) and 6.6 ml of Nitric acid (Sigma-Aldrich, 70%) were added to the beaker and stirred for 40 min. 5 grams of potassium permanganate (Sigma-Aldrich, ≥ 99.0%) was added slowly to keep the reaction temperature below 20 ^{0}C during addition. The reaction solution was stirred for 30 min at 40°C. 30ml of 20% Hydrogen peroxide (Fisher Chemical, 50%) was carefully added to the solution maintaining a temperature of <60ºC to quench the reaction. The solution was diluted with 200 ml of deionized water and later vacuum filtered to recover a vibrant yellow graphene oxide solution. Further, the GO solution was dialyzed for a week in a 2k MWCO

cellulose bag (Thermo Fisher, slide-a-lyzer flask) to remove the residual ions. Finally, reduced graphene oxide (rGO) was produced by hydrothermal reduction at 180°C for 4 hours.

4.3.2. Media preparation and inoculation of *Geobacter Sulfurreducens*

Geobacter medium was prepared by adding 1.5 g of Ammonium chloride (Fisher Chemical, +99%), 0.6 g of Sodium phosphate monobasic (Sigma-Aldrich, ≥ 99.0%), 0.1 g of Potassium chloride (Sigma-Aldrich, ≥ 99.0%), 2.5 g of Sodium bicarbonate (Mallinckrodt), 0.82 g of Sodium acetate (Sigma-Aldrich, ≥ 99.0%), 10 ml of Wolfe's Vitamin Solution (ATCC® MD-VS™) and 10.0 ml of modified Wolfe's Minerals (ATCC® MD-TMS™) to 1.0 L of distilled water. The medium was autoclaved at 121°C for 15 mins. 8.0 g of filter-sterilized Sodium fumarate (Sigma-Aldrich, ≥ 99.0%) was then added to the sterilized medium to reduce it. Under anaerobic conditions (80% N_2 and 20% CO_2), the *Geobacter sulfurreducens* (ATCC® 51573™) vial was thawed and inoculated in the prepared medium. The bacterial solution was subsequently incubated at 26°C-30°C for 2 weeks.

4.3.3. Device construction

The device consists of an anode and cathode chamber separated by a proton exchange membrane (Fuel Cell Store, Nafion 211). The anode and cathode are both 8.75 cm^2 pieces of carbon felt (Fuel Cell Store, AvCarb G200). The anode is connected to a 3.30 kΩ resistor that connects to a preamplifier (Stanford Research Systems, SRS570) that ends at the multimeter (Keithley 2110/2612) data acquisition system. The anode compartment is inoculated with geobacter suspension and an organic substrate of 0.01 M Sodium Acetate (Sigma Aldrich, ≥ 99%). The cathode compartment contains a solution of 0.02 M potassium hexacyanoferrate (Sigma Aldrich,

~99%). Once the electrical generation stabilizes, the rGO solution is distributed to the anode via a syringe.

4.3.4. Raman analysis

Graphene (rGO) and geobacter system was probed using WITEC Alpha 300-RA Raman spectrometer with a laser excitation wavelength of 532 nm. All the samples were studied using a 100X objective with an exposure time of ~5 mins. The Raman spot size is ~700 nm as determined using the equation:

$$Spot\ size = \frac{1.22\lambda}{NA}$$

Where λ is the laser wavelength and NA is the numerical aperture (0.9 for 100X objective).

4.3.5. SEM analysis

Field Emission SEM, the JSM-6320F, was used to obtain high-resolution micrographs of rGO - bacterial interface. A low accelerating voltage of 2kV with a working distance of 2.0 mm was chosen to optimize the image.

4.4. Results and Discussion

4.4.1. Characterization of the Geobacter-rGO interface

To characterize the interface between the geobacter cell membrane and the rGO sheets and to study the rGO's conformity, geobacter cell suspension was incubated with an rGO suspension for 1 hour. To deposit the cells on a substrate, a SiO_2/Si chip was dipped in the bacterial-rGO mixed-solution for 30 mins to help cell adhere to the SiO_2 surface. The resultant chip was probed using optical microscope, field emission SEM (FESEM) and Raman spectroscopy. The FESEM micrograph of the SiO_2/Si chip (Figure 4.3a), depicts two geobacter cells interfaced with rGO sheets. In one case, the geobacter is on top of an rGO sheet, while the other geobacter is wrapped

under the rGO sheet. The bare bacterium is noticeably more charged (higher intensity) compared to the rGO wrapped cell by a factor of 15%. This difference in intensity is attributed to the presence of conductive material on top of the bacterium, which minimizes the charging effect as seen in the exposed cell. Further, rGO's conformal nature(Mohanty et al. 2011) is observed on the wrapped bacteria by the formation of both longitudinal (due to relaxation of sheet) and transverse (due to strain in sheet) wrinkles as shown in figure 4.3a and b.(Deng et al. 2016) Note that majority of the observed geobacter cells were interfaced with rGO (bottom and/or atop).

Raman spectroscopy enables effective characterization of graphenic domain size of rGO and its carrier density due to the strong electronic coupling of the sp^2 in-plane (G), breathing (D) and second-order overtone of in-plane (2D) phonon vibration energies. Figure 4.3b illustrates the G band Raman spectra of rGO on SiO_2/Si substrate in air (black) and rGO interfaced with geobacter (red). From the spectrum, the domain size of the graphenic sp^2 regions of the rGO was calculated to be 17.8 nm using the Tuinstra and Koenig relationship,(Tuinstra and Koenig 1970; Cançado et al. 2006, 2011; A. C. Ferrari and Robertson 2000; Andrea C. Ferrari and Basko 2013) $L_a(nm) = 2.4 \times 10^{-10}\lambda^4 \left(\frac{I_D}{I_G}\right)^{-1}$, where L_a (nm) is the in-plane crystallite size, λ is the laser wavelength (532 nm), and I_D/I_G is the intensity ratio of D and G bands (1.079).

Graphene (rGO) acts as an electron acceptor when interfaced with the electrogenic bacterial cells. Based on the potential and flux of the electrons from the geobacter and the capacitance of rGO, a steady state electron concentration in rGO is expected to stabilize. This electron density in the rGO sheet was analyzed with Raman spectroscopy. It is important to note that geobacter cells with a typical size of 1.5-2 μm (projected area = 0.7 to1 μm^2) were probed with a 532 nm laser of the Raman spectroscope with a diffraction-limited spatial resolution of ~360 nm (spot size area =

0.385 μm^2). At the geobacter-rGO interface, the electrons shuttling from the membrane are taken

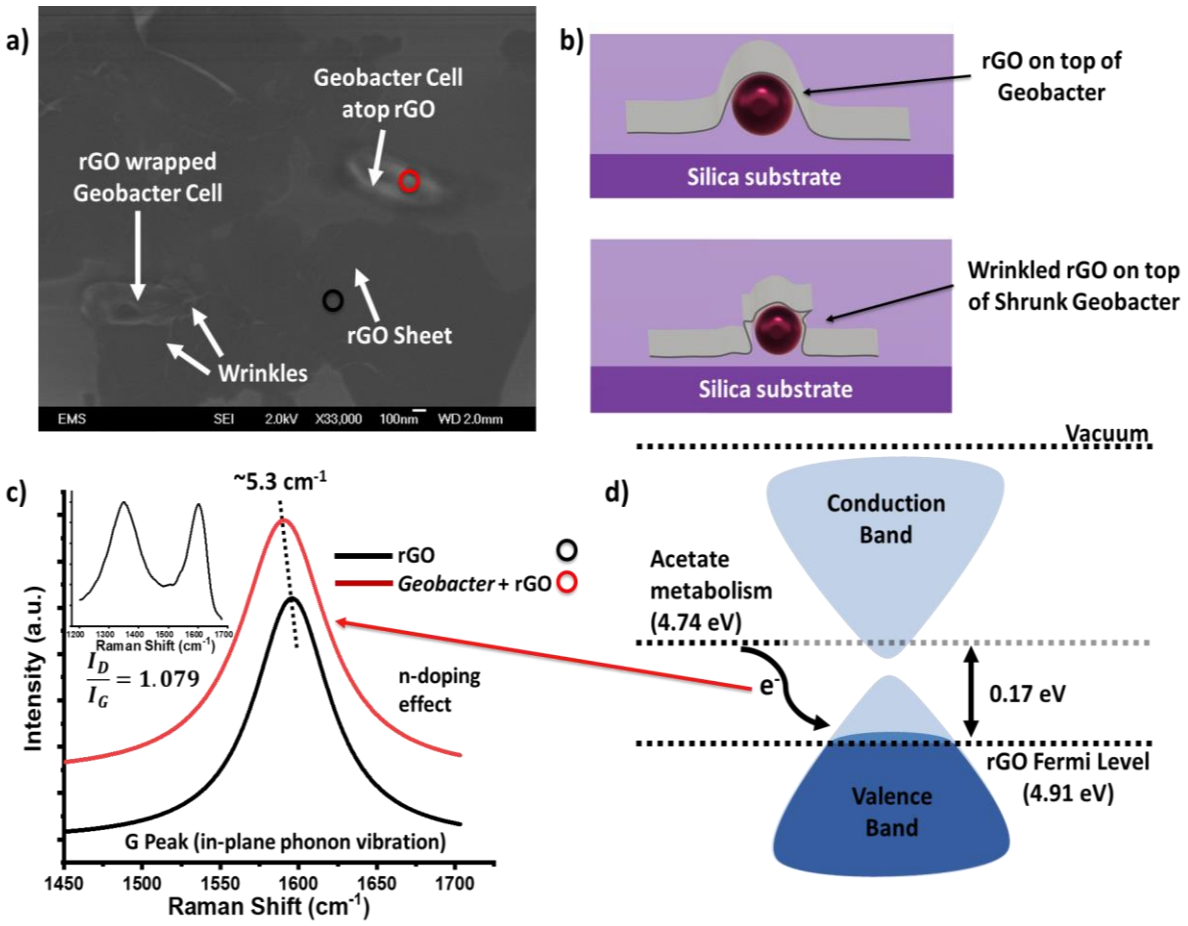

Figure 4.3. Optical characterization of rGO-bacterial interface. a) FESEM image showing bare rGO sheet, geobacter cell above rGO and rGO wrapped cell as well as the wrinkles formed on the graphenic sheet. b) Schematic showing the formation of wrinkles on the rGO sheet around geobacter. c) Raman spectra showing the G peak positions of rGO interfaced with air (black) and rGO interfaced with geobacter (red). (Inset left) Raman spectra of rGO showing D and G peaks. d) Band diagram of rGO depicting the favorable energetics for electron transfer.

up by the graphene, till it reaches its capacitance limit. Therefore, the electrogenic bacterial interfacing leads to rGO accepting electrons and undergoing a high degree of n doping. Raman spectroscopy was used to study the added electron density in rGO via measuring the induced red shift in the G peak position (~5.3 cm^{-1}) of rGO (Figure 4.3). The density of electrons added to rGO

(n) from the interfaced geobacter's metabolic activity is 3.44 x 10^{12} cm^{-2}, as calculated using the relationship between carrier concentration and Raman shift given by Das et al.(Das et al. 2008a) This added electron density can be used to calculate the quantum capacitance of rGO using the expression: $n\ e = C_{graphene}\ V_{electron}$, where $C_{graphene}$ is the quantum capacitance of rGO, $V_{electron}$ is the potential difference (0.17 eV) between the fermi level of rGO (4.91 eV)(Kang et al. 2013; Kumar, Bernardi, and Grossman 2013) and the electrons produced from the acetate metabolism (4.74 eV)(Logan et al. 2006), e is the charge on an electron, and n is the density of electrons added to rGO from geobacter (3.44 x 10^{12} cm^{-2}) (Figure 4.3c and d). $C_{graphene}$ is calculated to be 3.24 $\mu F cm^{-2}$, which is similar to the reported quantum capacitance value of pristine graphene.(Xia et al. 2009) This similarity can be attributed to the previously reported reduction of graphene oxide and rGO by the electrons from the geobacter.(Lehner et al. 2019; Salas et al. 2010; Goto et al. 2015) The physical interaction between rGO and geobacter confirmed from FESEM micrographs and the electron-transfer from geobacter to rGO shown by Raman analysis demonstrate the strong interface that will enable improved electron transfer from the geobacter membrane into the rGO. The high conductivity of rGO is known to shuttle the electrons into any low-potential region, which in the case of a MFC will be the connected (unmodified) anode to improve the total rate of electron transport of the system.

4.4.2. Membrane electron-transfer analysis

To study the electron-transport mechanism through the rGO-on-geobacter system, a MFC device was assembled with cell culture of wild type *Geobacter sulfurreducens* (ATCC® 51573™) and 0.01 M sodium acetate substrate in the anodic chamber, and 0.02 M potassium hexacyanoferrate in the cathode chamber [$Fe(CN)_6^{3-} \xrightarrow{Reduction} Fe(CN)_6^{4-}$] (Figure 4.1a). Note that the studied MFC

construct does not include a biofilm to study of the graphenic interface on the cell and not the biofilm (part of a future study). A resistor of 3.30 kΩ was connected between anode (unmodified) and cathode electrodes to complete the circuit. The electronic transfer from the anode is observed upon the introduction of the electrogenic bacteria in the anode chamber. To study the effect of interfacing rGO with geobacter, rGO suspension (preparation shown in experimental methods, and

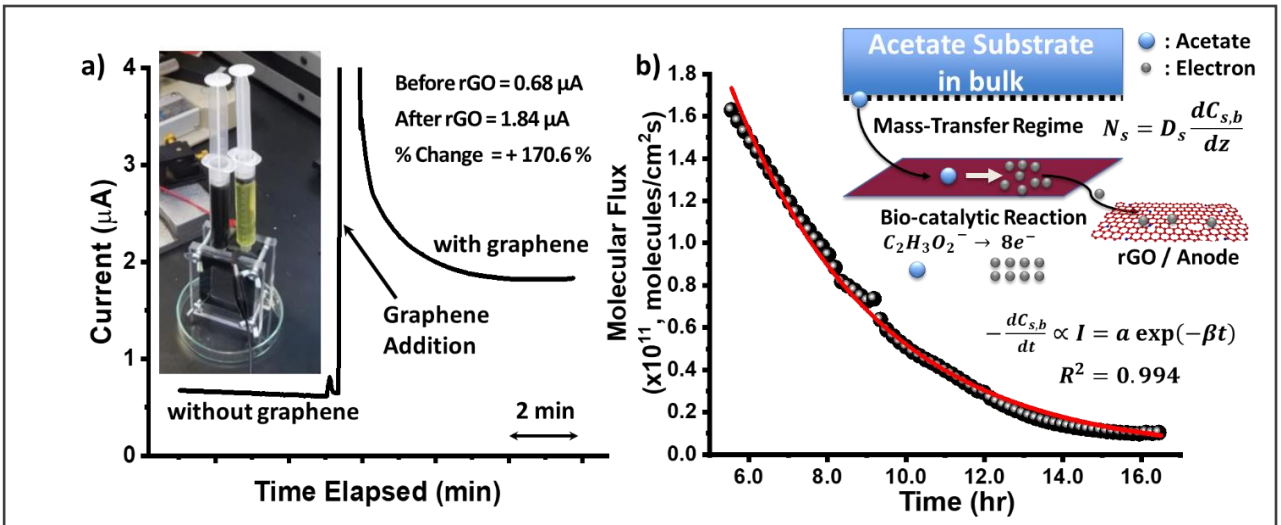

Figure 4.4. Evaluating the effect of rGO inside the MFC. a) Current response during device operation before and after injection of rGO solution. (Inset) Image of the MFC device. b) Modeling the molecular flux during the diffusion limited process after the device reaches steady state. An exponential function was applied to the system to fit the device output versus time. The solid red line represents the modeled equation. (Top right) Mass transfer mechanism of the substrate diffusion to the bacterial membrane for cellular respiration. Upon oxidation, electrons are transported via the interface into the circuit where the device current is proportional to the transient molecular flux by the exponential decay relation.

figure 4.2b) was introduced into the chamber once the electronic current stabilized (~15 min after device start-up). For each electron-transfer experiment, the system was allowed to operate without subsequent addition of substrate or medium.

The injection of only deionized (DI) water (control) decreases the overall electron transport rate (See Supporting information), attributed to the dilution of acetate substrate (that the bacteria use to catalyze electrons). The rate of electron transfer slowly decreased as the substrate was depleted

leaving less feed for the bacterial metabolic production of electrons. This dilution-effect is expected in every experiment where rGO solution is added. To improve the interface between the bacteria and the anode (unmodified), rGO sheets were introduced in the anodic chamber. Previous attempts of implementing graphene in a MFC have been focused on improving the conductivity of the electrodes.(Xiao et al. 2012; ElMekawy et al. 2017) Here, rGO suspension was utilized to interface with the membrane of the biological cells.(He et al. 2010; Nguyen and Berry 2012)

The rate of electron transfer from the geobacter membrane into the anode (unmodified) increased upon the injection of rGO solution, as shown in figure 4.4b, ascribed to the interface of the highly conductive rGO with the anode (unmodified), as depicted in figure 4.2a. These electrons, produced from the geobacter metabolism, are energetically favorable for transfer to the electron accepting rGO sheets upon conformal interfacing with the cell. At injection, the rate of electron transfer undergoes a sudden increase before stabilizing to a 170% higher flux. This is attributed to a) the convective flux from rGO addition disrupting the acetate concentration gradient near the cells, and b) the release of the electrons accumulated on the newly interfaced membrane with rGO. It is important to note that the addition of rGO into the system did not result in an observable stress induced cellular toxicity as seen in the live-dead assay. Further, the addition of rGO did not directly impact the life span of the fuel cell, also indicating negligible stress on the cell.

After the sudden release of the membrane-accumulated electrons, the rate of electron-transfer over time undergoes transient decrease, presumably due to the establishment of the substrate concentration gradient. Here, there are three serial transfer processes: (a) substrate molecular-transport from bulk into the cell, (b) the metabolic oxidation of substrate to produce electrons, and (c) transfer of electrons to the anode. Since the electron transport and the catalytic metabolism are

fast processes, the electron flux from the membrane is limited by the mass-transfer of the substrate molecules to the bacterium for metabolic oxidation. This response can be modeled by a pseudo steady-state mass-transfer equation: $N_s = k(C_{s,b} - C_{s,s})$, where N_s is the molecular flux (molecules/cm^2 s), $C_{s,b}$ and $C_{s,s}$ are the molecular substrate concentration (molecules/cm^3) in bulk and on the membrane, and k is the mass-transfer coefficient (cm/s). Since the reaction is fast, $C_{s,s}$ ~ 0. At equilibrium, the rate of electron production (or electrical current) is proportional to the

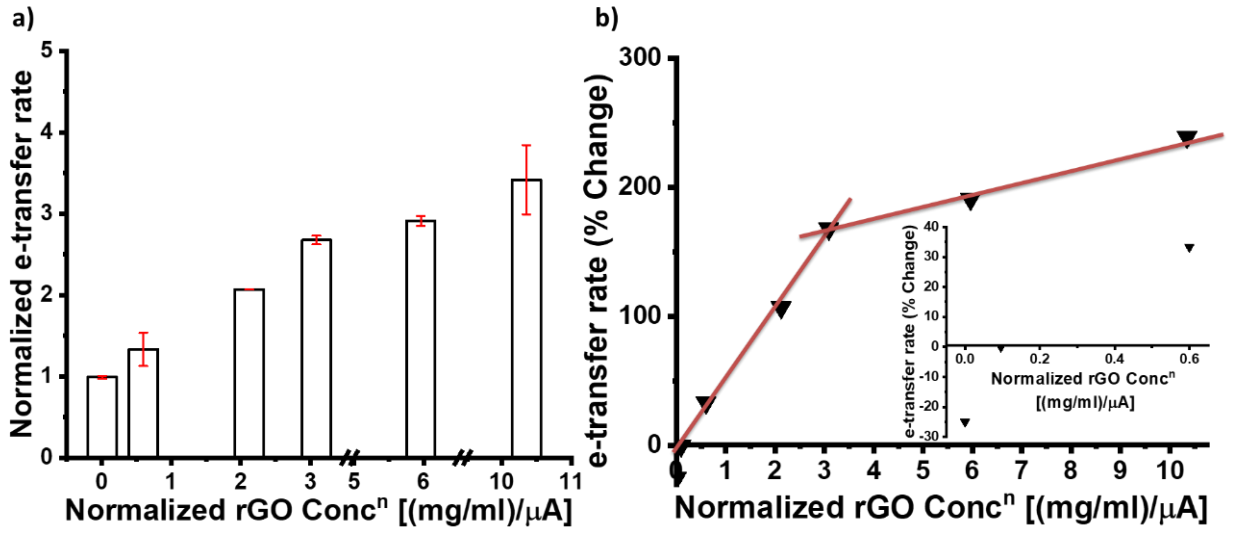

Figure 4.5. Performance study of the MFC device with respect to rGO concentration. a) Normalized current response of the device with control (DI water) and varying concentrations of rGO (0.01 – 10.35 [(mg/ml)/μA]) in the anodic chamber. The current was first allowed to stabilize after injection with the specific solution. The rGO concentrations were then normalized with the stabilized initial current response, which is directly proportional to the bacterial concentration. b) Percent difference in the power density with normalized rGO concentration. (Inset) Power density change for solutions with low normalized concentration of rGO (0 – 0.6 [(mg/ml)/μA])

substrate mass-transfer flux ($N_s = kC_{s,b}$). As the substrate is consumed, its concentration reduces following the mass-balance equation: $V\frac{dC_{s,b}}{dt} = -N_s * A$ where V is the bulk volume of the substrate (cm^3) and A is the cross-sectional area of the electrode (cm^2). This resulted in the expected mass-transfer limited exponential decay relation of the molecular flux of the substrate,

$-\frac{dC_{s,b}}{dt} \propto I = a\ exp\ (-\beta t)$, where a and β are fitting parameters corresponding to the diffusivity of the substrate in the mass transfer regime (Figure 4.4b).

To quantify the response at different rGO concentrations, lyophilized rGO powder was used to prepare different concentrations before introduction into the device. A correlation between the rate of the electron transfer and the rGO concentration (figure 4.5) shows that the electron transfer into the anode (unmodified) increases with rGO concentration. Since different devices have different initial interfacial properties, the rGO concentrations were normalized with the stabilized initial current, which is assumed to be directly proportional to the interfaced bacterial concentration. The units for the normalized concentration are (mg/ml)/μA. Further, since with the addition of rGO, the concentration of the substrate decreases (which should reduce the rate of the electron transfer at steady state), the increase in electron transfer implies that there are new channels created between the electron-producing bacterial membrane and the anode (unmodified) (figure 4.2). Since the number of cells and the number of electron-producing channels could not be controlled in each device, for all analysis, we normalized the rGO concentrations with the currents produced before rGO addition to obtain a normalized rGO concentration per (unmodified) anode-connected, electron-producing channels on the cell membrane. For the same reason, we also normalized the electron transfer rate after rGO interfacing with the initial currents produced without rGO. As shown in figure 4.5a, there is an increase in the electron transfer rate with the increase in rGO concentration, attributed to increased coverage of the bacterial cell. Further, there is a decline in the degree of increase in the electron-transfer-rate as shown by the reduction in the slope of the red trend lines in figure 4.5b. This is attributed to approaching more complete coverage of the

active electron-producing channels by rGO interfacing. As more coverage is achieved, there are lesser number of channels to cover.

The generated power density from the electrons flowing through the resistor was analyzed for each case under averaged electron-transfer rate. Power density ($\mu W/cm^2$) is given by, $P = \frac{I*V}{A}$, where I is the averaged device current (μA), V is the open circuit voltage (0.54 V) and A is the electrode area (8.75 cm^2). The device power density has a direct response to the current output which is proportional the rGO concentration inside of the anode chamber (Figure 4.5). The highest normalized concentration of rGO improved the power density from 0.0179 $\frac{\mu W}{cm^2}$ to 0.0606 $\frac{\mu W}{cm^2}$ (+239%). Increases in both the power density and the device current after the addition of rGO sheets are directly related to the amount of interfaced membrane proteins to the anode. Additional connected pathways via graphene increase the overall efficiency of each individual bacterium which collectively enhances the device performance.

4.5. Conclusions

In summary, we interfaced highly conductive graphenic sheets on electrogenic bacteria, which metabolize substrates into electrons that are transported into its membrane. These electrons at 4.74 eV reducing potential are then transferred onto the interfaced graphenic sheets (Fermi level = 4.91 eV) by adding ~34400 electrons per μm^2 under steady state as confirmed by phononic characterization. This effectively confirms the ease of electron transport from the bacteria to the graphene lattice. Controlling the concentration of graphene in the anode chamber resulted in an estimated 2-fold higher rate of electron transfer. The power density increased ~2 folds with 10.35 [(mg/ml)/μA] of rGO, indicating enhanced electron transport from increased rGO-microbial interaction. The conformal rGO sheet encases the cellular membrane, increasing the number of

connected proteins, which enhance the efficient transport of the electrons from the cellular surface. This resulting electron addition (n-doping) effect (~5.3 cm^{-1}) from the synergy of electrogenic bacteria and rGO correlates with the observed enhancement in device performance. To understand the macroscale impact of rGO in the MFC operation, further study needs to be done to explore the interaction of rGO and geobacter at a single cell level. This work will potentially lead to the development of synergistically designed, conformal-interfaces for electrogenic bacteria for next-generation microbe-driven systems.

CHAPTER 5

5. Investigating SERS of bacteria using graphene quantum dots (GQDs) as the enhancement substrate

5.1. Introduction

Raman spectroscopy has been extensively utilized for studying wide-ranging materials. It has demonstrated to be a powerful analytical tool for selective characterization of molecules in diverse fields ranging from physics, chemistry, material science and biology. However, one of the drawbacks of applying Raman spectroscopy, especially in biological systems, is its weak signal (intensity) arising from its low scattering cross-section (10^{-30} cm^2 $molecule^{-1}$). A way to subvert this limitation is Surface Enhancing Raman Scattering (SERS)(Fleischmann, Hendra, and McQuillan 1974; Jarvis and Goodacre 2004). The enhancement associated with the SERS process can be explained by 2 mechanisms: electromagnetic enhancement mechanism (EM) and chemical enhancement mechanism (CM).(Sharma et al. 2012; Ling et al. 2010) EM describes the significant increase in Raman cross section due to the enhancement of the local electromagnetic field. This electromagnetic enhancement is primarily contributed to the excitement of the surface plasmons when exposed to the incident light, roughly proportional to $|E|^4$ ($\sim 10^8$), where E is the intensity of the electromagnetic field. In contrast, CM involves a charge transfer between the substrate and the interfaced molecule, separating the positive and negative charge in the molecule further. This separation increases the polarizability of the molecule as well as the Raman cross-section.

The substrate used for SERS significantly affects the resulting spectra and in certain cases, the substrate might require modifications. The fabrication process required to prepare the substrate can be relatively complex, regardless of the enhancement mechanism involved. Various metals

including silver and gold have been utilized as the SERS substrate and the type of metal used often affects the efficiency of the resulting enhancement. Further, metal substrates might suffer from certain disadvantages: a) high cost, b) uncertain biological compatibility, and c) oxidization, especially silver. Hence, it is essential to explore new substrate, which is biocompatible, easy to handle, chemically inert and effective, to observe SERS. Due to these concerns, researchers have looked upon other compatible and affordable substrate like graphene for Raman enhancement.(Ling et al. 2010)

Graphene, a planar sheet sp^2 bonded carbon atoms, is chemical inert and has shown to be biocompatible as well. Previously, it has been shown that graphene can be utilized as a substrate for Raman enhancement. However, there are limited studies done in this field. Similar to graphene, graphene quantum dots (GQDs) have gained enormous attention in the past decade due to their unique properties. Along with possessing graphene-like properties (sp^2 carbon and chemically inert), GQDs show pronounced quantum confinement and edge lattice effect due to their small size. In this study, we utilize GQDs, synthesized *via* hydrothermal reduction, as a graphene enhancement substrate for bacterial cells (*Geobacter sulfurreducens* and *Shewanella Oniedensis*).

5.2. Experimental Methods

5.2.1. GQD Synthesis

Graphene oxide (GO) was synthesized by a modified hummers method. 1.0 gram of 300 mesh graphite powder (Alfa-Asear) were added to a beaker in an ice bath. 40 ml of Sulphuric acid (Fisher Chemical, 96%) and 6.6 ml of Nitric acid (Sigma-Aldrich, 70%) was added to the beaker and stirred for 40 min. 5 grams of potassium permanganate (Sigma-Aldrich, ≥ 99.0%) was then added slowly to keep the reaction temperature < 20°C. The solution was stirred for 30 min at 40°C.

Subsequently, 30ml of 20% Hydrogen peroxide (Fischer Chemical, 50%) was added to the solution to stop the reaction. The solution was then diluted with 200 ml of deionized water (DI) and vacuum filtered to recover a vibrant yellow graphene oxide solution. The GO solution was dialyzed for a week in a 2K MWCO cellulose bag (Thermo Fischer, slide-a-lyzer flask). Reduced graphene oxide (rGO) was then produced by hydrothermal reduction of the GO solution at 180C for 4 hours. The rGO solution was then intercalated with a similar ratio ~6:1 of Sulphuric Acid:Nitric Acid and placed in a bath sonicator for ~24 hours. Afterwards, the acid was removed *via* vacuum filtration with a 0.22 μm membrane to. The filtrate was later re-dispersed into DI water and neutralized with 1M Sodium hydroxide. The resulting solution was placed in a Teflon lined acid digestion vessel (Parr Reactor) and hydrothermally treated at 200°C for 10-12 hours to get GQD solution. Finally, the GQD solution was filtered through a 0.22 um membrane to remove any solids (big sheets of rGO).

5.2.2. Raman Data Analysis

The GQD solution was incubated with bacteria (*Geobacter sulfurreducens* and *Shewanella Oniedensis*) overnight to allow interaction. A SiO_2/Si chip was then placed in the GQD-bacteria solution and incubated for 1 hr. This chip was probed using WITEC Alpha 300-RA Raman spectrometer with a laser excitation wavelength of 532 nm. All the samples for this research was studied under 100X objective: exposure time ~5 mins and Raman spot size ~700 nm.

5.3. Results and Discussion

5.3.1. Characterization of GQDs

The hydrothermally synthesized GQDs were studied using AFM to characterize the size of the produced dots. The AFM scan (topography image) of the GQDs deposited on SiO_2/Si substrate is shown in figure 5.1a along with the height and size profile of the selected area in figure 5.2b. The diameters of the GQDs are predominantly in the range of 10-50 nm. Also, the topographic heights of these materials typically lie between 1-2 nm, comparable to the data related to 1-3 layer of functionalized graphene nanoribbons (GNR).(Xiaolin Li et al. 2008)

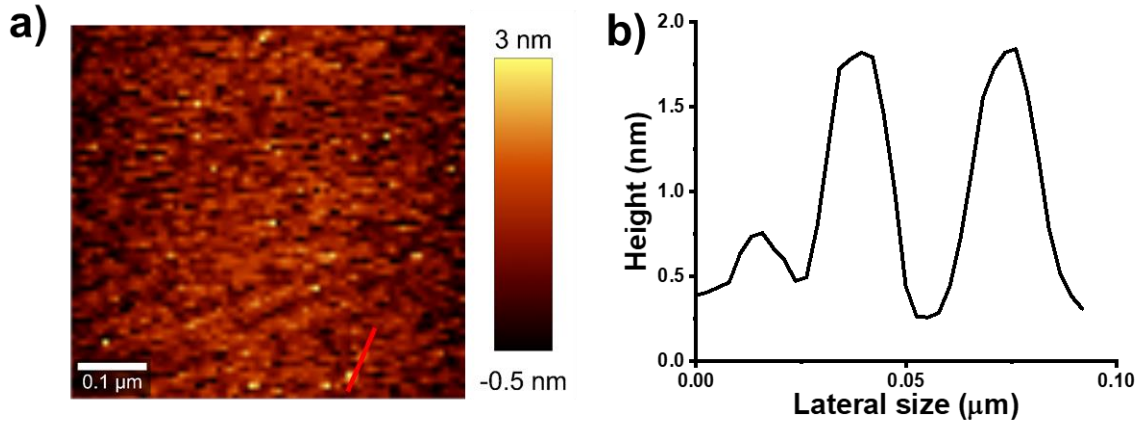

Figure 5.1. AFM profile of GQD. a) AFM image of the GQD deposited on a SiO_2/Si chip. b) Height profile along on the red line on a).

Further, the optical properties of the synthesized GQDs were studied using UV-Vis spectroscopy (Figure5.2). Previous studies have shown that GQDs with smaller dimension (<100 nm) possess several unique optical properties mainly due to the prominent effects of the edge lattice and quantum confinement.(D. Pan et al. 2010) The absorbance spectrum of the GQD showed a peak at ~200 nm which could be attributed to the electronic $\pi - \pi^*$ transition, common in pristine aromatic sp^2 domains, as shown in figure 5.2a.(Novoselov et al. 2004; D. Pan et al. 2010) Photoluminescence emission spectra of the GQDs for excitation at 320 nm showed a strong blue luminescence at ~430 nm (figure 5.2b).

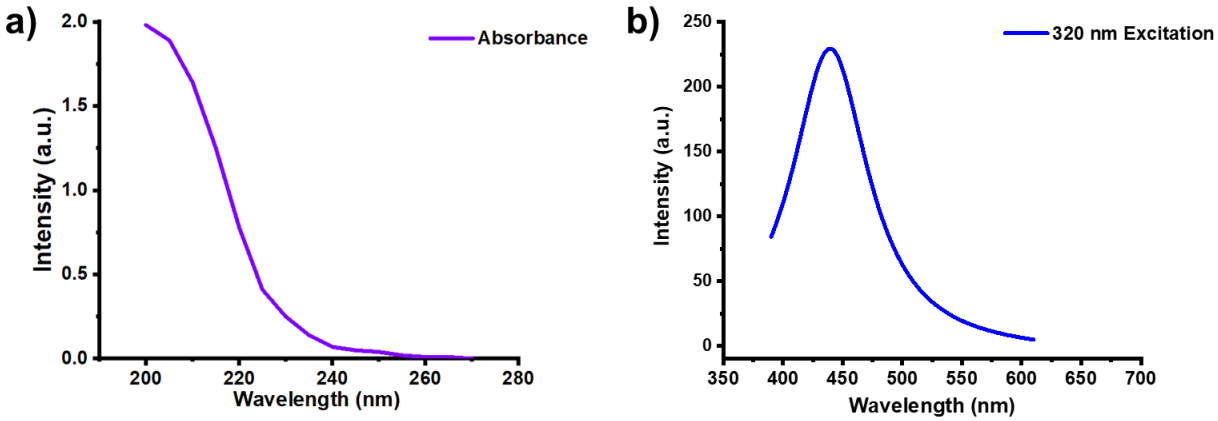

Figure 5.2. Characterization of GQD using UV-Vis Spectroscopy. a) Absorption spectrum of GQD. b) Photoluminescence emission spectrum of GQD for excitation at 320 nm.

5.3.2. Understanding the GQD-bacteria interface

To study the interaction of GQD with bacteria, the GQDs were incubated with bacteria (*Geobacter sulfurreducens* and *Shewanella Oniedensis*) overnight and observed under Raman spectroscopy. The Raman spectrum of GQD-bacteria interface showed an enhancement in the bacterial peaks confirming SERS effect as compared to the spectrum of bacteria on SiO_2/Si substrate without GQD

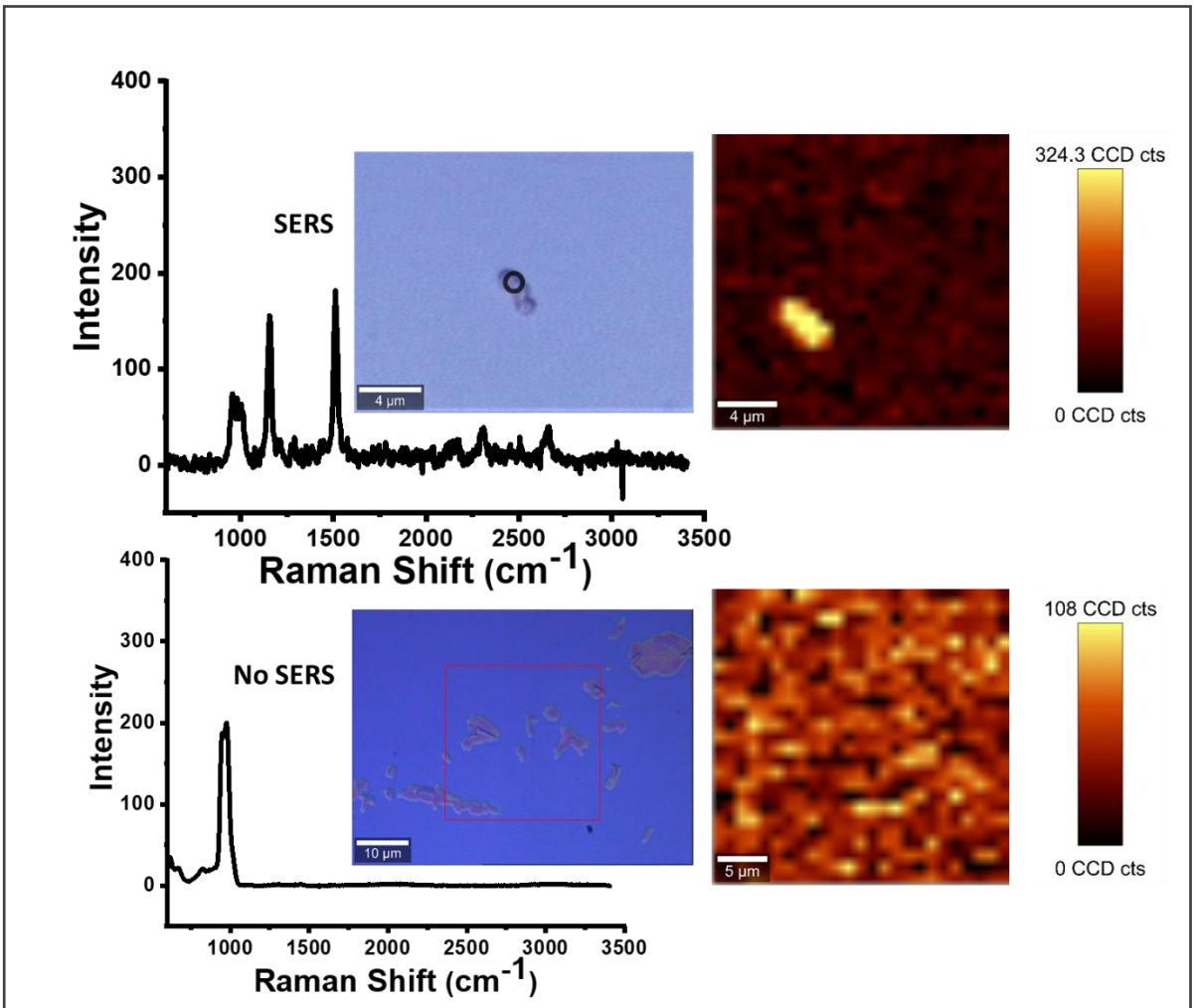

Figure 5.3. (Top) The Raman scan of GQD-bacteria interface with pronounced SERS (left); optical image of the bacteria incubated with GQD overnight (center); Raman intensity scan based on the bacterial peak at 1520 cm^{-1} with the scale bar (right). (Below) The Raman scan of just bacteria with no SERS (left); optical image of the bacteria incubated overnight (center); Raman intensity scan (red square in the optical image) based on the bacterial peak at 1510 cm^{-1} with the scale bar (right).

(Figure 5.3). The Raman enhancement from the GQD substrate was not strain dependent and could be observed with different types of bacteria (*Geobacter sulfurreducens* and *Shewanella Oniedensis*), as shown in figure 5.4. The peaks 1153 cm^{-1}, 1510 cm^{-1}, 2147 cm^{-1}, 2302 cm^{-1} and 2650 cm^{-1} are attributed to the enhanced bacterial peaks.

Although graphene has been used as a Raman enhancement substrate for chemical dyes, there has been no studies on the utilization of GQDs to observe the SERS of bacteria. One possible reason for this effect could be the chemical enhancement (CM) from the GQD substrate. When the GQDs were incubated with bacteria, they formed a close network with the bacteria. Such close interaction allowed charge transfer between GQDs and biomolecules associated with bacteria, resulting in the enhancement of the bacterial peaks. In contrast, there was no visible bacterial peaks when only SiO_2/Si was used as the substrate, conforming that the enhancement was due to the presence of GQD.

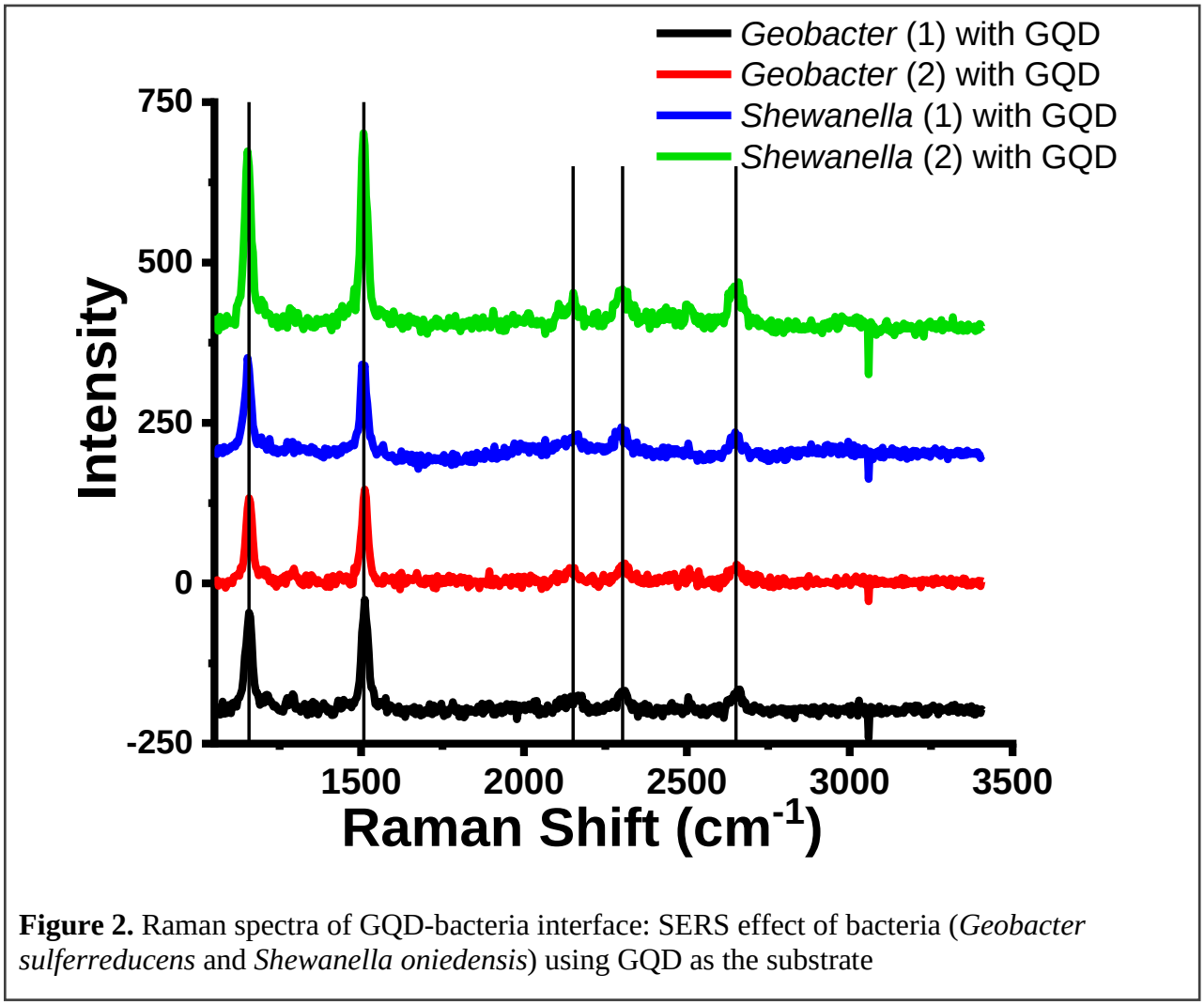

Figure 2. Raman spectra of GQD-bacteria interface: SERS effect of bacteria (*Geobacter sulferreducens* and *Shewanella oniedensis*) using GQD as the substrate

5.4. Conclusion

In this study, GQDs were used as the Raman enhancement substrate to study the SERS of bacteria for the first time. As a result of the interaction of GQDs with bacteria, the bacterial peaks 1153 cm^{-1}, 1510 cm^{-1}, 2147 cm^{-1}, 2302 cm^{-1} and 2650 cm^{-1} were enhanced. It is important to note that these peaks were not seen when bacteria on SiO_2/Si substrate were scanned. This result was attributed to the charge transfer between GQDs and bacteria due to the chemical enhancement mechanism. Further, SERS effect was observed in different types of bacteria (*Geobacter sulferreducens* and *Shewanella oniedensis*), demonstrating that it was not strain dependent. This research highlights the potential of GQD as a SERS substrate, however, further studies need to be done to understand the mechanism in detail and explore the applications in biosensing and disease detection.

CHAPTER 6

6. FUTURE WORKS AND CONCLUSION

6.1. Investigating graphene – tissue interfaces with Raman Spectroscopy

Glioblastoma multiforme (GBM) is the most common primary brain tumor affecting the adult population.(D.N. et al. 2016) The current standard of care for treatment of GBMs, employs a combination of surgical resection, chemotherapy, and radiation.(Stupp et al. 2005) Despite the current treatment paradigm, GBM carries a poor prognosis, with a median survival of only 15-months.(Stupp et al. 2005) Recent literature has confirmed that decrease of tumor burden via safe gross total resection correlates to improved survival outcomes.(Sanai et al. 2011; Y. M. Li et al. 2016; Brown et al. 2016; Incekara et al. 2019; I. W. Pan, Ferguson, and Lam 2015; Bloch et al. 2012; Byun et al. 2019) Given the intrinsic malignant nature of GBM cells and wide dispersion through the normal surrounding tissue, many technologies have been employed to improve intraoperative resection of grossly abnormal GBM tissue from the surrounding gliotic, edematous, or normal tissue.

Advances in microsurgical techniques, surgical tools, fluorescent agents and intraoperative imaging have enabled better identification of tumor borders, thereby allowing maximal gross total resection of tumor with preservation of surrounding normal tissue.(Bander, Magge, and Ramakrishna 2018) Since the introduction of the intraoperative microscope within the field of neurosurgery in the 1950's and 1960’s, as well as progress in the intraoperative tools, significant advances have been made in incorporating microsurgical techniques in neurosurgery for safer gross total tumor resection.(Kriss and Kriss 1998) Furthermore, introduction of intraoperative

fluorescent agents, as well as intraoperative magnetic resonance imaging in recent years have helped further advance surgical resection of brain tumors.(Kriss and Kriss 1998; Katsevman et al. 2019) The combination of such technologies have resulted in a synergistic improvement in achieving the end goal of gross total resection.(Coburger et al. 2015; Dobson 1989) This not only highlights the need for integration of imaging-based guidance intraoperatively, but also leads the way to the future development of real-time imaging-based devices to allow for virtual histopathologic interpretation of tissue intraoperatively. In the recent years, optimization of intraoperative technology to improve surgical guidance in tumor resection and tumor diagnostics has been rapidly growing, with a particular focus on utilization of Raman spectroscopy integrated into an intraoperative probe.

Raman spectroscopy has been heavily incorporated into biomedicine to study cells and tissues. Raman spectroscopy has been shown to be a versatile platform to investigate the chemical and spatial information of materials without labels. Even though other vibrational spectroscopy tools like IR exist for biomedical analysis, Raman offers unique advantages: a) Eliminates need for any contrast-enhancing agents, as the biomaterials can be probed in their native states, b) Raman spectroscopy can be readily used to study aqueous based samples (corresponding to small Raman cross-section of water) in contrast to spectroscopic techniques like FTIR, which exhibits high absorbance of water that interferes with the spectrum, and c) Raman scans range over large wavenumbers with the ability to provide higher spatial resolution as well. Along with these characteristics, Raman spectra depicts bands that are molecule specific providing direct and crucial information regarding the biochemical composition of the biomaterials.

The use of Raman spectroscopy in cancer studies as well as its subsequent application in intraoperative probes have been discussed in previous sections. While designing intraoperative probes, it is essential to incorporate a sensitive and specific platform. Numerous advantages of this versatile tool have been discussed, however, interpreting the Raman spectra and showing the bio-footprint of cells and tissues is somewhat challenging. Hence, it would be favourable to incorporate Raman based tool with a platform to enhance the detection, making it smoother to interpret the data.

The sensitivity of graphene to the presence of any chemical/ molecule has made it a suitable platform for biosensing devices. Based on previous success of incorporating graphene for studying cancer cells, the next step could be applying this sensitive material to analyze cancerous tissue. Here, we introduce graphene as a biosensing platform to improve the sensitivity of Raman signal, ease results interpretation, and future direction for incorporation of such technology in the operative arena.

6.1.1. Preliminary Results

GBM tissue was obtained from consented patients and placed in a PDMS mold with a center well to keep the tissue from dehydration. The tissue was then covered with CVD graphene transferred onto a glass coverslip and examined under Raman spectroscopy with a long working distance 50X objective (Figure 6.1). GBM tissue is known to be heterogenous as discussed in previously and different sections of the tumor were examined in this study.

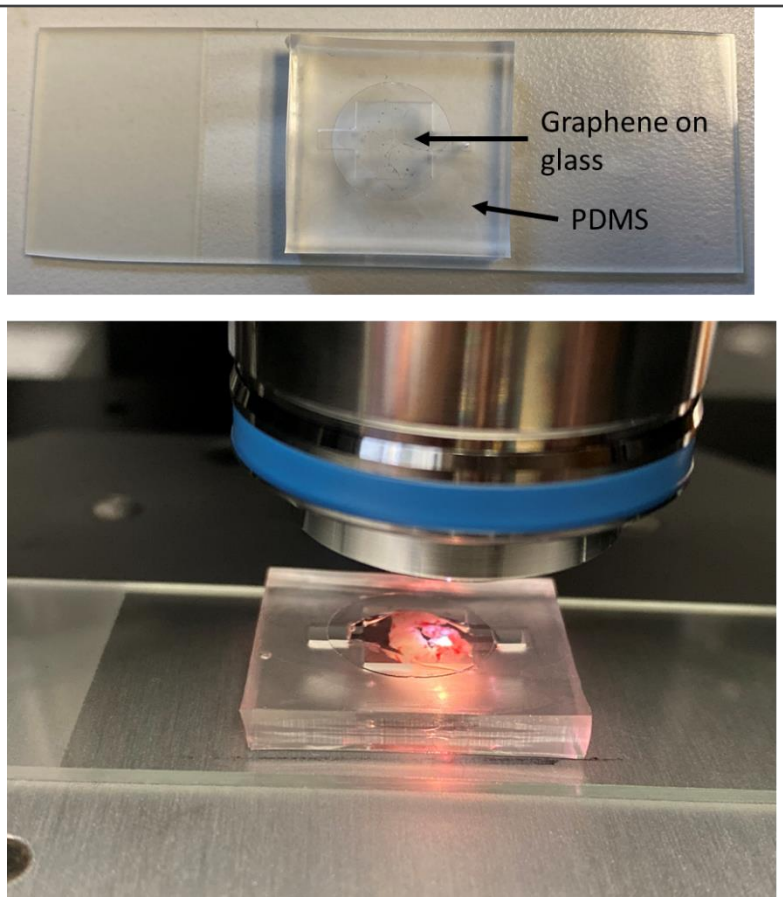

Figure 6.1. Experimental Set-up. (Top) Graphene, grown via CVD, was transferred onto a glass coverslip and placed on a PDMS mold. (Below) GBM tissue was placed in the PDMS well center and covered with the graphene/coverslip. The graphene – tissue interface was probed with Raman Spectroscopy.

Figure 6.2 shows the Raman spectra of 2 different areas of GBM tissue (tumor region and necrotic tissue area). It can be clearly seen that depending on which area is scanned, the Raman spectra is different, indicating the heterogeneity of the tissue region. Further studies need to be done with more samples from each region (tumor, necrotic and margin) to gather a comprehensive information which would help in the long-term goal: to develop graphene-based handheld intraoperative Raman probe.

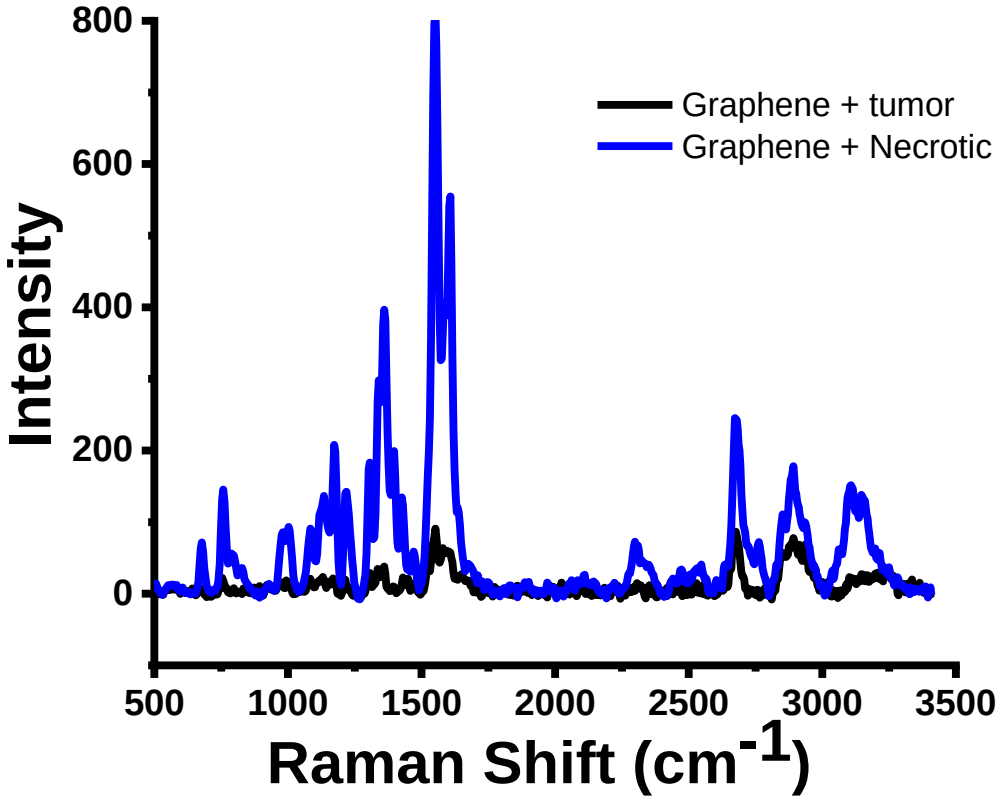

Figure 6.2. Raman spectra of graphene interfaced with tumor tissue (black) and necrotic tissue (blue)

6.2. Concluding remarks

This dissertation provides a detailed study on the interfaces of graphene with various biological systems. The research on graphene and its application is growing exponentially, ever since its discovery in 2006. The applications of graphene encompass a wide spectrum of fields, including biosensing, cellular transistor, drug delivery and energy. However, there is still a gap in knowledge regarding the graphene-bio interfaces. To develop an efficient graphene-based bio-devices, it is important to understand the fundamental concepts related to the type of interaction at the interface.

Chapter 1 introduces graphene and its properties, along with Raman spectroscopy, which is a versatile tool to study various materials especially carbon-based material like graphene. The factors influencing the type of interface formed between graphene materials and different biological systems are also reviewed. Further, the graphene phononics is discussed to understand the doping mechanism of graphene which is greatly influenced by its large quantum capacitance.

After the brief discussion on graphene phononics, chapter 2 reports on the interface of graphene with mammalian cells. In this study, graphene was interfaced with GBM cells (cancer) and astrocytes (normal) and examined with Raman spectroscopy. As cancer cells are known to be hyperactive as well as more electronegative (due to higher concentration of sialic acid in the outer membrane), GBM interfaced graphene showed a high degree of p-doping (~6.3 cm^{-1}) compared to astrocytes (~2.3 cm^{-1}). This study showed the first use of graphene phonons to differentiate cancer cells from normal at a single cell resolution.

Chapter 3 then describes the use of graphene-based platform to study neurodegenerative diseases. Here, CSFs obtained from patients with different diseases including ALS, MS and other types of motor neuron diseases was interfaced with graphene and probed with Raman spectroscopy. It was found that CSFs from different diseases n-doped graphene to a varying degree, showing that the effect was disease specific. The pathological and molecular characteristics of ALS including mitochondrial dysfunction, increased oxidative stress and detrimental immune activation have previously been shown to affect the CSF of diseased patients.(van Es et al. 2017; Bozzo et al. 2017) The composite dipole moment arising from the components of CSF was found to be disease-specific, directly correlating with the doping trend. This study also showed preliminary data indicating that CSFs taken from $SOD1^{G93A}$ transgenic rat ALS model at different stages of the

disease (early stage and late stage) exhibited different n-doping trend on graphene. It offers a unique approach to study this fatal disease and monitor the progression as well.

In chapter 4, the interaction of graphene with electrogenic bacteria is discussed. Here, reduced graphene oxide solution was used to form an interface with *Geobacter sulferreducens.* Electrogenic bacteria metabolizes substrate with electrons as the by product, which are then transported to its membrane. When the highly conductive rGO interfaces with geobacter, it conforms to the cell allowing more connections of the membrane proteins and the electrons are transferred to the rGO sheet. This interface was studied using FESEM and Raman spectroscopy. The electron addition onto the rGO sheet can be confirmed by the n-doping (~5.3 cm^{-1}) of the graphenic sheet. To understand the interaction further, rGO was introduced into the anode chamber of a MFC like device, which increased the power density ~2folds. This study gives an insight into the interface of electrogenic bacteria with graphene at a single cell level, which would be advantageous for fabricating nanodevices for energy source as well as understanding the effect of rGO in a macroscale MFC like setting.

Finally, chapter 5 introduces another graphene material, graphene quantum dots (GQDs) and its potential use as a Raman enhancement substrate. In this study, the GQDs were synthesized *via* a hydrothermal reduction route. The resulting GQDs were characterized with AFM to understand topological profile (diameter range: 10-50 nm and height: 1-2 nm) and with UV-Vis spectroscopy to study the optical properties (a strong photoluminescence emission peak at ~430 nm for excitation at 320 nm). The GQDs were then incubated with bacterial cells and examined under Raman spectroscopy. There was an enhancement in the bacterial peaks in the presence of GQDs which could be attributed to the chemical enhancement mechanism. This was the first time GQDs

were used to study the SERS of bacteria.

In conclusion, various graphene-biosystems interfaces (mammalian/bacterial cells, biofluids and tissue) were discussed in this thesis for applications in biomedicine and energy. However, further studies need to be done to get a more thorough idea regarding the potential of graphene-biointerfaces. For each interfaces formed, fundamental studies need to be done before, to understand the specific interaction involved.

7. REFERENCES

1. Akhavan, O. 2015. “Bacteriorhodopsin as a Superior Substitute for Hydrazine in Chemical Reduction of Single-Layer Graphene Oxide Sheets.” *Carbon* 81 (1): 158–66. https://doi.org/10.1016/j.carbon.2014.09.044.
2. Al-Chalabi, Ammar, Orla Hardiman, Matthew C. Kiernan, Adriano Chiò, Benjamin Rix-Brooks, and Leonard H. van den Berg. 2016. “Amyotrophic Lateral Sclerosis: Moving towards a New Classification System.” *The Lancet Neurology*. https://doi.org/10.1016/S1474-4422(16)30199-5.
3. Ang, Priscilla Kailian, Wei Chen, Andrew Thye Shen Wee, and Ping Loh Kian. 2008. “Solution-Gated Epitaxial Graphene as PH Sensor.” *Journal of the American Chemical Society* 130 (44): 14392–93. https://doi.org/10.1021/ja805090z.
4. Bander, Evan D., Rajiv Magge, and Rohan Ramakrishna. 2018. “Advances in Glioblastoma Operative Techniques.” *World Neurosurgery*. https://doi.org/10.1016/j.wneu.2018.04.023.
5. Basko, DM, S. Piscanec, and AC Ferrari. 2009. “Electron-Electron Interactions and Doping Dependence of the Two-Phonon Raman Intensity in Graphene.” *Physical Review B* 80 (16): 165413. https://doi.org/10.1103/PhysRevB.80.165413.
6. Batzill, Matthias. 2012. “The Surface Science of Graphene: Metal Interfaces, CVD Synthesis, Nanoribbons, Chemical Modifications, and Defects.” *Surface Science Reports* 67 (3–4): 83–115. https://doi.org/10.1016/j.surfrep.2011.12.001.
7. Bäumer, Dirk, Kevin Talbot, and Martin R. Turner. 2014. “Advances in Motor Neurone Disease.” *Journal of the Royal Society of Medicine* 107 (1): 14–21.

https://doi.org/10.1177/0141076813511451.

8. Bhattacharyya, Kiran, Benjamin S Goldschmidt, Mark Hannink, Stephen Alexander, and John A Viator. 2012. “Gold Nanoparticle Mediated Detection of Circulating Cancer Cells.” *Clinics in Laboratory Medicine* 32 (1): 89–101. https://doi.org/10.1016/j.cll.2012.01.001.
9. Bloch, Orin, Seunggu J. Han, Soonmee Cha, Matthew Z. Sun, Manish K. Aghi, Michael W. Mcdermott, Mitchel S. Berger, and Andrew T. Parsa. 2012. “Impact of Extent of Resection for Recurrent Glioblastoma on Overall Survival: Clinical Article.” *Journal of Neurosurgery*. https://doi.org/10.3171/2012.9.JNS12504.
10. Blum, L., N. Marzari, and R. Car. 2004. “Mechanism of the Hydrogen/Platinum(111) Fuel Cell.” *Journal of Physical Chemistry B* 108 (51): 19670–80. https://doi.org/10.1021/jp047188j.
11. Bond, Daniel R, Dawn E Holmes, Leonard M Tender, and Derek R Lovley. 2002. “Electrode-Reducing Microorganisms That Harvest Energy from Marine Sediments” 295 (January): 483–86.
12. Bond, Daniel R, and Derek R Lovley. 2003. “Electricity Production by Geobacter Sulfurreducens Attached to Electrodes Electricity Production by Geobacter Sulfurreducens Attached to Electrodes.” *Applied and Environmental Microbiology* 69 (3): 1548–55. https://doi.org/10.1128/AEM.69.3.1548.
13. Bozzo, F., A. Mirra, M. T. Carri, and M. T. Carrì. 2017. “Oxidative Stress and Mitochondrial Damage in the Pathogenesis of ALS: New Perspectives.” *Neuroscience Letters* 636: 3–8. https://doi.org/10.1016/j.neulet.2016.04.065.

14. Brown, Timothy J., Matthew C. Brennan, Michael Li, Ephraim W. Church, Nicholas J. Brandmeir, Kevin L. Rakszawski, Akshal S. Patel, et al. 2016. “Association of the Extent of Resection with Survival in Glioblastoma a Systematic Review and Meta-Analysis.” *JAMA Oncology*. https://doi.org/10.1001/jamaoncol.2016.1373.
15. Byun, Joonho, Young Hoon Kim, Soo Jung Nam, Ji Eun Park, Young Hyun Cho, Ho Sung Kim, Seok Ho Hong, Jeong Hoon Kim, Sang Joon Kim, and Chang Jin Kim. 2019. “Comparison of Survival Outcomes Between Partial Resection and Biopsy for Primary Glioblastoma: A Propensity Score-Matched Study.” *World Neurosurgery*. https://doi.org/10.1016/j.wneu.2018.09.237.
16. Cai, Weibo, Ting Gao, Hao Hong, and Jiangtao Sun. 2008. “Applications of Gold Nanoparticles in Cancer Nanotechnology.” *Nanotechnology, Science and Applications* 2008 (1): 10.2147/NSA.S3788. https://doi.org/10.2147/NSA.S3788.
17. Cançado, L. G., A. Jorio, E. H. Martins Ferreira, F. Stavale, C. A. Achete, R. B. Capaz, M. V. O. Moutinho, A. Lombardo, T. S. Kulmala, and A. C. Ferrari. 2011. “Quantifying Defects in Graphene via Raman Spectroscopy at Different Excitation Energies.” *Nano Letters* 11 (8): 3190–96. https://doi.org/10.1021/nl201432g.
18. Cançado, L. G., K. Takai, T. Enoki, M. Endo, Y. A. Kim, H. Mizusaki, A. Jorio, L. N. Coelho, R. Magalhães-Paniago, and M. A. Pimenta. 2006. “General Equation for the Determination of the Crystallite Size La of Nanographite by Raman Spectroscopy.” *Applied Physics Letters* 88 (16): 163106. https://doi.org/10.1063/1.2196057.
19. Casiraghi, C. 2009. “Doping Dependence of the Raman Peaks Intensity of Graphene Close to the Dirac Point.” *Physical Review B - Condensed Matter and Materials Physics*

80 (23). https://doi.org/10.1103/PhysRevB.80.233407.

20. Casiraghi, C., A. Hartschuh, E. Lidorikis, H. Qian, H. Harutyunyan, T. Gokus, K. S. Novoselov, and A. C. Ferrari. 2007. “Rayleigh Imaging of Graphene and Graphene Layers.” *Nano Letters* 7 (9): 2711–17. https://doi.org/10.1021/nl071168m.
21. Cheng, Liang Chien, Xiumei Jiang, Jing Wang, Chunying Chen, and Ru Shi Liu. 2013. “Nano-Bio Effects: Interaction of Nanomaterials with Cells.” *Nanoscale* 5 (9): 3547–69. https://doi.org/10.1039/c3nr34276j.
22. Chiò, Adriano, and Bryan J. Traynor. 2015. “Motor Neuron Disease in 2014: Biomarkers for ALS-in Search of the Promised Land.” *Nature Reviews Neurology*. https://doi.org/10.1038/nrneurol.2014.250.
23. Choi, Young-Eun, Ju-Won Kwak, and Joon Won Park. 2010. “Nanotechnology for Early Cancer Detection.” *Sensors* 10 (1): 428–55. https://doi.org/10.3390/s100100428.
24. Coburger, Jan, Vincent Hagel, Christian Rainer Wirtz, and Ralph König. 2015. “Surgery for Glioblastoma: Impact of the Combined Use of 5-Aminolevulinic Acid and Intraoperative MRI on Extent of Resection and Survival.” *PLoS ONE*. https://doi.org/10.1371/journal.pone.0131872.
25. Cui, Daxiang, Furong Tian, Cengiz S. Ozkan, Mao Wang, and Huajian Gao. 2005. “Effect of Single Wall Carbon Nanotubes on Human HEK293 Cells.” *Toxicology Letters* 155 (1): 73–85. https://doi.org/10.1016/j.toxlet.2004.08.015.
26. D.N., Louis, Perry A., Reifenberger G., von Deimling A., Figarella-Branger D., Cavenee W.K., Ohgaki H., Wiestler O.D., Kleihues P., and Ellison D.W. 2016. “The 2016 World Health Organization Classification of Tumors of the Central Nervous System: A

Summary." *Acta Neuropathologica*. https://doi.org/10.1007/s00401-016-1545-1 LK - http://sfx.hul.harvard.edu/sfx_local?sid=EMBASE&issn=14320533&id=doi:10.1007%2Fs00401-016-1545-1&atitle=The+2016+World+Health+Organization+Classification+of+Tumors+of+the+Central+Nervous+System%3A+a+summary&stitle=Acta+Neuropathol.&title=Acta+Neuropathologica&volume=131&issue=6&spage=803&epage=820&aulast=Louis&aufirst=David+N.&auinit=D.N.&aufull=Louis+D.N.&coden=ANPTA&isbn=&pages=803-820&date=2016&auinit1=D&auinitm=N.

27. D'Amico, Emanuele, Pam Factor-Litvak, Regina M Santella, and Hiroshi Mitsumoto. 2013. "Clinical Perspective on Oxidative Stress in Sporadic Amyotrophic Lateral Sclerosis." *Free Radical Biology & Medicine* 65: 509–27. https://doi.org/10.1016/j.freeradbiomed.2013.06.029.
28. Das, A., S. Pisana, B. Chakraborty, S. Piscanec, S. K. Saha, U. V. Waghmare, K. S. Novoselov, et al. 2008a. "Monitoring Dopants by Raman Scattering in an Electrochemically Top-Gated Graphene Transistor." *Nature Nanotechnology* 3 (4): 210–15. https://doi.org/10.1038/nnano.2008.67.
29. Das, A, S Pisana, B Chakraborty, S Piscanec, S K Saha, U V Waghmare, K S Novoselov, et al. 2008b. "Monitoring Dopants by Raman Scattering in an Electrochemically Top-Gated Graphene Transistor." *Nature Nanotechnology* 3 (4): 210–15. https://doi.org/10.1038/nnano.2008.67.
30. Deng, Shikai, Enlai Gao, Yanlei Wang, Soumyo Sen, Sreeprasad Theruvakkattil Sreenivasan, Sanjay Behura, Petr Král, Zhiping Xu, and Vikas Berry. 2016. "Confined,

Oriented, and Electrically Anisotropic Graphene Wrinkles on Bacteria." *ACS Nano* 10 (9): 8403–12. https://doi.org/10.1021/acsnano.6b03214.

31. Dikin, D A, S Stankovich, E J Zimney, R D Piner, G H Dommett, G Evmenenko, S T Nguyen, and R S Ruoff. 2007. "Preparation and Characterization of Graphene Oxide Paper." *Nature* 448 (7152): 457–60. https://doi.org/10.1038/nature06016.
32. Dobson, Susan Margaret. 1989. "Conceptualizing for Transcultural Health Visiting: The Concept of Transcultural Reciprocity." *Journal of Advanced Nursing*. https://doi.org/10.1111/j.1365-2648.1989.tb00906.x.
33. Dodge, J. C., C. M. Treleaven, J. A. Fidler, T. J. Tamsett, C. Bao, M. Searles, T. V. Taksir, et al. 2013. "Metabolic Signatures of Amyotrophic Lateral Sclerosis Reveal Insights into Disease Pathogenesis." *Proceedings of the National Academy of Sciences* 110 (26): 10812–17. https://doi.org/10.1073/pnas.1308421110.
34. Dresselhaus, Mildred S, Gene Dresselhaus, and Ado Jorio. 2008. *Group Theory: Application to the Physics of Condensed Matter*. *Springer*. Vol. 53. https://doi.org/10.1007/978-3-540-32899-5.
35. Dreyer, Daniel R, Sungjin Park, Christopher W Bielawski, and Rodney S Ruoff. 2010. "The Chemistry of Graphene Oxide." *Chemical Society Reviews* 39 (1): 228–40. https://doi.org/10.1039/B917103G.
36. Eda, Goki, Giovanni Fanchini, and Manish Chhowalla. 2008. "Large-Area Ultrathin Films of Reduced Graphene Oxide as a Transparent and Flexible Electronic Material." *Nature Nanotechnology* 3 (5): 270–74. https://doi.org/10.1038/nnano.2008.83.
37. Elias, D. C., R. V. Gorbachev, A. S. Mayorov, S. V. Morozov, A. A. Zhukov, P. Blake,

L. A. Ponomarenko, et al. 2011. “Dirac Cones Reshaped by Interaction Effects in Suspended Graphene.” *Nature Physics* 7 (9): 701–4. https://doi.org/10.1038/nphys2049.

38. ElMekawy, Ahmed, Hanaa M. Hegab, Dusan Losic, Christopher P. Saint, and Deepak Pant. 2017. “Applications of Graphene in Microbial Fuel Cells: The Gap between Promise and Reality.” *Renewable and Sustainable Energy Reviews* 72 (November 2016): 1389–1403. https://doi.org/10.1016/j.rser.2016.10.044.
39. Es, Michael A. van, Orla Hardiman, Adriano Chio, Ammar Al-Chalabi, R. Jeroen Pasterkamp, Jan H. Veldink, and Leonard H. van den Berg. 2017. “Amyotrophic Lateral Sclerosis.” *The Lancet*. https://doi.org/10.1016/S0140-6736(17)31287-4.
40. Fabbro, Alessandra, Denis Scaini, Verónica León, Ester Vázquez, Giada Cellot, Giulia Privitera, Lucia Lombardi, et al. 2016. “Graphene-Based Interfaces Do Not Alter Target Nerve Cells.” *ACS Nano* 10 (1): 615–23. https://doi.org/10.1021/acsnano.5b05647.
41. Fardin, M. A., O. M. Rossier, P. Rangamani, P. D. Avigan, N. C. Gauthier, W. Vonnegut, A. Mathur, J. Hone, R. Iyengar, and M. P. Sheetz. 2010. “Cell Spreading as a Hydrodynamic Process.” *Soft Matter* 6 (19): 4788. https://doi.org/10.1039/c0sm00252f.
42. Ferrari, A. C., J. C. Meyer, V. Scardaci, C. Casiraghi, M. Lazzeri, F. Mauri, S. Piscanec, et al. 2006. “Raman Spectrum of Graphene and Graphene Layers.” *Physical Review Letters* 97 (18): 187401. https://doi.org/10.1103/PhysRevLett.97.187401.
43. Ferrari, A. C., and J. Robertson. 2000. “Interpretation of Raman Spectra of Disordered and Amorphous Carbon.” *Physical Review B* 61 (20): 14095–107. https://doi.org/10.1103/PhysRevB.61.14095.
44. Ferrari, Andrea C. 2007. “Raman Spectroscopy of Graphene and Graphite: Disorder,

Electron-Phonon Coupling, Doping and Nonadiabatic Effects." *Solid State Communications* 143 (1–2): 47–57. https://doi.org/10.1016/j.ssc.2007.03.052.

45. Ferrari, Andrea C., and Denis M. Basko. 2013. "Raman Spectroscopy as a Versatile Tool for Studying the Properties of Graphene." *Nature Nanotechnology* 8 (4): 235–46. https://doi.org/10.1038/nnano.2013.46.
46. Ferrari, Mauro. 2005. "Cancer Nanotechnology: Opportunities and Challenges." *Nature Reviews Cancer* 5 (3): 161–71. https://doi.org/10.1038/nrc1566.
47. Fleischmann, M., P. J. Hendra, and A. J. McQuillan. 1974. "Raman Spectra of Pyridine Adsorbed at a Silver Electrode." *Chemical Physics Letters* 26 (2): 163–66. https://doi.org/10.1016/0009-2614(74)85388-1.
48. Gao, Wei, Lawrence B Alemany, Lijie Ci, and Pulickel M Ajayan. 2009. "New Insights into the Structure and Reduction of Graphite Oxide." *Nat. Chem.* 1 (5): 403–8. https://doi.org/10.1038/nchem.281.
49. Geim, A. K., and K.S. S. Novoselov. 2007. "The Rise of Graphene." *Nature Mater.* 6 (3): 183–91. https://doi.org/10.1038/nmat1849.
50. Geim, A K. 2009. "Graphene: Status and Prospects." *Science (New York, N.Y.)* 324 (5934): 1530–34. https://doi.org/10.1126/science.1158877.
51. Goto, Yuko, Naoko Yoshida, Yuto Umeyama, Takeshi Yamada, Ryugo Tero, and Akira Hiraishi. 2015. "Enhancement of Electricity Production by Graphene Oxide in Soil Microbial Fuel Cells and Plant Microbial Fuel Cells." *Frontiers in Bioengineering and Biotechnology* 3 (APR): 1–8. https://doi.org/10.3389/fbioe.2015.00042.
52. Gray, Elizabeth, James R. Larkin, Tim D.W. Claridge, Kevin Talbot, Nicola R. Sibson,

and Martin R. Turner. 2015. “The Longitudinal Cerebrospinal Fluid Metabolomic Profile of Amyotrophic Lateral Sclerosis.” *Amyotrophic Lateral Sclerosis and Frontotemporal Degeneration* 16 (7–8): 456–63. https://doi.org/10.3109/21678421.2015.1053490.

53. Griffiths, J R. 1991. “Are Cancer Cells Acidic?” *British Journal of Cancer* 64 (3): 425–27. https://doi.org/10.1038/bjc.1991.326.
54. Haltiwanger, S. 2010. “The Electrical Properties of Cancer Cells.” *Wind Power, 17.06*. http://scholar.google.com/scholar?hl=en&btnG=Search&q=intitle:The+Electrical+Properties+of+Cancer+Cells#1.
55. Hao, Yufeng, Yingying Wang, Lei Wang, Zhenhua Ni, Ziqian Wang, Rui Wang, Chee Keong Koo, Zexiang Shen, and John T.L. Thong. 2010. “Probing Layer Number and Stacking Order of Few-Layer Graphene by Raman Spectroscopy.” *Small* 6 (2): 195–200. https://doi.org/10.1002/smll.200901173.
56. He, Qiyuan, Herry Gunadi Sudibya, Zongyou Yin, Shixin Wu, Hai Li, Freddy Boey, Wei Huang, Peng Chen, and Hua Zhang. 2010. “Centimeter-Long and Large-Scale Micropatterns of Reduced Graphene Oxide Films: Fabrication and Sensing Applications.” https://doi.org/10.1021/nn100780v.
57. Holland, E C. 2000. “Glioblastoma Multiforme: The Terminator.” *Proceedings of the National Academy of Sciences of the United States of America* 97 (12): 6242–44. https://doi.org/10.1073/pnas.97.12.6242.
58. Holton, Oliver T, and Joseph W Stevenson. 2013. “The Role of Platinum in Proton Exchange Membrane Fuel Cells Evaluation of Platinum’s Unique Properties for Use in Both the Anode and Cathode of a Proton Exchange Membrane Fuel Cell.”

@BULLETPlatinum Metals Rev 57 (4): 259–71. https://doi.org/10.1595/147106713X671222.

59. Hooten, Kristopher G., David R. Beers, Weihua Zhao, and Stanley H. Appel. 2015. "Protective and Toxic Neuroinflammation in Amyotrophic Lateral Sclerosis." *Neurotherapeutics*. https://doi.org/10.1007/s13311-014-0329-3.
60. Howland, D. S., J. Liu, Y. She, B. Goad, N. J. Maragakis, B. Kim, J. Erickson, et al. 2002. "Focal Loss of the Glutamate Transporter EAAT2 in a Transgenic Rat Model of SOD1 Mutant-Mediated Amyotrophic Lateral Sclerosis (ALS)." *Proceedings of the National Academy of Sciences* 99 (3): 1604–9. https://doi.org/10.1073/pnas.032539299.
61. Huang, Mingyuan, Hugen Yan, Tony F. Heinz, and James Hone. 2010. "Probing Strain-Induced Electronic Structure Change in Graphene by Raman Spectroscopy." *Nano Letters* 10 (10): 4074–79. https://doi.org/10.1021/nl102123c.
62. Huang, Xiaohua, and Mostafa A. El-Sayed. 2010. "Gold Nanoparticles: Optical Properties and Implementations in Cancer Diagnosis and Photothermal Therapy." *Journal of Advanced Research*. https://doi.org/10.1016/j.jare.2010.02.002.
63. Hummers, William S., and Richard E. Offeman. 1958. "Preparation of Graphitic Oxide." *Journal of the American Chemical Society* 80 (6): 1339–1339. https://doi.org/10.1021/ja01539a017.
64. Incekara, Fatih, Stephan Koene, Arnaud J.P.E. Vincent, Martin J. van den Bent, and Marion Smits. 2019. "Association Between Supratotal Glioblastoma Resection and Patient Survival: A Systematic Review and Meta-Analysis." *World Neurosurgery*. https://doi.org/10.1016/j.wneu.2019.04.092.

65. Jarvis, Roger M., and Royston Goodacre. 2004. “Discrimination of Bacteria Using Surface-Enhanced Raman Spectroscopy.” *Analytical Chemistry* 76 (1): 40–47. https://doi.org/10.1021/ac034689c.

66. Jiang, Shan, Rui Cheng, Xiang Wang, Teng Xue, Yuan Liu, Andre Nel, Yu Huang, and Xiangfeng Duan. 2013. “Real-Time Electrical Detection of Nitric Oxide in Biological Systems with Sub-Nanomolar Sensitivity.” *Nat Commun* 4: 2225. https://doi.org/10.1038/ncomms3225.

67. Kalbacova, Marie, Antonin Broz, Jing Kong, and Martin Kalbac. 2010. “Graphene Substrates Promote Adherence of Human Osteoblasts and Mesenchymal Stromal Cells.” *Carbon* 48 (15): 4323–29. https://doi.org/10.1016/j.carbon.2010.07.045.

68. Kang, Boseok, Soojin Lim, Wi Hyoung Lee, Sae Byeok Jo, and Kilwon Cho. 2013. “Work-Function-Tuned Reduced Graphene Oxide via Direct Surface Functionalization as Source/Drain Electrodes in Bottom-Contact Organic Transistors.” *Advanced Materials*. https://doi.org/10.1002/adma.201302358.

69. Kato, Yasumasa, Shigeyuki Ozawa, Chihiro Miyamoto, Yojiro Maehata, Atsuko Suzuki, Toyonobu Maeda, and Yuh Baba. 2013. “Acidic Extracellular Microenvironment and Cancer.” *Cancer Cell International* 13 (1): 89. https://doi.org/10.1186/1475-2867-13-89.

70. Katsevman, Gennadiy A., Ryan C. Turner, Ogaga Urhie, Joseph L. Voelker, and Sanjay Bhatia. 2019. “Utility of Sodium Fluorescein for Achieving Resection Targets in Glioblastoma: Increased Gross- or near-Total Resections and Prolonged Survival.” *Journal of Neurosurgery*. https://doi.org/10.3171/2018.10.jns181174.

71. Keisham, Bijentimala, Arron Cole, Phong Nguyen, Ankit Mehta, and Vikas Berry. 2016.

"Cancer Cell Hyperactivity and Membrane Dipolarity Monitoring via Raman Mapping of Interfaced Graphene: Toward Non-Invasive Cancer Diagnostics." *ACS Applied Materials & Interfaces* 8 (48): 32717–22. https://doi.org/10.1021/acsami.6b12307.

72. Keisham, Bijentimala, Akop Seksenyan, Steven Denyer, Pouyan Kheirkhah, Gregory D Arnone, Pablo Avalos, Abhiraj D Bhimani, Clive Svendsen, Vikas Berry, and Ankit I. Mehta. 2019. "Quantum Capacitance Based Amplified Graphene Phononics for Studying Neurodegenerative Diseases." Research-article. *ACS Applied Materials & Interfaces* 11 (1): 169–75. https://doi.org/10.1021/acsami.8b15893.
73. Khan, Saida P., Gregory G. Auner, and Golam M. Newaz. 2005. "Influence of Nanoscale Surface Roughness on Neural Cell Attachment on Silicon." *Nanomedicine: Nanotechnology, Biology, and Medicine* 1 (2): 125–29. https://doi.org/10.1016/j.nano.2005.03.007.
74. Kiani, Mohammad Javad, Mohammad Taghi Ahmadi, Hediyeh Karimi Feiz Abadi, Meisam Rahmani, Amin Hashim, and Fauzan Khairi Che Harun. 2013. "Analytical Modelling of Monolayer Graphene-Based Ion-Sensitive FET to PH Changes." *Nanoscale Research Letters* 8 (1): 173. https://doi.org/10.1186/1556-276X-8-173.
75. Kim, S, B Keisham, and V Berry. 2020. "Cellular Nano-Transistor: An Electronic-Interface between Nanoscale Semiconductors and Biological Cells." *Materials Today Nano* 9 (March): 100063. https://doi.org/10.1016/j.mtnano.2019.100063.
76. Kriss, Timothy C., and Vesna Martich Kriss. 1998. "History of the Operating Microscope: From Magnifying Glass to Microneurosurgery." *Neurosurgery*. https://doi.org/10.1097/00006123-199804000-00116.

77. Kumar, Priyank V., Marco Bernardi, and Jeffrey C. Grossman. 2013. “The Impact of Functionalization on the Stability, Work Function, and Photoluminescence of Reduced Graphene Oxide.” *ACS Nano* 7 (2): 1638–45. https://doi.org/10.1021/nn305507p.

78. Lazzeri, Michele, and Francesco Mauri. 2006. “Nonadiabatic Kohn Anomaly in a Doped Graphene Monolayer.” *Physical Review Letters* 97 (26): 29–32. https://doi.org/10.1103/PhysRevLett.97.266407.

79. Leang, Ching, Xinlei Qian, Tünde Mester, and Derek R. Lovley. 2010. “Alignment of the C-Type Cytochrome OmcS along Pili of Geobacter Sulfurreducens.” *Applied and Environmental Microbiology* 76 (12): 4080–84. https://doi.org/10.1128/AEM.00023-10.

80. Lehner, Benjamin A E, Vera A E C Janssen, Ewa M Spiesz, Dominik Benz, Stan J. J. Brouns, Anne S. Meyer, and Herre S. J. van der Zant. 2019. “Creation of Conductive Graphene Materials by Bacterial Reduction Using Shewanella Oneidensis.” *ChemistryOpen* 8 (7): 888–95. https://doi.org/10.1002/open.201900186.

81. Li, Ning, Xuemin Zhang, Qin Song, Ruigong Su, Qi Zhang, Tao Kong, Liwei Liu, Gang Jin, Mingliang Tang, and Guosheng Cheng. 2011. “The Promotion of Neurite Sprouting and Outgrowth of Mouse Hippocampal Cells in Culture by Graphene Substrates.” *Biomaterials* 32 (35): 9374–82. https://doi.org/10.1016/j.biomaterials.2011.08.065.

82. Li, Xiaolin, Xinran Wang, Li Zhang, Sangwon Lee, and Hongjie Dai. 2008. “Chemically Derived, Ultrasmooth Graphene Nanoribbon Semiconductors.” *Science*. https://doi.org/10.1126/science.1150878.

83. Li, Xuesong, Weiwei Cai, Jinho An, Seyoung Kim, Junghyo Nah, Dongxing Yang, Richard Piner, et al. 2009. “Large-Area Synthesis of High-Quality and Uniform

Graphene Films on Copper Foils." *Science* 324 (5932): 1312–14. https://doi.org/10.1126/science.1171245.

84. Li, Yan Michael, Dima Suki, Kenneth Hess, and Raymond Sawaya. 2016. "The Influence of Maximum Safe Resection of Glioblastoma on Survival in 1229 Patients: Can We Do Better than Gross-Total Resection?" *Journal of Neurosurgery*. https://doi.org/10.3171/2015.5.JNS142087.
85. Li, Yilei. 2014. "Probing the Response of Two-Dimensional Crystals by Opical Spectroscopy," 9–18. https://doi.org/10.1007/978-3-319-25376-3.
86. Ling, Xi, Liming Xie, Yuan Fang, Hua Xu, Haoli Zhang, Jing Kong, Mildred S. Dresselhaus, Jin Zhang, and Zhongfan Liu. 2010. "Can Graphene Be Used as a Substrate for Raman Enhancement?" *Nano Letters* 10 (2): 553–61. https://doi.org/10.1021/nl903414x.
87. Liu, Hong, and Bruce E. Logan. 2004. "Electricity Generation Using an Air-Cathode Single Chamber Microbial Fuel Cell in the Presence and Absence of a Proton Exchange Membrane." *Environmental Science and Technology* 38 (14): 4040–46. https://doi.org/10.1021/es0499344.
88. Liu, Li, Sunmin Ryu, Michelle R. Tomasik, Elena Stolyarova, Naeyoung Jung, Mark S. Hybertsen, Michael L. Steigerwald, Louis E. Brus, and George W. Flynn. 2008. "Graphene Oxidation: Thickness-Dependent Etching and Strong Chemical Doping." *Nano Letters* 8 (7): 1965–70. https://doi.org/10.1021/nl0808684.
89. Liu, Ying, Yuliang Zhao, Baoyun Sun, and Chunying Chen. 2013. "Understanding the Toxicity of Carbon Nanotubes." *Accounts of Chemical Research* 46 (3): 702–13.

https://doi.org/10.1021/ar300028m.

90. Logan, Bruce E., Bert Hamelers, René Rozendal, Uwe Schröder, Jürg Keller, Stefano Freguia, Peter Aelterman, Willy Verstraete, and Korneel Rabaey. 2006. “Microbial Fuel Cells: Methodology and Technology.” *Environmental Science and Technology* 40 (17): 5181–92. https://doi.org/10.1021/es0605016.
91. Mager, Morgan D., Vanessa Lapointe, and Molly M. Stevens. 2011. “Exploring and Exploiting Chemistry at the Cell Surface.” *Nature Chemistry* 3 (8): 582–89. https://doi.org/10.1038/nchem.1090.
92. Malard, L. M., M. A. Pimenta, G. Dresselhaus, and M. S. Dresselhaus. 2009. “Raman Spectroscopy in Graphene.” *Physics Reports*. https://doi.org/10.1016/j.physrep.2009.02.003.
93. Mansoori, G Ali, Pirooz Mohazzabi, Percival McCormack, and Siavash Jabbari. 2007. “Nanotechnology in Cancer Prevention, Detection and Treatment: Bright Future Lies Ahead.” *World Review of Science* 4 (2/3): 226–57. https://doi.org/10.1504/WRSTSD.2007.013584.
94. Mehta, Ankit I., Andreas Linninger, Maciej S. Lesniak, and Herbert H. Engelhard. 2015. “Current Status of Intratumoral Therapy for Glioblastoma.” *Journal of Neuro-Oncology* 125 (1): 1–7. https://doi.org/10.1007/s11060-015-1875-1.
95. Meyer, Jannik C., A. K. Geim, M. I. Katsnelson, K. S. Novoselov, T. J. Booth, and S. Roth. 2007. “The Structure of Suspended Graphene Sheets.” *Nature* 446 (7131): 60–63. https://doi.org/10.1038/nature05545.
96. Mohanty, Nihar, and Vikas Berry. 2008. “Graphene-Based Single-Bacterium Resolution

Biodevice and DNA Transistor: Interfacing Graphene Derivatives with Nanoscale and Microscale Biocomponents." *Nano Letters* 8 (12): 4469–76. https://doi.org/10.1021/nl802412n.

97. Mohanty, Nihar, Monica Fahrenholtz, Ashvin Nagaraja, Daniel Boyle, and Vikas Berry. 2011. "Impermeable Graphenic Encasement of Bacteria." *Nano Letters* 11 (3): 1270–75. https://doi.org/10.1021/nl104292k.

98. "Nerve Cells." 2003. In *Introduction to Molecular Biophysics*, 319–40. CRC Press. https://doi.org/doi:10.1201/9780203009963.ch7.

99. Nevin, K. P., H. Richter, S. F. Covalla, J. P. Johnson, T. L. Woodard, A. L. Orloff, H. Jia, M. Zhang, and D. R. Lovley. 2008. "Power Output and Columbic Efficiencies from Biofilms of Geobacter Sulfurreducens Comparable to Mixed Community Microbial Fuel Cells." *Environmental Microbiology* 10 (10): 2505–14. https://doi.org/10.1111/j.1462-2920.2008.01675.x.

100. Nguyen, Phong, and Vikas Berry. 2012. "Graphene Interfaced with Biological Cells: Opportunities and Challenges." *Journal of Physical Chemistry Letters*. https://doi.org/10.1021/jz300033g.

101. Nguyen, Phong, Junwen Li, T. S. Sreeprasad, Kabeer Jasuja, Nihar Mohanty, Myles Ikenberry, Keith Hohn, Vivek B. Shenoy, and Vikas Berry. 2013. "Covalent Functionalization of Dipole-Modulating Molecules on Trilayer Graphene: An Avenue for Graphene-Interfaced Molecular Machines." *Small* 9 (22): 3823–28. https://doi.org/10.1002/smll.201300857.

102. Ni, Zhenhua, Yingying Wang, Ting Yu, and Zexiang Shen. 2008. "Raman

Spectroscopy and Imaging of Graphene." *Nano Research* 1 (4): 273–91. https://doi.org/10.1007/s12274-008-8036-1.

103. Novoselov, K. S., A. K. Geim, S. V. Morozov, D. Jiang, M. I. Katsnelson, I. V. Grigorieva, S. V. Dubonos, and A. A. Firsov. 2005. "Two-Dimensional Gas of Massless Dirac Fermions in Graphene." *Nature* 438 (7065): 197–200. https://doi.org/10.1038/nature04233.

104. Novoselov, K S, A K Geim, S V Morozov, D Jiang, Y Zhang, S V Dubonos, I V Grigorieva, and A A Firsov. 2004. "Electric Field Effect in Atomically Thin Carbon Films." *Science (New York, N.Y.)* 306 (5696): 666–69. https://doi.org/10.1126/science.1102896.

105. Olson, Eric J, Rui Ma, Tao Sun, Mona A Ebrish, Nazila Haratipour, Kyoungmin Min, Narayana R Aluru, and Steven J Koester. 2015. "Capacitive Sensing of Intercalated H2O Molecules Using Graphene." *ACS Applied Materials & Interfaces* 7 (46): 25804–12. https://doi.org/10.1021/acsami.5b07731.

106. Palermo, Vincenzo. 2013. "Not a Molecule{,} Not a Polymer{,} Not a Substrate... the Many Faces of Graphene as a Chemical Platform." *Chem. Commun.* 49 (28): 2848–57. https://doi.org/10.1039/C3CC37474B.

107. Pan, Dengyu, Jingchun Zhang, Zhen Li, and Minghong Wu. 2010. "Hydrothermal Route for Cutting Graphene Sheets into Blue-Luminescent Graphene Quantum Dots." *Advanced Materials* 22 (6): 734–38. https://doi.org/10.1002/adma.200902825.

108. Pan, I. Wen, Sherise D. Ferguson, and Sandi Lam. 2015. "Patient and Treatment Factors Associated with Survival among Adult Glioblastoma Patients: A USA

Population-Based Study from 2000-2010." *Journal of Clinical Neuroscience*. https://doi.org/10.1016/j.jocn.2015.03.032.

109. Park, Sung Young, Jaesung Park, Sung Hyun Sim, Moon Gyu Sung, Kwang S. Kim, Byung Hee Hong, and Seunghun Hong. 2011. "Enhanced Differentiation of Human Neural Stem Cells into Neurons on Graphene." *Advanced Materials* 23 (36): H263–67. https://doi.org/10.1002/adma.201101503.

110. Paulus, Geraldine L. C., Justin T. Nelson, Katherine Y. Lee, Qing Hua Wang, Nigel F. Reuel, Brittany R. Grassbaugh, Sebastian Kruss, et al. 2014. "A Graphene-Based Physiometer Array for the Analysis of Single Biological Cells." *Scientific Reports* 4: 6865. https://doi.org/10.1038/srep06865.

111. Perfézou, Maëlle, Anthony Turner, and Arben Merkoçi. 2012. "Cancer Detection Using Nanoparticle-Based Sensors." *Chem. Soc. Rev.* 41 (7): 2606–22. https://doi.org/10.1039/C1CS15134G.

112. Pericleous, Pericles, Maria Gazouli, Anna Lyberopoulou, Spyros Rizos, Nikolaos Nikiteas, and Efstathios P. Efstathopoulos. 2012. "Quantum Dots Hold Promise for Early Cancer Imaging and Detection." *International Journal of Cancer* 131 (3): 519–28. https://doi.org/10.1002/ijc.27528.

113. Pisana, Simone, Michele Lazzeri, Cinzia Casiraghi, Kostya S Novoselov, A K Geim, Andrea C Ferrari, and Francesco Mauri. 2007. "Breakdown of the Adiabatic Born-Oppenheimer Approximation in Graphene." *Nature Materials* 6 (3): 198–201. https://doi.org/10.1038/nmat1846.

114. Pope, Michael A., and Ilhan A. Aksay. 2015. "Four-Fold Increase in the Intrinsic

Capacitance of Graphene through Functionalization and Lattice Disorder." *Journal of Physical Chemistry C* 119 (35): 20369–78. https://doi.org/10.1021/acs.jpcc.5b07521.

115. Pumera, Martin. 2011. "Graphene in Biosensing." *Materials Today* 14 (7–8): 308–15. https://doi.org/10.1016/S1369-7021(11)70160-2.

116. Reich, Stephanie, and Christian Thomsen. 2004. "Raman Spectroscopy of Graphite." *Philosophical Transactions of the Royal Society of London. Series A: Mathematical, Physical and Engineering Sciences* 362 (1824): 2271 LP – 2288. https://doi.org/10.1098/rsta.2004.1454.

117. Richter, Hanno, Kevin Mccarthy, Kelly P Nevin, Jessica P Johnson, Vincent M Rotello, and Derek R Lovley. 2008. "Electricity Generation by Geobacter Sulfurreducens Attached to Gold Electrodes," no. 18: 4376–79. https://doi.org/10.1021/la703469y.

118. Riveragil, Pilar, Carmen Vazquez-Vazquez, Vincenzo Giannini, M. Pilar Callao, Wolfgang J. Parak, Miguel A. Correa-Duarte, and Ramon A. Alvarez-Puebla. 2013. "Plasmonic Nanoprobes for Real-Time Optical Monitoring of Nitric Oxide inside Living Cells." *Angewandte Chemie - International Edition* 52 (51): 13694–98. https://doi.org/10.1002/anie.201306390.

119. Salas, Everett C., Zhengzong Sun, Andreas Lüttge, and James M. Tour. 2010. "Reduction of Graphene Oxide via Bacterial Respiration." *ACS Nano* 4 (8): 4852–56. https://doi.org/10.1021/nn101081t.

120. Sanai, Nader, Mei Yin Polley, Michael W. McDermott, Andrew T. Parsa, and Mitchel S. Berger. 2011. "An Extent of Resection Threshold for Newly Diagnosed Glioblastomas: Clinical Article." *Journal of Neurosurgery*.

https://doi.org/10.3171/2011.2.JNS10998.

121. Santoro, Carlo, Catia Arbizzani, Benjamin Erable, and Ioannis Ieropoulos. 2017. "Microbial Fuel Cells: From Fundamentals to Applications. A Review." *Journal of Power Sources* 356: 225–44. https://doi.org/10.1016/j.jpowsour.2017.03.109.

122. Santoro, Carlo, Mounika Kodali, Sadia Kabir, Francesca Soavi, Alexey Serov, and Plamen Atanassov. 2017. "Three-Dimensional Graphene Nanosheets as Cathode Catalysts in Standard and Supercapacitive Microbial Fuel Cell." *Journal of Power Sources* 356: 371–80. https://doi.org/10.1016/j.jpowsour.2017.03.135.

123. Sasaki, Ken Ichi, Keiko Kato, Yasuhiro Tokura, Satoru Suzuki, and Tetsuomi Sogawa. 2012. "Decay and Frequency Shift of Both Intervalley and Intravalley Phonons in Graphene: Dirac-Cone Migration." *Physical Review B - Condensed Matter and Materials Physics* 86 (20): 1–6. https://doi.org/10.1103/PhysRevB.86.201403.

124. Schedin, F, Ak K Geim, Sv V Morozov, Ew W Hill, P Blake, Mi I Katsnelson, and Ks S Novoselov. 2007. "Detection of Individual Gas Molecules Adsorbed on Graphene." *Nature Materials* 6 (9): 652–55. https://doi.org/10.1038/nmat1967.

125. Schröder, Uwe. 2007. "Anodic Electron Transfer Mechanisms in Microbial Fuel Cells and Their Energy Efficiency." *Phys. Chem. Chem. Phys.* 9 (21): 2619–29. https://doi.org/10.1039/B703627M.

126. Schwamb, Timo, Brian R Burg, Niklas C Schirmer, and Dimos Poulikakos. 2009. "An Electrical Method for the Measurement of the Thermal and Electrical Conductivity of Reduced Graphene Oxide Nanostructures." *Nanotechnology* 20 (40): 405704. https://doi.org/10.1088/0957-4484/20/40/405704.

127. Sharma, Bhavya, Renee R. Frontiera, Anne Isabelle Henry, Emilie Ringe, and Richard P. Van Duyne. 2012. “SERS: Materials, Applications, and the Future.” *Materials Today* 15 (1–2): 16–25. https://doi.org/10.1016/S1369-7021(12)70017-2.

128. Si, Yongchao, and Edward T. Samulski. 2008. “Synthesis of Water Soluble Graphene.” *Nano Letters* 8 (6): 1679–82. https://doi.org/10.1021/nl080604h.

129. Siegel, R, K Miller, and A Jemal. 2015. “Cancer Statistics , 2015 .” *CA Cancer J Clin* 65 (1): 29. https://doi.org/10.3322/caac.21254.

130. Smart, S.K., A.I. Cassady, G.Q. Lu, and D.J. Martin. 2006. “The Biocompatibility of Carbon Nanotubes.” *Carbon* 44 (6): 1034–47. https://doi.org/10.1016/j.carbon.2005.10.011.

131. Sreeprasad, T. S., and Vikas Berry. 2013. “How Do the Electrical Properties of Graphene Change with Its Functionalization?” *Small*. https://doi.org/10.1002/smll.201202196.

132. Sreeprasad, T. S., Phong Nguyen, Ahmed Alshogeathri, Luke Hibbeler, Fabian Martinez, Nolan McNeil, and Vikas Berry. 2015. “Graphene Quantum Dots Interfaced with Single Bacterial Spore for Bio-Electromechanical Devices: A Graphene Cytobot.” *Scientific Reports* 5 (1): 9138. https://doi.org/10.1038/srep09138.

133. Staff, Nathan P., and Stanley H. Appel. 2016. “The Immune System Continues to Knock at the ALS Door.” *Neuromuscular Disorders*, 2016. https://doi.org/10.1016/j.nmd.2016.04.010.

134. Stankovich, Sasha, Dmitriy A. Dikin, Richard D. Piner, Kevin A. Kohlhaas, Alfred Kleinhammes, Yuanyuan Jia, Yue Wu, SonBinh T. Nguyen, and Rodney S. Ruoff.

2007. “Synthesis of Graphene-Based Nanosheets via Chemical Reduction of Exfoliated Graphite Oxide.” *Carbon* 45 (7): 1558–65. https://doi.org/10.1016/j.carbon.2007.02.034.

135. Stankovich, Sasha, Richard D Piner, Xinqi Chen, Nianqiang Wu, SonBinh T Nguyen, and Rodney S Ruoff. 2006. “Stable Aqueous Dispersions of Graphitic Nanoplatelets via the Reduction of Exfoliated Graphite Oxide in the Presence of Poly(Sodium 4-Styrenesulfonate).” *J. Mater. Chem.* 16 (2): 155–58. https://doi.org/10.1039/B512799H.

136. Stupp, Roger, Warren P. Mason, Martin J. Van Den Bent, Michael Weller, Barbara Fisher, Martin J.B. Taphoorn, Karl Belanger, et al. 2005. “Radiotherapy plus Concomitant and Adjuvant Temozolomide for Glioblastoma.” *New England Journal of Medicine*. https://doi.org/10.1056/NEJMoa043330.

137. Sundaram, Ravi Shankar, Cristina Gómez-Navarro, Kannan Balasubramanian, Marko Burghard, and Klaus Kern. 2008. “Electrochemical Modification of Grapheme.” *Advanced Materials* 20 (16): 3050–53. https://doi.org/10.1002/adma.200800198.

138. Talbott, E.O., A.M. Malek, and D. Lacomis. 2016. “The Epidemiology of Amyotrophic Lateral Sclerosis.” In *Handbook of Clinical Neurology*, 138:225–38. https://doi.org/10.1016/B978-0-12-802973-2.00013-6.

139. Tannock, I F, and D Rotin. 1989. “Acid PH in Tumors and Its Potential for Therapeutic Exploitation.” *Cancer Research* 49 (16): 4373–84. https://doi.org/2545340.

140. Tarasiuk, Joanna, Alina Kułakowska, Wiesław Drozdowski, Johannes Kornhuber, and Piotr Lewczuk. 2012. “CSF Markers in Amyotrophic Lateral Sclerosis.” *Journal of Neural Transmission*. https://doi.org/10.1007/s00702-012-0806-y.

141. Thomsen, G. M., G. Gowing, J. Latter, M. Chen, J.-P. Vit, K. Staggenborg, P. Avalos, et al. 2014. “Delayed Disease Onset and Extended Survival in the SOD1G93A Rat Model of Amyotrophic Lateral Sclerosis after Suppression of Mutant SOD1 in the Motor Cortex.” *Journal of Neuroscience* 34 (47): 15587–600. https://doi.org/10.1523/JNEUROSCI.2037-14.2014.

142. Tuinstra, F., and J. L. Koenig. 1970. “Raman Spectrum of Graphite.” *The Journal of Chemical Physics* 53 (3): 1126–30. https://doi.org/10.1063/1.1674108.

143. Tung, Vincent C., Matthew J. Allen, Yang Yang, and Richard B. Kaner. 2009. “High-Throughput Solution Processing of Large-Scale Graphene.” *Nature Nanotechnology* 4 (1): 25–29. https://doi.org/10.1038/nnano.2008.329.

144. Turner, Martin R., and Michael Benatar. 2015. “Ensuring Continued Progress in Biomarkers for Amyotrophic Lateral Sclerosis.” *Muscle and Nerve* 51 (1): 14–18. https://doi.org/10.1002/mus.24470.

145. Vendrell, Marc, Kaustabh Kumar Maiti, Kevin Dhaliwal, and Young-Tae Chang. 2013. “Surface-Enhanced Raman Scattering in Cancer Detection and Imaging.” *Trends in Biotechnology* 31 (4): 249–57. https://doi.org/10.1016/j.tibtech.2013.01.013.

146. Voggu, Rakesh, Barun Das, Chandra Sekhar Rout, and C N R Rao. 2008. “Effects of Charge Transfer Interaction of Graphene with Electron Donor and Acceptor Molecules Examined Using Raman Spectroscopy and Cognate Techniques.” *Journal of Physics: Condensed Matter* 20 (47): 472204. https://doi.org/10.1088/0953-8984/20/47/472204.

147. Voiry, Damien, Jieun Yang, Jacob Kupferberg, Raymond Fullon, Calvin Lee, H. Y. Hu Young Jeong, Hyeon Suk Shin, and Manish Chhowalla. 2016. “High-Quality

Graphene via Microwave Reduction of Solution-Exfoliated Graphene Oxide." *Science* 3398 (6306): 1–7. https://doi.org/10.1126/science.aah3398.

148. Wang, Xuan, Linjie Zhi, and Klaus Müllen. 2008. "Transparent, Conductive Graphene Electrodes for Dye-Sensitized Solar Cells." *Nano Letters* 8 (1): 323–27. https://doi.org/10.1021/nl072838r.

149. Wang, Ying, Zhaohui Li, Jun Wang, Jinghong Li, and Yuehe Lin. 2011. "Graphene and Graphene Oxide: Biofunctionalization and Applications in Biotechnology." *Trends in Biotechnology*. https://doi.org/10.1016/j.tibtech.2011.01.008.

150. Warburg, Otto. 1956. "On the Origin of Cancer Cells." *Science* 123 (3191): 309–14. http://science.sciencemag.org/content/123/3191/309.abstract.

151. Wu, Zhang Ting, Wei Wei Zhao, Wei Yu Chen, Jie Jiang, Hai Yan Nan, Xi Tao Guo, Zheng Liang, Yu Ming Chen, Yun Fei Chen, and Zhen Hua Ni. 2015. "The Influence of Chemical Solvents on the Properties of CVD Graphene." *Journal of Raman Spectroscopy* 46 (1): 21–24. https://doi.org/10.1002/jrs.4582.

152. Xia, Jilin, Fang Chen, Jinghong Li, and Nongjian Tao. 2009. "Measurement of the Quantum Capacitance of Graphene." *Nature Nanotechnology* 4 (8): 505–9. https://doi.org/10.1038/nnano.2009.177.

153. Xiao, Li, Jacqueline Damien, Jiayan Luo, Hee Dong Jang, Jiaxing Huang, and Zhen He. 2012. "Crumpled Graphene Particles for Microbial Fuel Cell Electrodes." *Journal of Power Sources* 208: 187–92. https://doi.org/10.1016/j.jpowsour.2012.02.036.

154. Yu, P.Y., and Manuel Cardona. 2005. *Fundamentals of Semiconductors: Physics and Materials Properties*. *Fundamentals of Semiconductors: Physics and Materials*

Properties, Edited by PY Yu and M. Cardona. XVIII, 639 p. 250 Illus. in Color, 116 Problems. 3rd Rev. and Enlargeded. 2005. Corr. 3rd Printing 3-540-25470-6. Berlin: Springer, 2005. Vol. 1. https://doi.org/10.1007/978-3-642-00710-1.

155. Yu, Xin, Bernard Munge, Vyomesh Patel, Gary Jensen, Ashwin Bhirde, Joseph D. Gong, Sang N. Kim, et al. 2006. "Carbon Nanotube Amplification Strategies for Highly Sensitive Immunodetection of Cancer Biomarkers." *Journal of the American Chemical Society* 128 (34): 11199–205. https://doi.org/10.1021/ja062117e.

156. Zhang, Yi, Luyao Zhang, and Chongwu Zhou. 2013. "Review of Chemical Vapor Deposition of Graphene and Related Applications." *Accounts of Chemical Research* 46 (10): 2329–39. https://doi.org/10.1021/ar300203n.

157. Zhao, Weihua, David R. Beers, Kristopher G. Hooten, Douglas H. Sieglaff, Aijun Zhang, Shanker Kalyana-Sundaram, Christopher M. Traini, et al. 2017. "Characterization of Gene Expression Phenotype in Amyotrophic Lateral Sclerosis Monocytes." *JAMA Neurology* 74 (6): 677–85. https://doi.org/10.1001/jamaneurol.2017.0357.

158. Zhu, Yanwu, Shanthi Murali, Weiwei Cai, Xuesong Li, Ji Won Suk, Jeffrey R. Potts, and Rodney S. Ruoff. 2010. "Graphene and Graphene Oxide: Synthesis, Properties, and Applications." *Advanced Materials* 22 (35): 3906–24. https://doi.org/10.1002/adma.201001068.

8. APPENDIX

8.1. Supporting Information: Detection of Cancer Cell via Raman Mapping of Interfaced Graphene: Towards Non-Invasive Cancer Diagnostics

8.1.1. Effect of cell interfaced with graphene (Raman G peak)

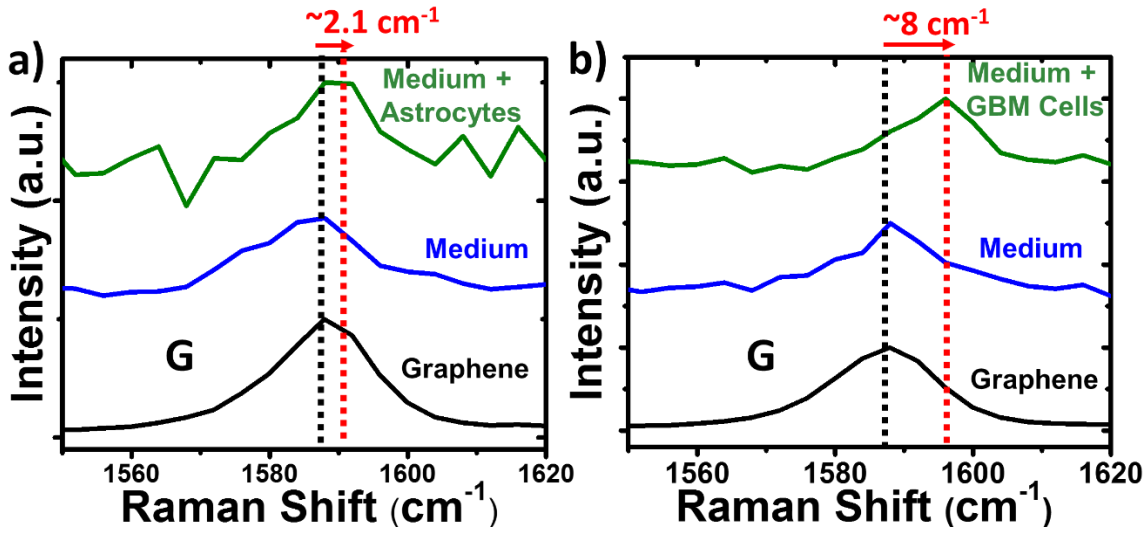

Figure A1. Raman spectra showing the G peak positions of graphene on air (black), graphene covered in cellular growth medium (blue) and graphene interfaced with the cell covered in medium (green) for a) Astrocyte. b) GBM cell. The G peak position of graphene interfaced with GBM cell shows a large blue shift, ~8 cm^{-1} compared to that interfaced with Astrocyte, ~2.1 cm^{-1}.

8.1.2. Effect of cell growth medium and PBS on graphene

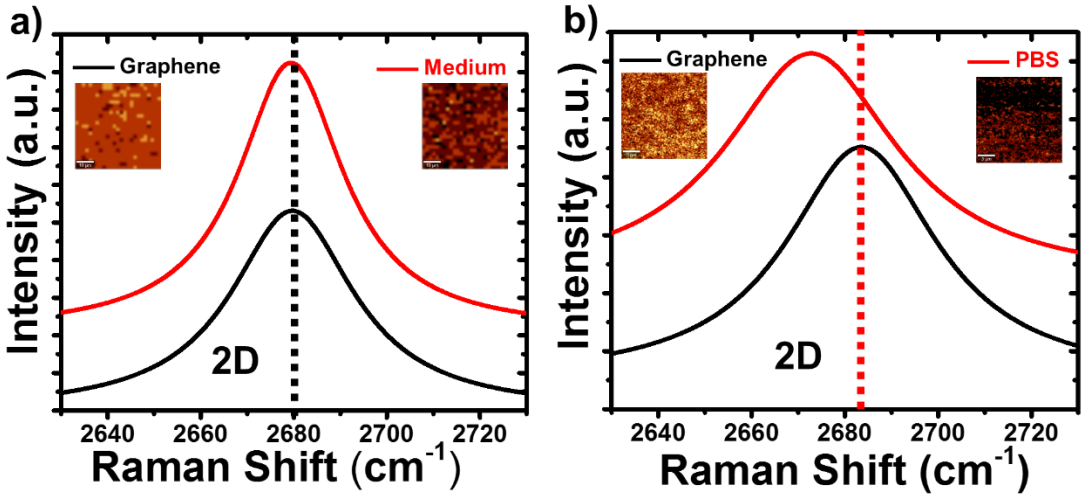

Figure A2. Raman spectra of graphene on air (black), graphene covered in a) cellular growth medium (red) and b) Phosphate buffer solution (red). Both spectra show n-doping on graphene when interfaced with different solvent medium.

8.1.3. Effect of high cell density on graphene

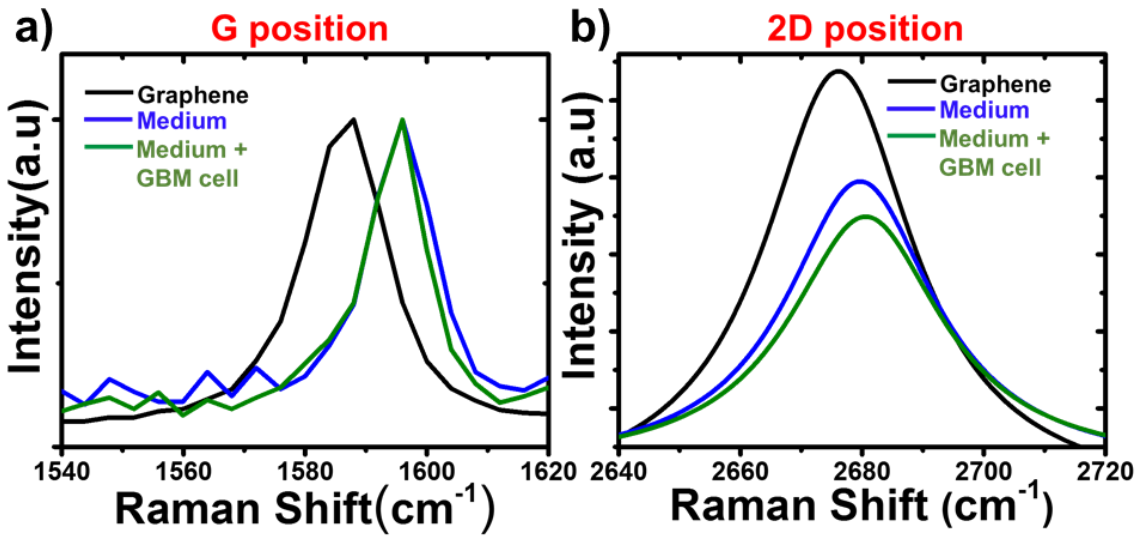

Figure A3. Raman spectra of graphene on air (black), graphene covered in cellular growth medium (blue) and graphene interfaced with GBM cell covered in medium (green) showing the a) G peak and b) 2D peak positions. When the cell density is >4 x 10^6 cells/ml, G peak shift is saturated while 2D peak remains unaffected and shows the general trend of graphene interfaced with GBM cells.

When the GBM cell density was very high (>4 x 10^6 cells/ml), saturation in graphene's G peak shift was observed (Figure S3a). Such G position saturation due to high degree of doping has been reported before(Das et al. 2008b; Pisana et al. 2007) which is attributed to the non-adiabatic removal of the Kohn anomaly at Γ(Lazzeri and Mauri 2006). In our study, the phenomena can be explained by the excessive amount of proton concentration in the solution, which is further adsorbed onto graphene platform. Further, it was challenging to decipher the cells from the medium (both were G-peak saturated). However, 2D peak exhibited a significant difference between the areas underneath the cell and the growth medium (Figure S3b). The saturation can be mitigated by modifying the sample preparation process, where graphene on SiO_2/Si chip was

dipped in the GBM cell solution in medium and incubated for 2 hours. Subsequently, the chip was washed with fresh medium, removing any unattached cell as well as replacing the old medium with the new one.

8.2. Supporting Information: Quantum Capacitance Based Amplified Graphene Phononics for Studying Neurodegenerative Diseases

The Raman spectra of the CVD grown graphene transferred on SiO_2/Si is shown in Figure S1 depicting the D, G and 2D bands, along with the optical image. The 2D/G intensity ratio was calculated to be ~2.4 and the full width at half maximum (FWHM) of 2D peak was ~29.9 cm^{-1}.(Hao et al. 2010) These values correspond to graphene monolayer produced via CVD.(Xuesong

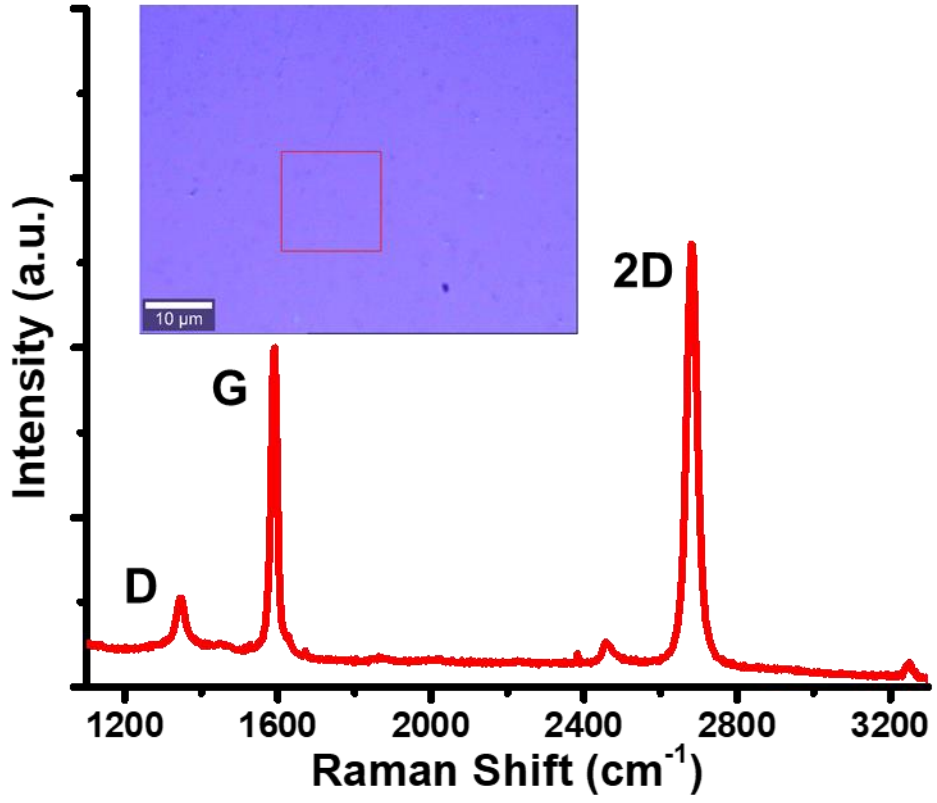

Figure A4. Raman Spectra of CVD graphene on SiO_2/Si substrate. (Inset) Optical image of graphene transferred SiO_2/Si substrate.

Li et al. 2009) Further, the weak D peak indicates that the CVD grown graphene is of high quality (sp^2 C orbitals).(L. Liu et al. 2008)

8.2.1. Average dipole moment comparison for different sample groups

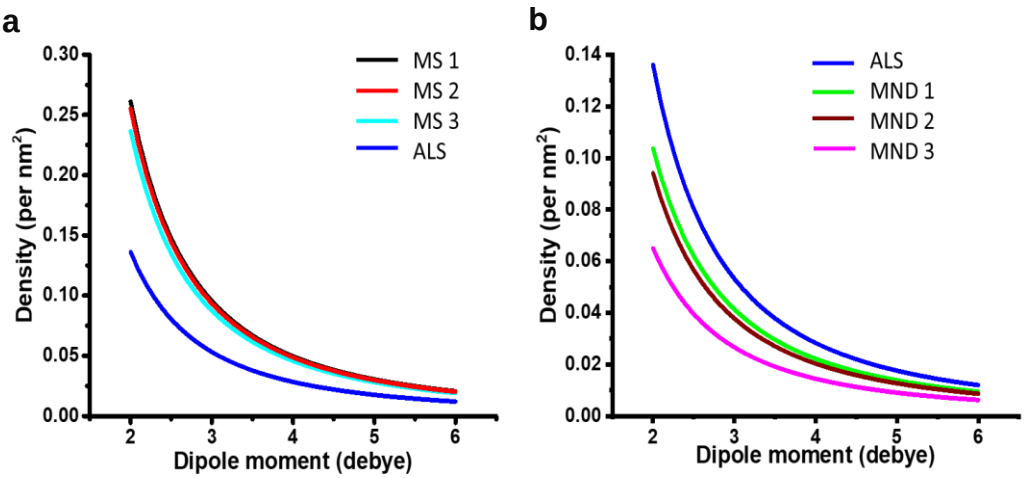

Figure A5. Calculated average induced dipole moment of human a) MS and b) MND CSF samples.

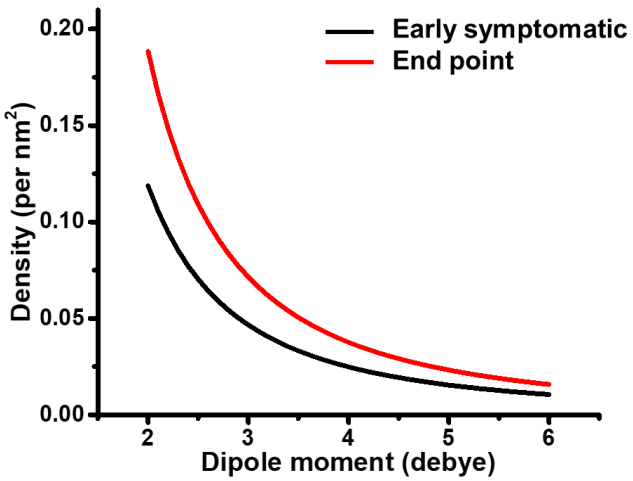

Figure A6. Calculated average induced dipole moment of CSF samples from rats at early symptomatic and end point stages.

8.3. Supporting Information: Graphene-Interface with Electrogenic Bacterial Membrane: Electron Transport and Energetics

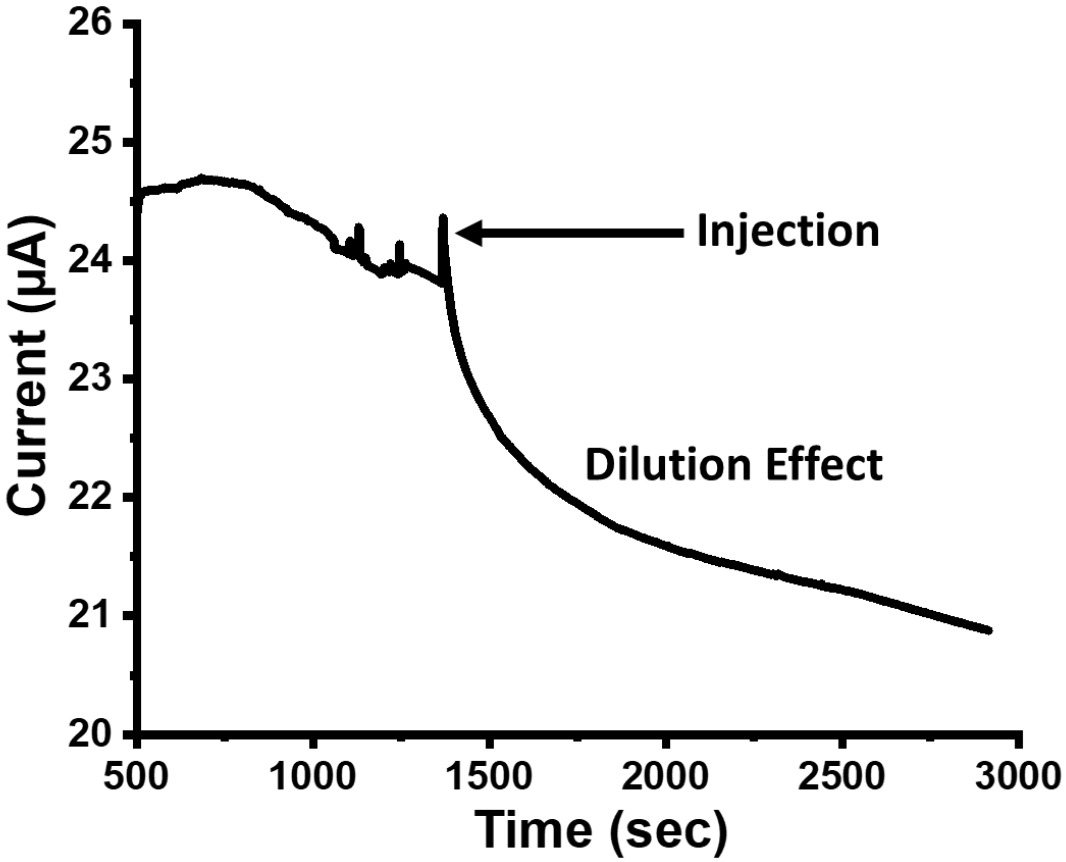

Figure A7. Current response for the MFC construct during operation. DI water was injected at the indicated point as a control experiment to observe the effect on the device from the injection. An instant increase is observed due to the convection on the electrode surface followed by a steady decline in current due to the dilution of the substrate inside of the anodic chamber. The dilution is proportional to the current by decreasing the biocatalyst's access to the substrate, an operational current drop is observed.

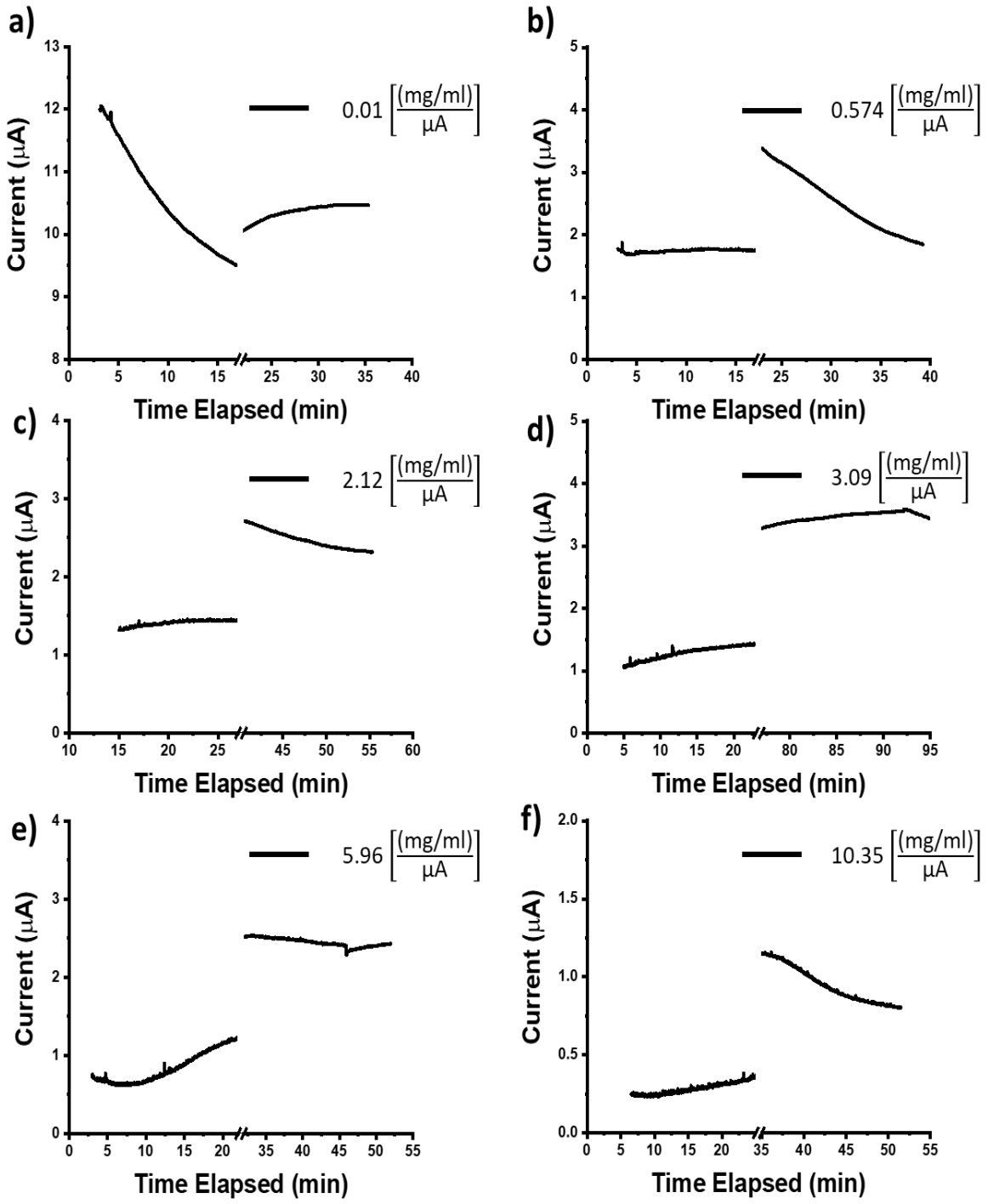

Figure A8. Raw current data collected by varying rGO (reduced graphene oxide) concentration inside device. The rGO solution was injected in the anodic chamber and allowed to operate until completion. The data has been truncated to show the current output of the device before and after the injection. The convection effect has not been illustrated and it was not involved in the calculations. The variation in the current is directly related to the amount of biocatalyst inside the apparatus and the cell count was not controlled.

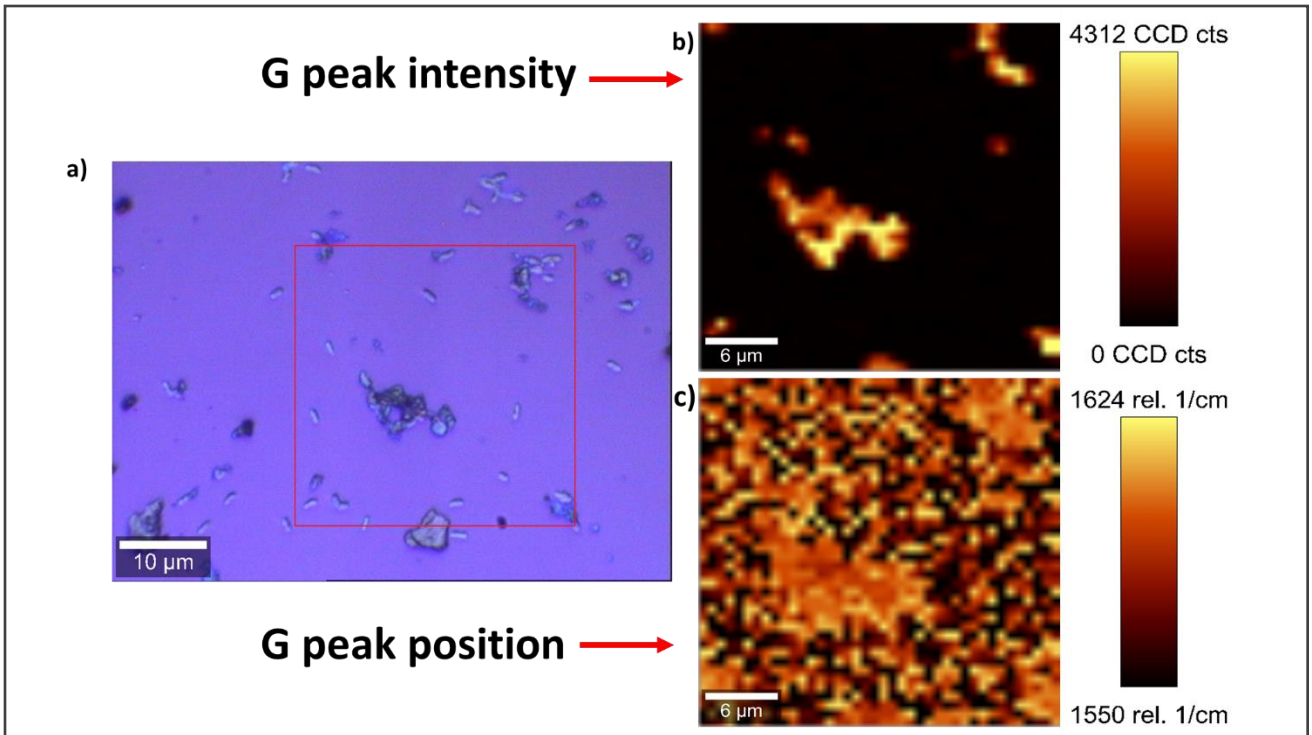

Figure A9. Raman characterization of rGO-geobacter interface. a) Optical image showing rGO and Geobacter on SiO_2/Si substrate, scale 10 µm. The red square represents the scanned area. b) and c) shows the G peak intensity and position, respectively, of the interfaced rGO

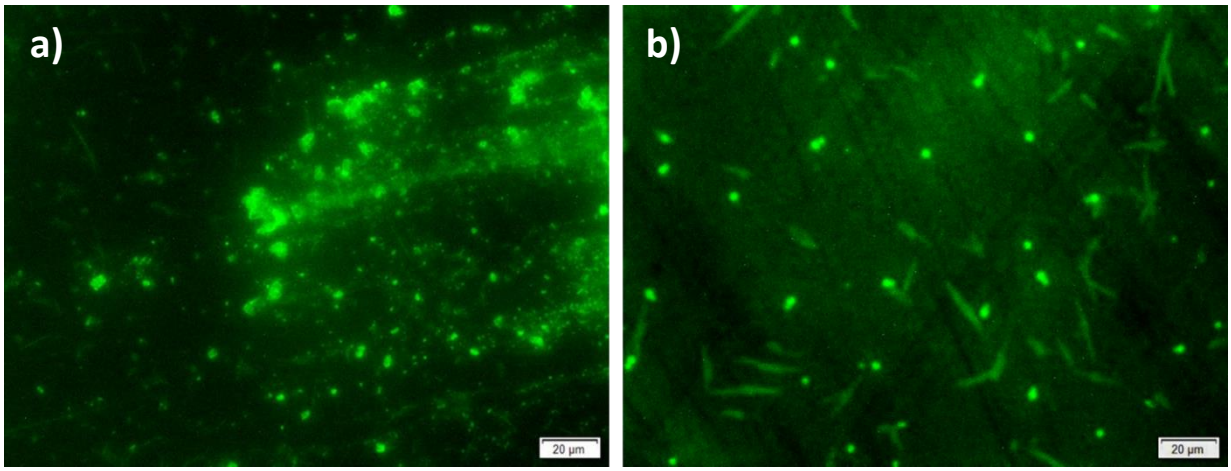

Figure A10. Live-dead bacterial assay. Geobacter cell solution was incubated with rGO solution overnight to perform the live-dead assay. Significant bacterial cells were observed to be still alive as shown in the images.

Table A1. Summary of the effect of different concentrations of rGO associated with the performance of the MFC device.

Devices	Normalized rGO Concentration [(mg/ml)/µA]	Average Electron Transfer Rate (10^6)	Device Power density
1	0 (DI water)	0.721	-28.0 %
2	0.01	0.989	-1.07 %
3	0.6	1.33	33.2 %
4	2.12	2.07	107 %
5	3.09	2.67	168 %
6	5.96	2.91	191 %
7	10.35	3.42	239 %

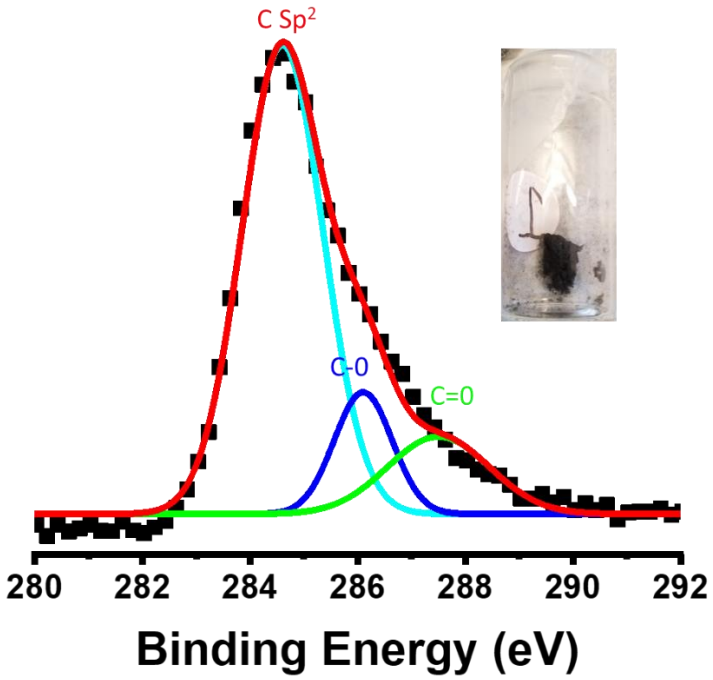

Figure A11. XPS spectrum at the C1S peak of the rGO sample showing the SP^2 hybridized carbon and functionalization with different carbon-oxygen bonding. (Insert) Picture of rGO powder after lyophilization.

UNIVERSITY OF ILLINOIS
AT CHICAGO

Office for the Protection of Research Subjects (OPRS)
Office of the Vice Chancellor for Research (MC 672)
203 Administrative Office Building
1737 West Polk Street
Chicago, Illinois 60612-7227

Approval Notice

Amendment to Research Protocol and/or Consent Document – Expedited Review

UIC Amendment # 1

November 2, 2016

Ankit Mehta, MD

Neurosurgery

912 S Wood Street

51N NPI, M/C 799

Chicago, IL 60612

Phone: (312) 996-4842 / Fax: (312) 996-9018

RE: Protocol # 2016-0006
"Tumor Biomarker-Graphene Cell Signature"

Dear Dr. Mehta:

Members of Institutional Review Board (IRB) #3 have reviewed this amendment to your research and/or consent form under expedited procedures for minor changes to previously approved research allowed by Federal regulations [45 CFR 46.110(b)(2) and/or 21 CFR 56.110(b)(2)]. The amendment to your research was determined to be acceptable and may now be implemented.

Please note the following information about your approved amendment:

Amendment Approval Date: November 2, 2016

Amendment:

Summary: UIC Amendment #1, dated October 7, 2016 (received 10/10/16, modifications received 10/26/16), is an investigator-initiated revision to the consent document to clarify incorrect statements. This is a research study about tumor markers from brain tumors, not tumor cells from metastatic lesions as previously described. The initial review application form and research protocol were updated to incorporate this change. Documentation of continuing education was provided for Laura McGuire.

Approved Subject Enrollment #: 10

Performance Sites: UIC

Research Protocol:

a) Tumor Biomarker - Graphene Cell Signature, Vers# 2.4, 10/26/2016

Informed Consent:

a) Combined Consent/Authorization: Graphene Tumor Biomarker, Version 1.3, 10/7/2016

Please note the Review History of this submission:

Receipt Date	Submission Type	Review Process	Review Date	Review Action
10/10/2016	Amendment	Expedited	10/21/2016	Modifications Required
10/26/2016	Response To Modifications	Expedited	11/02/2016	Approved

Please be sure to:

→ **Use only the IRB-approved and stamped consent document(s) and/or HIPAA Authorization form(s) enclosed with this letter when enrolling subjects.**

→ Use your research protocol number (2016-0006) on any documents or correspondence with the IRB concerning your research protocol.

→ Review and comply with all requirements on the enclosure,
"**UIC Investigator Responsibilities, Protection of Human Research Subjects**"
(http://tigger.uic.edu/depts/ovcr/research/protocolreview/irb/policies/0924.pdf)

Please note that the UIC IRB #3 has the right to ask further questions, seek additional information, or monitor the conduct of your research and the consent process.

Please be aware that if the scope of work in the grant/project changes, the protocol must be amended and approved by the UIC IRB before the initiation of the change.

We wish you the best as you conduct your research. If you have any questions or need further help, please contact the OPRS at (312) 996-1711 or me at (312) 413-3788. Please send any correspondence about this protocol to OPRS at 203 AOB, M/C 672.

Sincerely,

Rachel Olech, B.A., CIP

Assistant Director, IRB # 3

Office for the Protection of Research Subjects

Enclosure(s):

1. **Informed Consent Document:**
   a) Combined Consent/Authorization: Graphene Tumor Biomarker, Version 1.3, 10/7/2016

cc: Fady Charbel, Neurosurgery, M/C 799

Approval Notice

Amendment – Expedited Review

UIC Amendment # 1

September 13, 2019

Maria Tsoukas, MD, PhD

Dermatology

Phone: (312) 996-8667 / Fax: (312) 996-1188

RE: **Protocol # 2019-0303**
"Tissue Analysis for Skin Cancer Diagnosis using a Graphene Phononics Based Sensing Platform"

Dear Dr. Tsoukas:

Your application was reviewed and approved on September 13, 2019. The amendment to your research may now be implemented.

Please note the following information about your approved amendment:

Amendment Approval Date: September 13, 2019

Amendment:

Summary: UIC Amendment #1, dated 08/26/2019 and received via OPRS Live on 08/30/2019, includes a revised Appendix-P adding Virginia Jones (Alvarado) and Lacey Zimmerman as key research personnel.

Please be sure to:

→ Use your research protocol number (2019-0303) on any documents or correspondence with the IRB concerning your research protocol.

→ Review and comply with the policies of the UIC Human Subjects Protection Program

(HSPP) and the guidance ***Investigator Responsibilities***.

Please note that the IRB has the right to ask further questions, seek additional information, or monitor the conduct of your research and the consent process.

Please be aware that if the scope of work in the grant/project changes, the protocol must be amended and approved by the UIC IRB before the initiation of the change.

We wish you the best as you conduct your research. If you have any questions or need further help, please contact the OPRS at (312) 996-1711 or me at (312) 355-3949. Please send any correspondence about this protocol to OPRS via OPRS Live.

Sincerely,

Eddie Mendoza
IRB Coordinator, IRB # 3
Office for the Protection of Research Subjects

cc: Maria Tsoukas, Dermatology

Cancer Cell Hyperactivity and Membrane Dipolarity Monitoring via Raman Mapping of Interfaced Graphene: Toward Non-Invasive Cancer Diagnostics

Author: Bijentimala Keisham, Arron Cole, Phong Nguyen, et al
Publication: Applied Materials
Publisher: American Chemical Society
Date: Dec 1, 2016

VITA

Education

PhD. Chemical Engineering — August 2014-Present

University of Illinois, Chicago

M.Tech. Chemical Engineering — July 2010-May 2012

National Institute of Technology, Trichy, India

B.Tech. Biotechnology — August 2006-June 2010

Amity University, Uttar Pradesh, India

Selected Publications

1. Bijentimala Keisham, Arron Cole, Ankit Mehta and Vikas Berry, *"Cancer Cell Hyperactivity and Membrane Dipolarity Monitoring via Raman Mapping of Interfaced Graphene: Towards Non-Invasive Cancer Diagnostics"*, ACS Applied Materials and Interfaces, 8 (48), 32717-32722, 2016 [Featured in ScienceDaily, The Engineer, AzoNano, etc.]

2. Bijentimala Keisham, Akop Seksenyan, Steven Denyer, Pouyan Kheirkhah, Gregory Arnone, Pablo Avalos, Abhiraj D. Bhimani, Clive Svendsen, Vikas Berry and Ankit Mehta, *"Quantum Capacitance Based Amplified Graphene Phononics for Studying Neurodegenerative Diseases",* ACS Applied Materials and Interfaces, 11 (1), 169–175, 2019 [Featured in Nature India, The Hindu, Economic Times, ScienceDaily, etc.]

3. Sungjoon Kim, Bijentimala Keisham, and Vikas Berry, *"Cellular Nano-Transistor: An Electronic-Interface between Nanoscale Semiconductors and Biological Cells"*, Accepted, Materials Today Nano

4. S Deng, D Rhee, WK Lee, S Che, B Keisham, V Berry, TW Odom, "*Graphene Wrinkles Enable Spatially Defined Chemistry*", Nano letters 19 (8), 5640-5646

5. Sheldon Cotts, Bijentimala Keisham, Jay Rawal and Vikas Berry, "*Graphene-Interface with Electrogenic Bacterial Membrane for Electron-Harvestation*", Submitted

6. Bijentimala Keisham, Sungjoon Kim and Vikas Berry, "*Exploring Graphene Biointerfaces With Raman Spectroscopy*", Under preparation

7. Bijentimala Keisham, Sheldon Cotts, and Vikas Berry, "*Investigating SERS of bacteria using graphene quantum dots (GQDs) as the enhancement substrate*", Under preparation

Presentations

1. **Bijentimala Keisham**, Akop Seksenyan, Steven Denyer, Pouyan Kheirkhah, Gregory Arnone, Pablo Avalos, Abhiraj D. Bhimani, Clive Svendsen, Vikas Berry and Ankit Mehta, *"Quantum Capacitance Based Amplified Graphene Phononics for Studying Neurodegenerative Diseases",* **2019 MRS Spring Meeting,** April 2019

2. **Bijentimala Keisham,** Sheldon Cotts and Vikas Berry, *"Increased electron transport inside microbial fuel cell through interfacing graphene with Geobacter",* **2019 MRS Spring Meeting,** April 2019

3. **Bijentimala Keisham**, Akop Seksenyan, Steven Denyer, Pouyan Kheirkhah, Gregory

Arnone, Pablo Avalos, Abhiraj D. Bhimani, Clive Svendsen, Vikas Berry and Ankit Mehta, *"Graphene Based Sensing Platform for Studying Amyotrophic Lateral Sclerosis",* **2018 AIChE Annual Meeting,** November 2018

4. Sheldon Cotts, **Bijentimala Keisham** and Vikas Berry**,** *"Increased electron transport inside microbial fuel cell through interfacing graphene with Geobacter",* **2018 AIChE Annual Meeting,** November 2018

5. Akop Seksenyan, **Bijentimala Keisham**, Steven Denyer, Pouyan Kheirkhah, Gregory Arnone, Pablo Avalos, Abhiraj D. Bhimani, Clive Svendsen, Vikas Berry and Ankit Mehta, *"Graphene based biomarker platform for amyotrophic lateral sclerosis",* **Neuroscience 2018, Poster Presentation,** November 2018

6. **Bijentimala Keisham**, Arron Cole, Ankit Mehta and Vikas Berry, *"Cancer Cell Hyperactivity and Membrane Dipolarity Monitoring via Raman Mapping of Interfaced Graphene: Towards Non-Invasive Cancer Diagnostics",* **2017 AIChE Annual Meeting,** October 2017

7. **Bijentimala Keisham**, Arron Cole, Ankit Mehta and Vikas Berry, *"Cancer Cell Hyperactivity and Membrane Dipolarity Monitoring via Raman Mapping of Interfaced Graphene: Towards Non-Invasive Cancer Diagnostics",* **9th Annual Midwest Regional Conference, AIChE,** March 2017

8. **Bijentimala Keisham**, Arron Cole, Ankit Mehta and Vikas Berry, "*2D micro-Raman mapping of cell interfaced with graphene to determine surface potential and cellular activity: An ultrasensitive biosensor for non-invasive cancer diagnosis*", **2015 UIC**

College of Medicine Research Forum, Poster Presentation, UIC, December 2015